UNIVERSIDAD COMPLUTENSE DE MADRID
FACULTAD DE CIENCIAS QUÍMICAS

TESIS DOCTORAL

Papel de la amidohidrolasa de ácidos grasos en el desarrollo de la glándula mamaria adulta y en cáncer de mama

Role of fatty acid amide hydrolase in adult mammary gland development and breast cancer

MEMORIA PARA OPTAR AL GRADO DE DOCTOR

PRESENTADA POR

Isabel Tundidor Pérez

Directores

Eduardo Pérez Gómez
Cristina Sánchez García

Madrid

UNIVERSIDAD COMPLUTENSE DE MADRID
FACULTAD DE CIENCIAS QUÍMICAS

TESIS DOCTORAL

PAPEL DE LA AMIDOHIDROLASA DE ÁCIDOS GRASOS EN EL DESARROLLO DE LA GLÁNDULA MAMARIA ADULTA Y EN CÁNCER DE MAMA

ROLE OF FATTY ACID AMIDE HYDROLASE IN ADULT MAMMARY GLAND DEVELOPMENT AND BREAST CANCER

MEMORIA PARA OPTAR AL GRADO DE DOCTOR

PRESENTADA POR

Isabel Tundidor Pérez

DIRECTORES

Dr. Eduardo Pérez Gómez
Dra. Cristina Sánchez García

TESIS DOCTORAL

UNIVERSIDAD COMPLUTENSE DE MADRID

Facultad de Ciencias Químicas

UNIVERSIDAD
COMPLUTENSE
MADRID

PAPEL DE LA AMIDOHIDROLASA DE ÁCIDOS GRASOS EN EL DESARROLLO DE LA GLÁNDULA MAMARIA ADULTA Y EN CÁNCER DE MAMA

ROLE OF FATTY ACID AMIDE HYDROLASE IN ADULT MAMMARY GLAND DEVELOPMENT AND BREAST CANCER

Isabel Tundidor Pérez

Directores:

Dr. Eduardo Pérez Gómez
Dra. Cristina Sánchez García

AGRADECIMIENTOS

Tengo que empezar dándote las gracias a ti, Cris. Por haber visto potencial en mí y por no haber fallado jamás en ofrecerme comprensión, apoyo y confianza ciega. Ni soy la primera ni seré la última de tus predocs en decirte esto, pero tengo que recordártelo: eres inspiración. Edu, eres el mejor ejemplo de que la genialidad no está reñida con la sencillez, y esa combinación solo se encuentra en los mejores mentores. Gracias por estar siempre ahí para recordarme que en una sola cabecita no hay espacio para tantas preguntas y que, en ocasiones, hay que hacerse solo las correctas. Me has salvado de mí misma una y mil veces. Sandra, gracias por enseñarme de la mejor manera en mis inicios, y por toda tu ayuda en estos últimos meses. Recuerdo lo orgullosa que me sentí de ti el día de tu defensa, y solo espero que cuando me toque a mí pueda sentir que he terminado ligeramente cerca. María, gracias por llegar para ser referente y por contagiarnos a todos tu entusiasmo y tu pasión por la ciencia. Cada vez que te oigo hablar recuerdo por qué me dedico a esto. Manolo, ¿qué puedo decir sobre ti que no se haya dicho ya? Qué *savoir-faire*, qué estilo y qué elegancia. Gracias por las enseñanzas, profesionales y existenciales. Evita, me lo dijo Cris cuando nos presentó nada más llegar, y tras los años veo que no exageraba: si no estás, el laboratorio se viene abajo. Gracias por ser tan condenadamente eficaz. Y por hacer que una noche de cervezas contigo cunda más que 6 meses de terapia.

No se comparte poyata con alguien durante 5 años sin que se cree inevitablemente un vínculo, pero ese vínculo se blinda cuando además de poyata se comparten ilusiones y miedos, alegrías y frustraciones, éxitos y fracasos. Habéis conseguido que sintiese el laboratorio como más casa que mi casa, y que el síndrome del impostor fuese algo más fácil con lo que lidiar. Lo mejor de esta etapa habéis sido vosotros. Isra, eres de las personas que más admiro en el mundo. Naciste ya con la habilidad de estar a la altura de cualquier circunstancia, y gracias a tus consejos yo también he podido estarlo en muchas de ellas. Por favor, no dejes nunca de mandarme memes casposos. Juan, qué bonitas son las personas que dan lo que no les sobra, y tú eres una de ellas. Gracias por los bailes, los abrazos y las meriendas, pero, sobre todo, gracias por la RISA. Marta, compañeira, qué hubiese sido de mí todo este tiempo si no hubieses estado cerca. Tu técnica de pipetting ninja ha contribuido a una buena parte de los resultados que aquí se recogen, pero tu apoyo incondicional, tu energía y tu lealtad impregnan todas y cada una de estas páginas. Gracias por haber formado parte de esto conmigo. *De verdad de la buena*. Carlos, pequeña enciclopedia andante. Muy pronto asumí que jamás iba a llegar a ser lo que tú eres, pero creo que aspirar a ello me ha convertido en un poco mejor científica. Gracias por ser respuesta a mis continuas preguntas. Alba, gracias por haberte tomado la molestia de conocerme tan bien en tan poco tiempo. Gracias por tu entrega y tu implicación, porque son de las cosas más reales que ahora mismo me rodean. Nunca me olvido de que al mismo

tiempo estás librando tus propias batallas, y eso les da todavía más valor. Esti, siempre he sentido que hay mucho de ti en mí (y viceversa). Gracias por hacerme sentir comprendida, da igual cuándo leas esto o los km de distancia que nos separen.

A la gente del laboratorio que no he mencionado individualmente: gracias por haber formado parte de este ecosistema conmigo. Estoy segura de haber aprendido algo de todos y cada uno de vosotros a lo largo de estos 5 años. Al final todos terminamos siendo un recuerdo en la memoria de la gente, y vosotros habéis hecho todo lo posible por ser uno bueno.

Dejando a un lado todo el apoyo emocional, desde luego esta tesis no hubiese salido adelante sin el soporte técnico y científico de decenas de personas de la universidad y de centros asociados. De los CAIs de microscopía, de genómica y del animalario. De colaboradoras como María Caffarel o Gema Moreno (gracias por las muestras humanas, han sido valiosísimas para esta investigación). Y de la generosidad de un montón de gente que ha estado siempre disponible para ayudar de manera desinteresada. Especial mención a Sonia Castillo y a su equipo, por habernos prestado material en momentos de escasez. Al grupo de Maite Grande en la UFV, por ayudarnos con la colonia de los FAAH KO. A Nerea y Sara, por el microscopio de la planta 12. A Javier Lacadena, por su diligencia sin precedentes. Y allá donde se esconda, a Alexandra Elbakyan, por concedernos nuestro más que merecido derecho a la ciencia libre.

La UCM no ha sido el único escenario en el que la ciencia me ha llevado a conocer a gente sin cuyo apoyo esta tesis no hubiese sido posible. Juan, Álvaro, gracias por hacer que un solo año de universidad sentara las bases de un recorrido tan largo. Musasis fue durante muchos años mi día a día y hoy lo recuerdo con un cariño infinito. Nacho, fuiste mi mentor en el laboratorio desde la beca de introducción a la investigación en 3º de carrera, y de alguna manera nunca has dejado de serlo. Gracias por todo lo que me has enseñado, dentro y fuera del laboratorio. Gracias por haber hecho posible el experimento más guay de la tesis. Pero por encima de todo, gracias por seguir aquí. Lucía, Marta, Noe y Rebe, gracias por acompañarme durante todo este camino (y todo el que queda). Convertisteis en soportable (e incluso divertido) el levantarse a las 4 AM para desayunar la bebida energética del Mercadona y ponerse a subrayar apuntes, y desde entonces habéis sido un apoyo absoluto y una fuente inagotable de recursos para gestionar mi mundo emocional. Aunque no nos pongamos de acuerdo para compartir ciudad, os siento ahora tan presentes como cuando compartíamos pupitre.

Lejos de las probetas y los matraces, tengo que agradecerle todo a Ainhoa, Elena, María, Sara y Susana: salimos de los escombros de aquel derrumbe y nos reconstruimos juntas, y seguimos haciéndolo cada día. Gracias por hacerme sentir, cada vez que estoy con vosotras, que lo que me separa de todos mis problemas son mucho más de 50 km. A toda la gente de Barrelhouse, gracias por ser procuradores

últimos de salud mental. Espero de corazón que el swing haya llegado a mi vida para quedarse. Y a Carlos, por aparecer para recordarme que las cosas se pueden elegir fáciles. Gracias por el calor del hogar.

Por último, gracias a mi familia. A mis tíos, tías, primos, y primas (y a Larry, qué demonios): gracias por ser transversales, permanentes e incondicionales. Gracias a mis padres, por haberme concedido una vida que me permitiese el lujo de elegir mis propias preocupaciones. Mamá, sé que te hubieras recorrido las 50 provincias de España con tal de que terminase estudiando lo que quería estudiar. Gracias por haber sembrado en mí las cosas de las que más orgullosa me siento. Papá, gracias por hacer más de lo que tú crees que has hecho. Tú me enseñaste a cuestionarme y cuestionar, y al fin y al cabo es eso lo que me ha terminado trayendo aquí. Y Ana, gracias por existir. Tuve una infancia feliz porque te tuve a ti, y eso me salvó la vida. Os debo todo.

TABLE OF CONTENTS

RESUMEN

El cáncer de mama es el cáncer más frecuente en el mundo. Según el Observatorio Global de Cáncer de la Organización Mundial de la Salud, en 2020 se diagnosticaron más de 2.3 millones de nuevos casos, superando por primera vez al cáncer de pulmón en incidencia. Gracias al diagnóstico precoz y a la aparición de terapias dirigidas para los subtipos mayoritarios, el pronóstico de las pacientes con cáncer de mama en etapa temprana ha mejorado notablemente en los últimos años. Sin embargo, la existencia de subtipos tumorales con una biología más agresiva para las cuales no existe terapia dirigida o que presentan resistencia a las terapias convencionales supone un desafío clínico no resuelto. Por otro lado, la enfermedad metastásica afecta a un 30 % de las pacientes y, aunque es potencialmente tratable, a día de hoy se considera incurable. Todo esto hace necesaria la búsqueda de nuevas terapias, así como de nuevas herramientas de cribado que identifiquen a las pacientes con mayor probabilidad de sufrir una enfermedad más agresiva y permitan adaptar su manejo clínico. En este contexto, conocer los mecanismos moleculares que gobiernan el desarrollo de la glándula mamaria adulta y que se ven alterados durante la formación y progresión del cáncer de mama puede resultar de extrema utilidad para entender la biología que subyace a los fenotipos tumorales más agresivos y así poder desarrollar nuevas herramientas para su abordaje en la clínica.

El sistema endocannabinoide (SEC) es un sistema de comunicación celular que se encuentra implicado en el control de múltiples procesos biológicos y cuya desregulación se ha identificado en diversas patologías, incluido el cáncer. Este sistema está formado por receptores acoplados a proteínas G (los receptores cannabinoides), sus ligandos endógenos (los endocannabinoides) y las enzimas encargadas de la síntesis y degradación de estos últimos. A lo largo de las últimas décadas, la mayor parte de la investigación acerca del SEC en cáncer se ha centrado en el hecho ampliamente demostrado de que su activación farmacológica produce respuestas antitumorales. Sin embargo, muy pocos estudios han abordado cuál es el papel de este sistema en la generación y progresión del cáncer. Debido a que el SEC controla procesos celulares tan importantes en la biología del cáncer como la proliferación, la diferenciación y la muerte celular, su posible participación en los procesos tumorales es una cuestión muy relevante cuya respuesta podría tener importantes implicaciones traslacionales.

La amidohidrolasa de ácidos grasos (FAAH, por sus siglas en inglés) es una de las enzimas encargadas de la degradación de los endocannabinoides y, como tal, una de las principales reguladoras de la disponibilidad y la actividad biológica de los mismos. Como aproximación al estudio del papel del SEC en el cáncer de mama, el trabajo de esta tesis se centra en responder cuál es el papel de FAAH en el desarrollo de la glándula mamaria adulta y en cáncer de mama.

Los resultados generados por este trabajo apuntan a que FAAH juega un papel importante como impulsor de la diferenciación celular tanto en la mama sana como transformada. En primer lugar, encontramos que (i) los niveles de expresión de esta enzima aumentan durante la diferenciación de las células luminales de la glándula mamaria, (ii) que su actividad es necesaria para que esta diferenciación tenga lugar *in vitro*, y que (iii) su silenciamiento en ratones produce defectos en el desarrollo mamario durante la lactancia. En el contexto tumoral, descubrimos que (i) la expresión de FAAH está significativamente asociada al subtipo luminal de cáncer de mama (donde, a su vez, se relaciona con un mejor pronóstico de las pacientes), que (ii) su actividad promueve un viraje del fenotipo tumoral hacia estados más diferenciados, y que (iii) actúa como inhibidor de la progresión tumoral y la metástasis a pulmón.

En conjunto, estos resultados establecen por primera vez que FAAH tiene un papel como supresor tumoral en cáncer de mama y que, a su vez, ofrece potencial para ser estudiado como biomarcador con valor pronóstico y como diana terapéutica en esta enfermedad.

ABSTRACT

Breast cancer is the most common cancer worldwide. According to the Global Cancer Observatory of the World Health Organization, more than 2.3 million new cases were diagnosed in 2020, surpassing lung cancer in incidence for the first time. Thanks to early diagnosis and the development of targeted therapies for the most prevalent subtypes, the prognosis of early-stage breast cancer patients has notably improved in recent years. However, the existence of tumor subtypes with a more aggressive biology for which there is no targeted therapy or that are resistant to conventional therapies represents an unresolved clinical challenge. On the other hand, metastatic disease affects 30 % of patients and, although potentially treatable, is currently considered incurable. All of this makes necessary to seek for new therapies, as well as new screening tools that identify patients with a greater probability of suffering a more aggressive form of the disease and help clinical decisions. In this context, knowing the molecular mechanisms that govern the development of the adult mammary gland and that are altered during the formation and progression of breast cancer can be extremely useful to understand the biology that underlies the most aggressive tumor phenotypes and thus, to be able to develop new tools for its clinical management.

The endocannabinoid system (ECS) is a cell communication system that is involved in the control of multiple biological processes and whose dysregulation has been identified in various pathologies, including cancer. This system is composed of G protein-coupled receptors (cannabinoid receptors), their endogenous ligands (endocannabinoids) and the enzymes responsible for the synthesis and degradation of the latter. Over the past decades, most research on the ECS in cancer has been focused on the widely demonstrated fact that pharmacological activation of cannabinoid receptors produces antitumor responses. However, very few studies addressed the role of this system in the generation and progression of cancer. Because the ECS controls cellular processes as important in cancer biology as proliferation, differentiation and cell death, its possible participation in tumor processes is a very relevant question whose answer could have important translational implications.

Fatty acid amide hydrolase (FAAH) is one of the enzymes responsible for the degradation of endocannabinoids and, as such, one of the main regulators of their availability and biological activity. As an approach to studying the role of the ECS in breast cancer, the work of this thesis focuses on establishing the role of FAAH in the development of the adult mammary gland and in breast cancer.

The results generated by this work suggest that FAAH plays an important role as a driver of cell differentiation in both the healthy and the transformed mammary gland. First, we found that (i) the expression levels of this enzyme increase during the differentiation of mammary gland luminal cells, (ii) that its activity is necessary

for this differentiation to take place *in vitro*, and (iii) that its silencing in mice produces defects in mammary gland development during lactation. In the tumor context, we discovered that (i) the expression of FAAH is deeply associated with the luminal subtype of breast cancer (where it is related to a better prognosis of patients), that (ii) its activity promotes a shift of the tumor phenotype towards more differentiated states, and that (iii) it acts as an inhibitor of tumor progression and lung metastasis.

Together, these results establish for the first time that FAAH has a role as a tumor suppressor in breast cancer and that it offers potential to be studied as a biomarker with prognostic value and as a therapeutic target in this disease.

ABBREVIATIONS

2-AG: 2-arachidonoylglycerol

7-AAD: 7-aminoactinomycin D

AA: arachidonic acid

AC: adenylyl cyclase

AEA: arachidonoylethanolamide

ATCC: American Type Culture Collection

BSA: bovine serum albumin

BC: breast cancer

CB_1R: cannabinoid receptor 1

CB_2R: cannabinoid receptor 2

CBD: cannabidiol

CBRs: cannabinoid receptors

CK: cytokeratin

CNS: central nervous system

COX-2: cyclooxygenase-2

CXCR4: C-X-C chemokine receptor type 4

DAGL: diacylglycerol lipase

DEGs: differentially expressed genes

DMEM: Dulbecco's modified Eagle's medium

DTT: dithiothreitol

eCB(s): endocannabinoid(s)

ECM: extracellular matrix

ECS: endocannabinoid system

EGF: epidermal growth factor

EMA: European Medicines Agency

EMT: endocannabinoid membrane transporter

EMT: epithelial-to-mesenchymal transition

ER: estrogen receptor

ETA: ethanolamine

FABP: fatty acid binding protein

FACS: fluorescence-activated cell sorting

FBS: fetal bovine serum

FDA: Food and Drug Administration

FMO: fluorescence minus one

FSC/SSC: forward/side scatter

GES: gene expression signature

GFP: green fluorescent protein

GO: Gene Ontology

GPCR: G protein-coupled receptor

H&E: hematoxylin and eosin

IHQ: immunohistochemistry

JAK: Janus kinase

KEGG: Kyoto Encyclopedia of Genes and Genomes

LOX-12, LOX-15: lipoxygenase 12 and 15

MAG: monoacylglycerol

MAPKs: mitogen-activated protein kinases

MaSC: mammary stem cell

MetAEA: methanandamide

MEC: mammary epithelial cell

MEM: minimum essential medium

MFI: mean fluorescence intensity

MMP: matrix metalloproteinase

MTT: 3-(4,5-Dimethylthiazol-2-yl)-2,5-diphenyltetrazolium bromide

NAE: N-acylethanolamine

NAPE-PLD: N-acylphosphatidylethanolamine-specific phospholipase D

NAT: N-acyltransferase

RPMI: Roswell Park Memorial Institute

RT: room temperature

SCR: scrambled

scRNA-seq: single-cell RNA sequencing

O/N: overnight

OEA: oleoylethanolamide

PEA: palmitoylethanolamide

PCNA: proliferating cell nuclear antigen

PR: progesterone receptor

PI3K: phosphoinositide 3-kinase

PI-MECs: parity-induced mammary epithelial cells

PMSF: phenylmethylsulfonyl fluoride

P: progesterone

PRL: prolactin

PRLR: prolactin receptor

ROS: reactive oxygen species

SDF-1: stromal cell-derived factor 1

SEA: stearoylethanolamide

SNPs: single nucleotide polymorphisms

STAT: signal transducer and activator of transcription

STR: short tandem repeats

TEBs: terminal end buds

THC: Δ^9-tetrahydrocannabinol

TIMP: tissue inhibitor of metalloproteinase

TMA: tissue microarray

TNBC: triple-negative breast cancer

VEGF: vascular endothelial growth factor

INTRODUCTION

THE MAMMARY GLAND

The mammary gland is a unique glandular organ that distinguishes mammals from all other animals and whose function is to produce and secrete milk to nourish offspring. It is also the only glandular organ that reaches full development after birth, and as such, it provides a unique model for biologists to study development and organ specificity.

ANATOMICAL STRUCTURE OF THE ADULT MAMMARY GLAND

The functional mammary gland is composed of an epithelial system of ducts and lobuloalveolar secretory units embedded in a mesenchyme-derived fat pad (**FIG. I1**). The ductal structure is composed of two main cellular lineages arranged in concentric layers: the luminal cells, that surround a central lumen, and the myoepithelial or basal cells, found between the former and the basement membrane (Visvader & Stingl, 2014) (**FIG. I1**). They can be distinguished by different protein expression profiles. The luminal layer is characterized by expression of epithelial cell adhesion molecules, BCL2, GATA3 and low molecular weight cytokeratins (CK7, 8/18 and 19). Regarding the expression of hormone receptors (HR), luminal cells include hormone receptor (HR)+ sensing cells and HR- alveolar cells, which are those in charge of milk secretion during lactation. On the other hand, myoepithelial cells do no express HRs and are characterized by the expression of high molecular weight cytokeratins (CK5/6, 14 and 17), smooth muscle actin (SMA), calponin, p63, integrin β4, laminin γ2, P-cadherin, nerve growth factor receptor (NGFR), CD10, caveolin 1 or S-100 proteins (Badowska-Kozakiewicz *et al*., 2016).

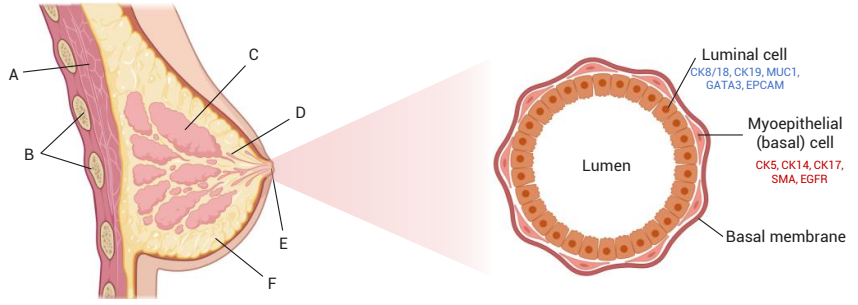

Figure I1. Anatomy of the human mammary gland. On the left, sagittal cut of the human mammary gland. A: chest muscle; B: ribs; C: lobules; D: duct system; E: nipple; F: fat. On the right, transversal cut of a mammary duct.

AN OVERVIEW OF MOUSE MAMMARY GLAND DEVELOPMENT

The development of the mammary gland consists of the following phases: embryonic, pubertal and during each round of pregnancy (**FIG. I2**).

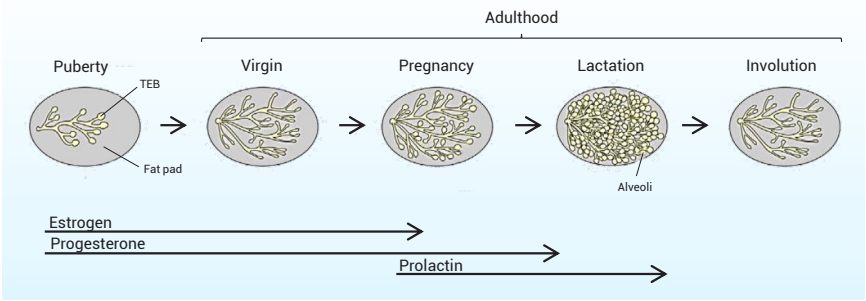

Figure I2. Stages of the mammary gland development. Adapted from Visvader & Lindeman, 2014.

In utero

In mice, the embryonic phase of the mammary gland development occurs between embryonic day (E) 10.5 and E18.5. The ventral epidermal ridges (also referred to as milk lines) derive from the ectoderm and form the base on which five placodes develop and subsequently invaginate to form the nipples. As mouse develops, this rudimentary structure starts invading the mammary fat pad, a process that culminates with the formation of a primitive ductal structure, which remains quiescent until puberty (Anderson *et al*., 2007; Inman *et al*., 2015).

Puberty

At the onset of puberty and driven by the influence of estrogen (E), epidermal growth factor (EGF) and insulin growth factor (IGF)-1, ductal elongation and branching begins. Highly proliferative structures named terminal end buds (TEBs) lead the way through the stroma in a radial pattern until they reach the margins of the fat pad, which appears to occur by 10 to 12 weeks of age. This ductal structure is maintained into adulthood (Anderson *et al*., 2007; Inman *et al*., 2015). In the pubertal and adult female, the mammary gland undergoes developmental modifications tightly associated with ovarian/uterine reproductive cyclical repetitions. During ovulation (also called estrus in mice), peak levels of E stimulate the high production of luteinizing hormone from the pituitary gland, causing the release of the ovum from the ovary whereupon the luteal phase begins. In preparation for a potential pregnancy, the corpus luteum keeps up progesterone (P) production for a few days thus triggering secondary and tertiary branching from the ductal tree, which augments mammographic density. If fertilization does not occur, the corpus luteum is degraded and reduced levels of P mark the end of a cycle, which induces clearance

of mammary epithelial cells (MECs) through cell death and lobuloalveolar shedding (Slepicka *et al*., 2021).

Pregnancy

During each round of pregnancy, a unique hormonal milieu triggers extensive proliferation and specialization of MECs. P induces extensive side-branching and, in combination with prolactin (PRL), promotes the differentiation of alveolar progenitors into pre-secretory structures, thus initiating the so-called phase I of lactogenesis. At this stage, the luminal space encased by alveolar MECs is filled with a proteinaceous substance whose identity is not clear but may represent milk proteins, glycoproteins such as MUC1, lactoferrin, and possibly immunoglobulins (Anderson *et al*., 2007; Inman *et al*., 2015).

Lactation

During gestation, PRL is prevented from exerting its effect on milk secretion by elevated levels of P. Following parturition, the downregulation of P releases the break for the lactogenic switch (also named lactogenesis II) and PRL drives terminal differentiation of alveolar MECs and orchestrates milk production through the activation of the JAK/STAT signaling pathway (**BOX 1**). PRL levels decrease as lactation is established, but nursing stimulates its new release from the pituitary

BOX 1 | **STAT signaling in mammary gland development**

The signal transducer and activator of transcription (STAT) family of transcription factors comprises seven members that are activated by cytokine receptors and receptor-associated Janus kinases (JAK). STAT activation requires phosphorylation in tyrosine residues to form homo- and heterodimers that translocate to the nucleus, where they regulate the transcription of a number of genes. STAT proteins have been shown to be involved in normal mammary gland development and function. Specifically, STAT5 is required for the proliferation of alveolar progenitors and their differentiation into milk-producing cells in response to PRL. During pregnancy, PRL binds PRL receptor (PRLR), which dimerizes and activates JAK2, that in turn phosphorylates STAT5. Activated STAT5 dimerizes and translocates to the nucleus, where it binds to and induces transcription from promoters containing g-interferon activation sites (GAS) (TTCNNNGAA) such as *CSN2* (the gene encoding β-Casein), *WAP* (the gene encoding whey acidic protein), and other milk-protein genes. Phosphorylation of STAT5 reaches the highest levels in late gestation (lactogenesis I) and early lactation (lactogenesis II) and decreases at day 2 of involution. Accordingly, STAT5 knockout mice have impaired lobuloalveolar development during pregnancy and fail to lactate. On the other hand, STAT3 is essential for the early phase of mammary gland involution as it initiates cell death and tissue remodeling. Consistent with this, knockout mice for STAT3 show reduced levels of apoptosis and delayed post-lactational regression (Caffarel *et al*., 2012).

and from the mammary gland itself. From this moment, the sucking stimulus is the main responsible for the maintenance of systemic and local levels of lactogenic hormones that will sustain continued milk production, as well as for the release of oxytocin that will cause the contraction of myoepithelial cells necessary to allow milk delivery. Examination of the histology of the mammary gland throughout lactation reveals prominent lobuloalveolar units with a luminal space distended with secretory material and few adipocytes. This change is thought to reflect delipidation of adipocytes rather than a decrease in their number (Anderson *et al*., 2007; Inman *et al*., 2015).

Involution

Upon weaning, the stimuli for milk production are lost and the mammary gland undergoes a process of post-lactational regression or involution that results in a structure that resembles the pre-pregnant state. Mammary gland involution proceeds through an initial reversible stage in which cessation of suckling and milk accumulation in the acinar lumen are sufficient to activate widespread (i.e., 80 %) apoptosis of the secretory alveolar cells. Approximately 48 h after weaning, involution progresses to a second irreversible stage as a response to the gradual reduction of circulating hormones. This second phase is characterized by glandular collapse and tissue remodeling of the breast, which requires the activation of matrix metalloproteinases (MMPs) and the inactivation of their inhibitors, the tissue inhibitors of metalloproteinases (TIMPs) (Schwertfeger *et al*., 2001). In this context, it is worth mentioning the existence of the parity-induced mammary epithelial cells (PI-MECs), a subpopulation of alveolar-like cells that originate during the first pregnancy but do not undergo apoptosis during involution, thus serving as alveolar precursors during subsequent pregnancies (Anstine *et al*., 2019).

THE MAMMARY EPITHELIAL CELL HIERARCHY

Multipotency in the adult mammary gland

The ability of the mammary gland to undergo successive cycles of growth and involution implicates the existence of a population of mammary stem cells (MaSCs) capable of generating the entire epithelial architecture. The remarkable regenerative capacity of mammary epithelium was first demonstrated in the late 1950s thanks to the development of the transplantation assay (DeOme *et al*., 1959). Small numbers of epithelial cells were able to regenerate the entire ductal epithelial tree when transplanted into de-epithelialized (cleared) mammary fat pads, and cell populations from these outgrowths were able to reconstitute the gland again in subsequent cleared fat pads, showing strong stem cell-like behavior. Following the discovery of MaSCs, the search for molecular markers specific to the stem cell population became a major focus within the field. Many of these studies used

flow cytometry or fluorescence-activated cell sorting (FACS) to isolate different epithelial cell populations which were then tested for reconstitution efficiency by injecting them into cleared mammary fat pads at limiting dilutions (Stingl *et al*., 2006; Shackleton *et al*., 2006; Zeng and Nusse, 2010; Spike *et al*., 2012; Plaks *et al*., 2013). Most of the cells showing regenerative capacity had a $CD49f^{hi}$ $CD29^{hi}$ $CD24^{+/mod}$ $Sca1^{low}$ phenotype. Notably, this immunophenotype characterizes the wider basal population, which comprises MaSCs, mature myoepithelial cells and presumptive basal progenitor intermediates.

Although the transplantation assay has been historically considered the gold standard assay for the detection of MaSCs, it has been highly questioned given that it may not accurately represent cellular differentiation as it would intrinsically occur *in vivo*. The drastic micro-environmental changes transplantation entails have been suggested to bestow multipotent potential onto cells that would otherwise be restricted to specific differentiation. Overcoming this weakness, lineage tracing technology allows for the tracking of stem cells and their progeny within the context of the normal tissue environment. Various studies using lineage tracing analyses have led to controversy surrounding the existence of a multipotent entity in the adult mammary gland. In the first inducible cell fate mapping study in the mammary gland, Van Keymeulen and colleagues (Van Keymeulen *et al*., 2011) reported that only unipotent cells remain after birth and that they are the only responsible for maintenance of adult lineages. Subsequent studies, however, supported the existence of multi- and bi-potent mammary epithelial cell populations within the mammary gland that could give rise to all mature lineages (Rios *et al*., 2014; Wang *et al*., 2015).

The conflicting results generated from transplantation studies with those from lineage tracing have been a source of controversy in the field. The primary question remains: does a multipotent stem cell exist after birth?

A new model for the differentiation hierarchy of MECs

Although transplantation and lineage tracing have been essential to our understanding of mammary gland biology, they have led to a highly compartmentalized view of the mammary epithelial hierarchy in which fetal MaSCs give rise to a series of downstream intermediates which become increasingly lineage-restricted moving from multi- to bi- to uni-potent progenitor states, until terminally differentiating into mature epithelial populations (**FIG. I3A**). This historical model of the mammary epithelial cell differentiation hierarchy has been proven to be insufficient to fully characterize the complete spectrum of epithelial intermediate populations or their spatial and temporal relationships.

In the last two years, the remarkable advances in single-cell RNA sequencing (scRNA-seq) have allowed the uncovering of the transcriptional heterogeneity

within the mammary gland, resulting in a new, more flexible model of epithelial differentiation. Several independent laboratories have used scRNA-seq to identify epithelial subpopulations across embryonic and adult (both nulliparous and reproductive) stages (Bach *et al*., 2017; Giraddi *et al*., 2018; Sun *et al*., 2018; Nguyen *et al*., 2018). According to their results, until birth, the mammary epithelium consists of largely homogeneous populations with a hybrid (i.e., luminal and basal) gene expression profile. This dual expression signature will become increasingly more lineage restricted throughout puberty, yet the precise timing of the postnatal development where the major bifurcation between luminal and basal lineages takes place remains unclear. In the adult mammary gland, luminal and basal phenotypes further segregate into a continuum of transcriptionally distinct subpopulations that cannot be characterized by the expression of a single gene and likely represent cells spanning various transitional stages of differentiation (**FIG. I3B**). That being said, and although specific populations with stem potential may exist, the sc-RNA sequencing studies reported to date have failed to detect a transcriptionally distinct multipotent stem cell population within the adult murine gland.

The new model of the mammalian epithelial hierarchy has led to a major conceptual shift in which the rigid boundaries separating discrete population states have been deconstructed and the fluid, gradual progression of epithelial differentiation has been acknowledged. This new model has important implications for mammary development, carcinogenesis, and metastasis, and provides novel insights into the underlying cellular states that may promote malignant phenotypes.

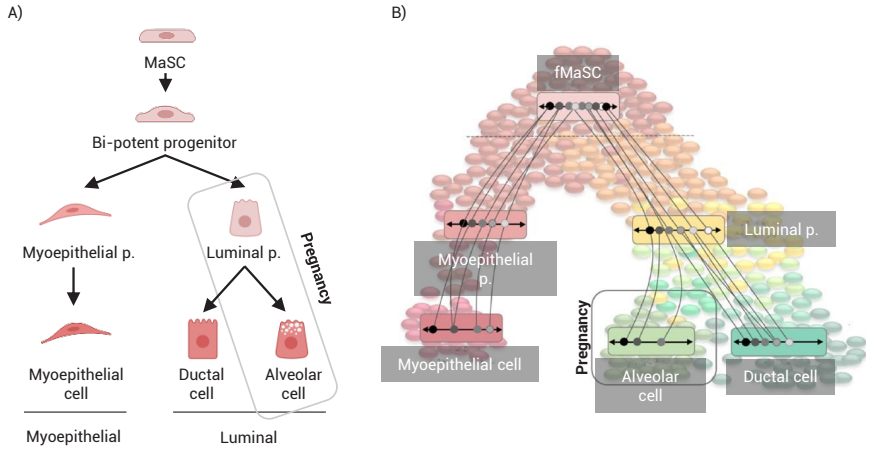

Figure I3. Different models of the MEC differentiation hierarchy. A) Historical model of the MEC differentiation hierarchy. MaSCs can self-renew and give rise to multi and bi-potent progenitors that maintain myoepithelial and luminal lineages in the postnatal gland. B) New model of MEC differentiation hierarchy. Each MEC undergoes differentiation, passing through the same phenotypic compartments but taking a slightly different transcriptional path each time, resulting in a continuous array of differentiation states. Grayscale circles (ranging from white to black) on the horizontal lines represent the various epigenetic and transcriptomic states found within each phenotypic compartment. Adapted from Anstine *et al*., 2019.

BREAST CANCER

As explained in the previous sections, the mammary gland is a highly dynamic organ that suffers profound changes throughout the female's life. From the onset of puberty, the epithelial component and the surrounding tissue architecture go through cyclic phases of remodeling where cells proliferate, differentiate or apoptose in response to different hormonal stimuli. The same molecular mechanisms that control mammary gland development can result in aberrant growth and cancer formation when they are disrupted. As a result, it is estimated that 1 out of every 8 women will develop breast cancer (BC) during her lifetime (Harbeck *et al*., 2019).

EPIDEMIOLOGY

BC is the most frequent malignancy and the leading cause of cancer death in women. In 2020, an estimated 2.3 million women were newly diagnosed with BC and approximately 3 % of them died out of advanced disease (WHO, 2020). Incidence varies worldwide, being higher in developed regions, which is reflective of both a higher exposure to risk factors (unhealthy lifestyle in terms of diet and exercise, longer exposure to sexual hormones due to non or late parity, hormone-replacement therapy for menopause, etc.) and a higher technical capacity to detect the disease by imaging techniques. Despite its lower incidence, mortality is usually higher in developing countries due to late detection and limited access to treatment (Harbeck *et al*., 2019).

Approximately 10 % of BCs are inherited and associated with a family history. Several syndromes related to germline mutations of genes involved in DNA repair have been shown to be linked to the inherited BC risk. Mutations of tumor suppressors BRCA1 and BRCA2 are associated with an average cumulative risk of developing BC by the age of 80 years. Others include mutations of ATM, PTEN, PALB2 and TP53 (Harbeck *et al*., 2019). The vast majority of BCs, however, are sporadic and do not have a hereditary component.

CLASSIFICATION

BC classification has gradually shifted over the years from being purely descriptive to be more integrative, considering both clinical features and molecular biomarkers.

Histopathologic analysis reveals great heterogeneity both at the cellular level and in the architectural structure. Histologically, BC broadly categorizes into *in situ* carcinoma and invasive (or infiltrating) carcinoma (**FIG. I4**). According to the latest edition of the World Health Organization classification (WHO, 2019), the most frequent histologic type is invasive carcinoma of no special type (NST), formerly

invasive ductal carcinoma (70-75 %). The remaining breast carcinomas are classified into special types based on the dominating growth pattern. Of the special types, lobular carcinomas are most common (10 % to 15 % of total BC), whereas some of the others (e.g., apocrine, cribriform, mucinous, etc.) are extremely rare (< 1 %).

Together with the histotype, the assessment of the histological grade is a routine analysis that reflects the potential aggressiveness of the disease and provides valuable prognostic information. Tumor grade (also referred to as differentiation grade) is determined according to the Bloom and Richardson's system (Bloom & Richardson, 1957), modified by Elston and Ellis in 1991 (Elston & Ellis, 1991), and it classifies breast tumors into G1, G2 or G3 according to three criteria: proportion of tubule formation, mitotic rate and degree of nuclear pleomorphism. G1 (or well-differentiated) tumors display a tissue organization close to normal mammary gland (most tubules are well structured, mitotic rates are low and nuclear pleomorphisms are rare), and tend to spread slowly, while G3 (or poorly differentiated) tumors show major disorganized tissue structure (poor normal tubule formation, high mitotic counts and high nuclear pleomorphism), and an aggressive behavior.

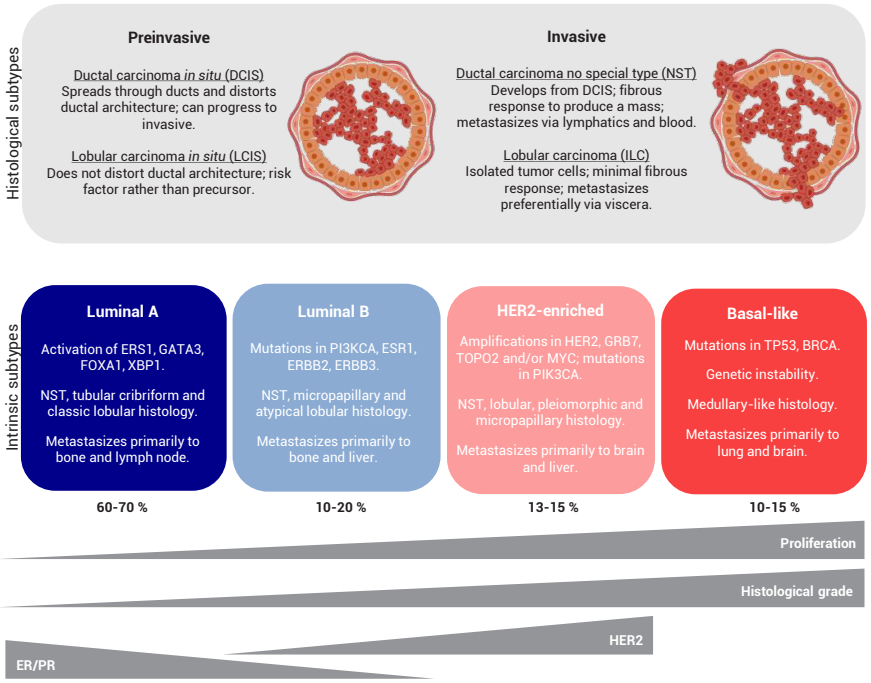

Figure I4. BC classification is based on histological and genomic criteria. Histological classification categorizes the heterogeneity found in BC based on architectural features and growth pattern. The histological subtypes described here are the most frequent. On the other hand, the intrinsic subtypes of Perou and Sørlie are based on a 50-gene expression signature (PAM50) and classify BC into transcriptionally similar clusters. Adapted from Harbeck *et al.*, 2019.

Histopathological classification is insufficient in terms of prognosis and predictive implications, and its clinical utility is quite modest. With the advent of the -omics, extensive molecular profiling has been performed on thousands of BC samples over the last few decades, allowing to improve the existing classification scheme and to predict response to therapy. Studies conducted by Perou and Sørlie and coworkers (Perou *et al*., 2000; Sørlie *et al*., 2001) demonstrated that breast tumors could be stratified into at least four main molecular subtypes (the so-called intrinsic subtypes) with diverse tumor characteristics and clinical outcomes: luminal A and B, HER2-enriched and basal-like (**FIG. I4**). The existence of a fifth subtype defined by a normal breast tissue profiling (and thereby termed "normal-like") was suggested in the original classification, but due to its poor characterization and limited clinical relevance will not be taken into consideration here.

- Luminal A and B

Luminal tumors (70-80 % of BCs) are defined by the expression of estrogen receptor (ER) and a gene signature typical of the luminal epithelium of the mammary gland. While luminal A presents low-risk features such as high expression of progesterone receptor (PR), low grade, low proliferation and a low-risk gene expression signature (GES), luminal B usually displays no PR expression, higher grade, higher proliferation and higher-risk GES. Some luminal B tumors can also be HER2+ (Harbeck *et al*., 2019).

Therapeutic management of BC types luminal A or B encompasses surgical and/or pharmacological approaches aimed to block estrogenic signaling, which supports proliferation and survival of tumor cells, mainly through ER type α. Targeted therapies include the removal of the ovaries as primary source of endogenous estrogen and/or the use of selective estrogen receptor modulators (like the partial agonist tamoxifen or the inhibitor of dimerization fulvestrant), or inhibitors of aromatase, the main enzyme responsible for estrogen synthesis (Nilsson *et al*., 2011). Luminal B tumors which overexpress HER2 are also candidates for anti-HER2 therapy (see below).

- HER2-enriched

HER2-enriched tumors (13-15 % of BCs) are characterized by the overexpression of the human epidermal growth factor receptor 2 (HER2). HER2 belongs to the epidermal growth factor receptor (EGFR) family, which consists of four members (ErbB1/HER1/EGFR, ErbB2/HER2, ErbB3/HER3 and ErbB4/HER4). They all have intrinsic tyrosine kinase activity and dimerize upon ligand binding to subsequently activate numerous oncogenic processes, including proliferation and survival (Zhang *et al*., 2007). The HER2-enriched subtype frequently displays G2 or G3 features, low or absent expression of ER and PR, and medium to high proliferation rates (Harbeck *et al*., 2019).

The outcome of HER2-enriched BC patients has considerably improved since the incorporation to the clinic of Herceptin® (the commercial name for trastuzumab, a humanized monoclonal antibody targeting the extracellular domain of HER2) and Tykerb® (the commercial name for lapatinib, a small molecule inhibitor of EGFR and HER2 tyrosine kinase activity) (Higgins & Baselga, 2011).

- Basal-like

Basal-like tumors comprise a particularly aggressive molecular subtype defined by a robust cluster of genes characteristic of the basal/myoepithelial cells in the mammary gland. Most basal-like tumors lack expression of ER, PR and HER2, therefore they are also referred to as triple-negative (TNBC) (Harbeck *et al*., 2019).

Despite its low prevalence (10-15 %), this highly proliferative group of tumors is a major clinical challenge as there is no standard targeted therapy for them and they relapse rapidly. Efforts are being made to improve chemotherapy responses and they include, for example, the use of angiogenesis inhibitors such as Avastin® (bevacizumab) combined with poly (adenosine diphosphate–ribose) polymerase (PARP) inhibitors (Higgins & Baselga, 2011).

Molecular classification of BC is a field in constant growth and new tumor types are being acknowledged that cannot be included in the aforementioned categories. For example, the later defined claudin-low group is triple-negative but does not express a basal-like gene signature. Instead, it is characterized by a high enrichment of epithelial to mesenchymal transition markers and cancer stem cell-like features (Herschkowitz *et al*., 2007).

All in all, therapeutic decision for BC patients is currently guided by histology (tumor type and grade) and immunodetection of clinically relevant biomarkers (ER, PR, HER2, Ki67), complemented in some cases with genetic signature tests (i.e., PAM 50, MammaPrint™, MapQuant Dx™, Oncotype DX™) (Harbeck *et al*., 2019).

The origin of BC heterogeneity

As it has been mentioned, BC molecular subtypes differ greatly in terms of proliferation rate, invasiveness, metastatic potential, and response to anticancer therapy, resulting in diverse patient outcomes. Thus, dissecting the molecular events that determine whether malignant transformation of the mammary gland results in one tumor type or another has become a major focus of contemporary BC research.

Molecular profiling studies have revealed that the gene expression patterns of some of the intrinsic cancer subtypes align with those of normal mammary epithelial cell

lineages. The gene expression profile of claudin-low tumors most closely resembles that of MaSCs, whereas basal-like tumors closely resemble luminal progenitors, and luminal A and B tumors resemble the mature luminal cell (Lim *et al.*, 2009; Prat *et al.*, 2010) (**FIG. I5**). This has led to the idea that phenotypically similar tumors arise from cells residing in the exact same cellular state and maintain their differentiation status during malignant transformation, regardless of the nature of the oncogenic mutations they acquire along the way. This theory, which states that tumor phenotype of BC is a simple legacy from the phenotype of the precursor cell, is termed the cell-of-origin theory.

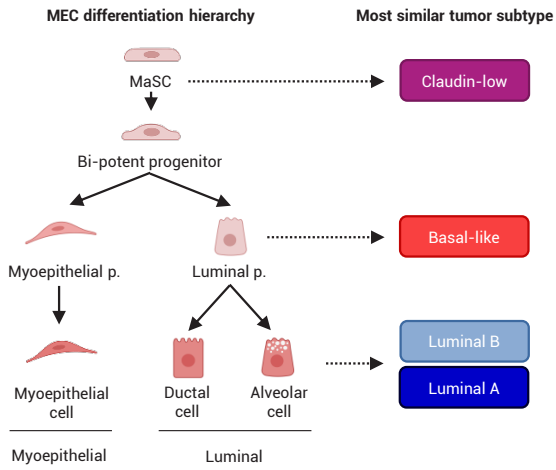

Figure I5. Schematic model of the human breast epithelial hierarchy and possible relationships with BC subtypes. Gene expression profiling of these subpopulations revealed similarities to specific subtypes of BC, depicted on the right-hand side. Adapted from Lim *et al.*, 2009.

However, this model is inconsistent with the fact that those populations in the healthy mammary gland most susceptible to accumulate mutations (i.e., stem/progenitor subset, due to their longevity and ability to self-renew) display a genetic signature that does not correlate with that of the most frequent intrinsic subtype (i.e., luminal A). Likewise, not all cancer subtypes have been associated with a cell of origin (i.e., HER2-enriched). The possibility that all tumors within the same intrinsic subtype come from the same cell of origin is thus slim and does not fully explain BC diversity. Instead, it can now be presumed that cells residing anywhere along the continuous differentiation trajectory may acquire tumor-initiating mutations, and that many of those mutated genes may act as determinants of tumor differentiation in addition to exerting oncogenic effects. This would explain the inability to identify a single lineage that contributes to HER2-enriched tumors because amplification of HER2 may occur in an array of cell states rather than a single cell. Therefore, it is fairly accepted today that tumor phenotype is influenced by both the cell of origin and the particular collection of oncogenic mutations they

acquire. Recently, it has been suggested that while MaSCs likely initiate claudin-low BC, luminal progenitors serve as the origin of both luminal and basal-like BC, and that their mutational profile will determine if the developing tumor adopts one tumor phenotype or the other (Skibinski & Kuperwasser, 2015).

METASTATIC DISEASE

Despite the advances in BC treatment and patient outcome over the last two decades, women continue to relapse and die of advanced disease. In Western countries, the proportion of patients who experience metastatic recurrence is 20–30%. NST invasive carcinoma tends to metastasize to the lungs, distant lymph nodes and central nervous system (CNS) via the lymphatic system and blood, whereas invasive lobular carcinoma (ILC) has three times more metastases in the viscera (i.e., peritoneum, gastrointestinal tract, and ovaries) (Chen *et al*., 2018). The intrinsic subtype also influences the timing and the specific organ BC cells metastasize to. Luminal A and B subtypes tend to relapse late (after 5 years of first presentation) and have a tropism for bone and lymph nodes. Since the era of anti-HER2 targeted therapy, HER2-positive BCs show better prognosis, but they escape therapy through brain metastasis. TNBCs are prone to early recurrences (within 2–3 years of first presentation) and tend to form lung and brain metastases (**FIG. I4**) (Harbeck *et al*., 2019).

The molecular basis of organotropic metastasis

Understanding the molecular mechanisms of organotropic metastasis is essential for improving biomarker-based prediction and prognosis, and for the consequent development of proper therapeutic strategies. Stephen Paget's "seed and soil" theory stated that metastases require both the dissemination of cancer cells (the "seed") and a special affinity for the growth-enhancing milieu of specific organs (the "soil") (Paget, 1889). In a complementary view, James Ewing proposed 40 years later that organ specificity is purely determined by mechanical forces and circulatory patterns between the primary tumor and the secondary site (the "mechanical theory", Ewing *et al*., 1928). Both Paget's and Ewing's theories are probably correct: Ewing focused on the migration step (the act of travelling) and Paget focused on immigration (the process of arriving). However, Ewing's theory falls quite short in explaining different organotropic preferences by tumor cells from the same primary site. Much effort has been done to identify tissue-specific gene signatures that predict metastatic organotropism, revealing that the transcriptome profiles of circulating tumor cells (CTCs) that end up landing in bone (Kang *et al*., 2003), lung (Minn *et al*., 2005) and brain (Bos *et al*., 2009) have very little in common. Collectively, these studies reveal that most of the predictive markers (which include growth and survival factors, chemokines, cell adhesion receptors and extracellular

proteases) also work as functional mediators of organ-specific metastasis, providing advantages both in the primary tumor and in the host organ microenvironment.

Involvement of chemokine receptors in BC metastasis

Tumor cell migration and metastasis share many similarities with leukocyte trafficking, which is critically regulated by chemokines and their receptors. Chemokines are a superfamily of 8-10 kDa cytokine-like proteins with the ability to bind G protein-coupled receptors and induce actin polymerization in leukocytes, a process that is a prerequisite for cell motility and migration (Zlotnik *et al*., 2000). Müller and colleagues demonstrated for the first time that tumor cells express their own set of functionally active chemokine receptors, and that they play a significant role in organotropic metastases (Müller *et al*., 2001). Out of all known chemokine receptors, C-X-C chemokine receptor type 4 (CXCR4) was found to be highly expressed in BC compared to normal breast tissue. Moreover, CXCR4 expressing BC cells showed to be attracted to tissues with high expression of stromal cell-derived factor 1 (SDF1; the only known ligand for CXCR4, also known as CXCL12), which coincidentally represent the main sites for BC metastasis: bones, lymph nodes, lungs and liver. Several studies have since validated the role of the CXCR4-SDF1 axis in regulating BC metastasis and suggested its involvement in other hallmarks of cancer such as proliferation (Smith *et al*., 2004), angiogenesis (Bachelder *et al*., 2002), stemness (Abblet *et al*., 2014) and modulation of the tumor microenvironment (Guo *et al*., 2016).

THE ENDOCANNABINOID SYSTEM

In order to understand the molecular bases of BC generation and progression, it is essential to know the molecular mechanisms that govern mammary gland development and homeostasis. The preclinical information obtained on the mechanisms that control the physiopathology of the mammary gland will make it possible to propose new therapeutic targets for the treatment of BC, especially in advanced disease, which continues to be an unresolved clinical challenge, as well as new screening tools that allow the early identification of patients at a highest risk of suffering it. Previous studies have shown that the endocannabinoid system (ECS) is involved in the control of cell fate (understood in terms of the "decision" between proliferation, differentiation, death, etc.) both in tumor cells and non-transformed cells. For this reason, we decided to focus our work on the study of this system in the physiopathology of the mammary gland.

The ECS is a cell signaling system that plays multiple roles in the regulation of several aspects of cell physiology, and it was discovered in an attempt to elucidate the molecular basis of the body's response to cannabis (**BOX 2**). This system is composed of a plethora of biomolecules that revolve around three main elements:

(i) the cannabinoid receptors, (ii) their endogenous ligands (the endocannabinoids) and (iii) the enzymes responsible for the synthesis, transport, degradation and bioconversion of eCBs (**FIG. I6**) (Lu & Mackie, 2016).

BOX 2 | **Cannabinoid research: an historical perspective**

Research on the chemistry of cannabis began in the late 19th century, following a major trend at that time focused on the quest for active natural products. The cannabis plant (*Cannabis sativa* L.) produces a unique mixture of chemical constituents, the most studied being the group of terpenophenolic compounds known as phytocannabinoids or simply cannabinoids. Out of the >150 cannabinoids produced by *C. sativa*, Δ^9-tetrahidrocannabinol (THC) is the most relevant owing to its high potency and abundance in plant preparations. In 1964, THC was structurally characterized and identified as responsible for the psychotropic effects of cannabis (Gaoni & Mechoulam, 1964). The second breakthrough in cannabinoid research provided answer to the conceptual question of why our brain reacts to cannabis: in 1988, Dr. Allyn Howlett's group obtained the first unequivocal evidence for the presence of a specific GPCR in the CNS underlying the behavioral effects of cannabinoids (Devane *et al*., 1988), and its cloning was reported soon later (Matsuda *et al*., 1990). This receptor is now known as CB_1 receptor (CB_1R) and seems to be the only responsible for the psychotropic effects of THC. A second cannabinoid-selective receptor, CB_2R, was identified shortly thereafter by sequence homology and presumed to be mainly present in the periphery (Munro *et al*., 1993). The observation that quantitative distribution of CB_1R was remarkably similar across species suggested a conserved physiological function and thus initiated an immediate quest for its endogenous ligands. As THC is a lipophilic molecule, it was assumed that any endogenous cannabinoid would probably be a lipid. Indeed, the use of methods for the separation of lipids made possible the identification by Dr. Mechoulam's group of the first endocannabinoid, N-arachidonoylethanolamine, named anandamide, based on the Sanskrit word "ananda" meaning "inner bliss" (Devane *et al*., 1992). Because its pharmacological activity did not fully recapitulate the behavioral effects of THC (Smith *et al*., 1994), the existence of a second endocannabinoid was postulated, and soon identified as 2-arachidonoylglycerol (2-AG) (Mechoulam *et al*., 1995; Sugiura *et al*., 1995). The discovery of the cannabinoid receptors and their natural ligands laid the ground for the study of the ECS, which currently constitutes a very active field in biomedicine.

More than 20 years of preclinical research have implicated the ECS in a variety of physiological processes, both in the nervous system and in various peripheral organs, and its de-regulation has been observed in several diseases. These studies have suggested that modulating the ECS activity may have therapeutic potential in many pathological conditions affecting humans, including chronic pain, chemotherapy-induced nausea and vomiting, epilepsy, motor symptoms associated to neurodegeneration, gastrointestinal diseases, obesity, and diabetes, among others (Pacher *et al*., 2006).

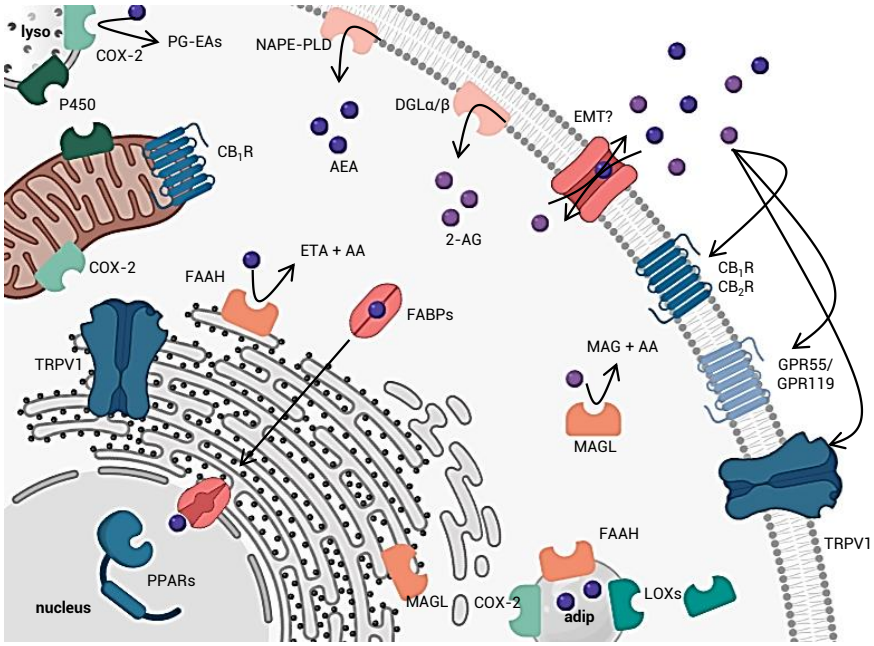

Figure I6. Overview and subcellular localization of the main elements of the ECS. Endocannabinoids (eCBs) are produced and degraded within both the plasma and organelle membranes, and therefore most of the metabolic machinery is membrane-associated. eCBs [anandamide (AEA) and 2-arachidonoylglycerol (2-AG)] are depicted in purple, cannabinoid receptors (CB_1R and CB_2R) and related receptors (GPR55, GPR119, TRPV1 and PPARs) in blue, biosynthetic enzymes [N-acylphosphatidylethanolamine-specific phospholipase D (NAPE-PLD) and diacylglycerol lipase α/β (DAGL α/β)] in pink, hydrolytic enzymes (fatty acid amide hydrolase (FAAH) and monoacylglycerol lipase (MAGL) in orange, oxidative enzymes [cyclooxygenase-2 (COX-2), lipoxygenases-12 and 15 (LOX-12, LOX-15) and cytochrome P450 oxygenases] in green and eCB transporters (fatty acid binding proteins (FABPs) and the predicted eCB membrane transporter (EMT)] in red. lyso: lysosome. adip: adiposome.

MAIN COMPONENTS

(i) Cannabinoid receptors

The discovery of the main psychoactive component of *Cannabis sativa*, THC, provided the foundation for cannabis research (**BOX 2**) and the following discovery of the cannabinoid receptors (CBRs): cannabinoid receptor type 1 (CB_1R) and 2 (CB_2R). CB_1R and CB_2R are G protein-coupled receptors (GPCRs), and they primarily mediate the actions of plant-derived, endogenous and synthetic cannabinoids in the body. Surprisingly, they share little sequence homology: only 44 % at the protein level or 68 % in the transmembrane domain, which is thought to contain the binding sites for cannabinoids (Munro *et al.*, 1993). They also differ in tissue distribution. CB_1R is the most abundant GPCR in the mammalian brain and was initially considered to be a neuronal receptor, yet more recent studies identify CB_1R receptors in virtually all peripheral tissues and cell types, where they elicit important regulatory functions

(Kunos *et al*., 2009). CB_2R receptors, on the other hand, are highly expressed in the spleen and regarded as the predominant cannabinoid receptor of the immune system, although functionally relevant expression has been found in specific regions of the brain and in the endothelium, myocardium, vascular smooth muscle, gut, pancreas and reproductive organs (Pacher & Mechoulam, 2011).

CB_1R and CB_2R receptors couple primarily to heterotrimeric G proteins of the $G_{i/o}$ classes, and their signaling is considerably complex. It is now well stablished that stimulation of CBRs may result into G protein-dependent inhibition of adenylyl cyclase (AC), modulation of ion channel functions or activation of members of multifunctional mitogen-activated protein kinases (MAPKs) and PI3K pathways, in addition to other G-protein independent actions such as the synthesis of the lipid second messenger ceramide (Pacher *et al*., 2006). Nonetheless, accumulating evidence suggest that CBR signaling is highly pleiotropic and that CB_1R and CB_2R each can modulate multiple pathways and give rise to markedly different cellular responses that can be ligand-, dose- and/or tissue-specific (Ibsen *et al*., 2017). Importantly, CBR signaling repertoire is further enriched by their ability to crosstalk with a large variety of other receptors and even to function in homo- and heterodimers with some of them, both GPCRs (e.g., CB_2R-CXCR4 heteromers [Coke *et al*., 2016]) and non-GPCRs (e.g., CB_2R-HER2 heteromers [Pérez-Gómez *et al*., 2015]).

(ii) Endocannabinoids

The endocannabinoids (eCBs) are endogenous lipophilic substances that engage cannabinoid receptors and partially recapitulate the pharmacological effects of THC. The first discovered (**BOX 2**) and best-characterized eCBs are the arachidonic acid derivatives arachidonoylethanolamide [anandamide (AEA)] and 2-arachidonoylglycerol (2-AG), belonging to the N-acylethanolamine (NAE) and monoacylglycerol (MAG) families, respectively (**FIG. I7**). While they were first identified as retrograde neurotransmitters to prevent excessive neuronal activity at the presynaptic site, today we know they are involved in a myriad of physiological processes like determination of cell fate, immune response, energy homeostasis and reproduction, among many others (Maccarrone *et al*., 2015).

The intrinsic pharmacology of the eCBs is different; 2-AG is a full agonist for both CB_1R and CB_2R, whereas AEA is a partial agonist and shows higher affinity for CB_1R than for CB_2R. Besides canonical cannabinoid receptors, several studies now support that the eCBs can bind to and activate other targets such as the orphan receptors GPR55 and GPR119, the transient receptor potential vanilloid (TRPV) ion channel family, and the peroxisome proliferator-activated receptors (PPAR) α and γ (De Petrocellis & Di Marzo, 2010).

Also, there are additional, structurally similar endogenous substances that do not

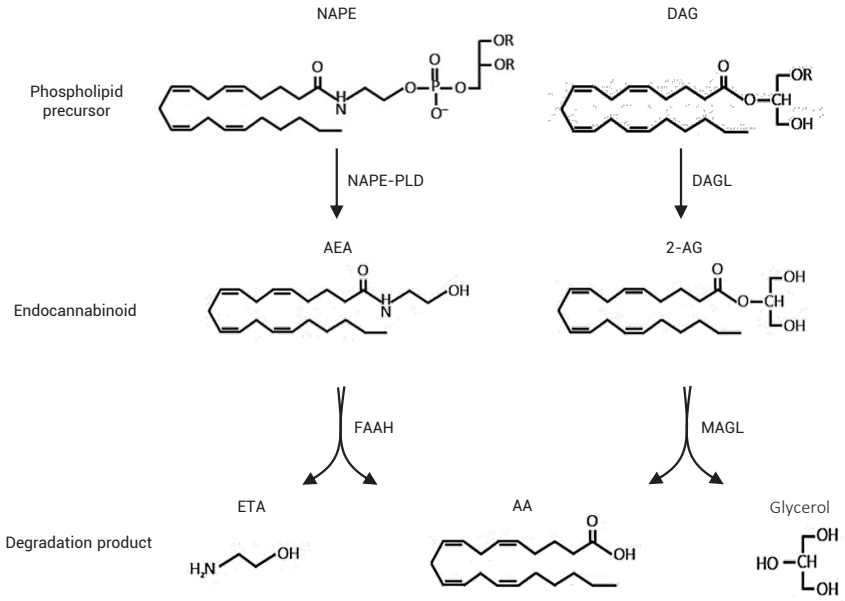

Figure I7. Key players in the biosynthesis and degradation of eCBs. Anandamide (AEA) and 2-AG both come from cell membrane phospholipid remodeling. Most AEA appears to be produced from N-arachidonoylphosphatidylethanolamine (NAPE), while 2-AG is produced from 2-arachidonoyl-containing phospholipids. Fatty acid amide hydrolase (FAAH) and monoacylglycerol lipase (MAGL) mainly orchestrate the breakdown of AEA and 2-AG, respectively. ETA: ethanolamine; AA: arachidonic acid.

bind to CBRs but contribute to the effect of eCBs and therefore are considered *bona fide* members of the ECS. These include NAEs other than AEA such as palmitoylethanolamide (PEA), stearoylethanolamide (SEA) and oleoylethanolamide (OEA), which are the amides of palmitic, stearic and oleic acids, respectively. These compounds lack affinity for CB_1R and CB_2R but are active at non-canonical CBRs such as PPARα and TRPV1. NAEs can also act as entourage compounds for eCBs, i.e., they may enhance their action by inhibiting their inactivation (Bisogno *et al.*, 1998; Di Marzo *et al.*, 2001). MAGs other than 2-AG, N-acylaminoacids, N-acyldopamines, -taurines and -serotonines are also considered eCB-like molecules (Iannotti & Piscitelli, 2019).

(iii) Endocannabinoid metabolic machinery

The last constituents of the ECS to be described were the components of the enzymatic machinery responsible for the biosynthesis, degradation, transport, and bioconversion of eCBs.

Both AEA and 2-AG are mostly synthesized on demand (when and where needed) from phospholipid precursors in the cell membrane, yet their metabolism occurs through different pathways. Biosynthetic routes for AEA and related NAEs are

multiple and apparently redundant. Among them, the sequential action of Ca^{2+}-dependent N-acyltransferase (NAT) and N-acylphosphatidylethanolamine-specific phospholipase D (NAPE-PLD) appears the most relevant. α/β-Hydrolase domain-containing protein 4 (ABDH4), glycerophosphodiesterase-1 (GDE1) and tyrosine-protein phosphatase non-receptor type 22 (PTPN22) have also been identified as AEA-synthesizing enzymes. On the contrary, only two diacylglycerol lipases (DAGLα and β) seem to be responsible for the production of 2-AG and other members of the MAG family (**FIG. I7**) from diacylglycerol (DAG), which is a hydrolysis product from the cleavage of phosphatidylinositol bisphosphate (PIP2) by phospholipase C (PLC). Once synthesized, eCBs are released via diffusion through the plasma membrane -possibly facilitated by a still unidentified eCB membrane transporter (EMT)-, where they act as autocrine and paracrine factors.

The classical dogma that eCBs are synthesized on demand has been recently revisited, suggesting that metabolic regulation is complemented by intracellular trafficking and storage in adiposomes. Fatty acid binding proteins (FABPs), albumin and heat shock protein 70 have been discussed as intracellular binding proteins that coordinate the delivery of eCBs to their catabolic enzymes or intracellular targets (Maccarrone *et al*., 2010).

The eCB-mediated effects are very weak and transient compared to those of THC, and that can be attributed to their fast recycling to the cytoplasm and subsequent catabolism. Signaling of AEA and other NAEs is primarily terminated by fatty acid amide hydrolase (FAAH), which hydrolizes these compounds to free fatty acids and ethanolamine (ETA). *N*-acylethanolamine-hydrolyzing acid amidase (NAAA), initially described as a PEA-hydrolyzing enzyme, participates to a lesser extent in AEA degradation. 2-AG is preferentially hydrolyzed to arachidonic acid (AA) and glycerol by monoacylglycerol lipase (MAGL), however FAAH and other serine hydrolases (ABHD6 and ABHD12) have been proposed as secondary degraders. These hydrolytic enzymes are the main responsible for regulating the biological availability of eCBs *in vivo* and therefore function as ultimate determinants of the eCB tone (Maccarrone *et al*., 2015).

Alternatively, due to the presence of an arachidonate moiety in both AEA and 2-AG molecules, they can function also as substrates for the same enzymes implicated in AA metabolism: cyclooxygenase-2 (COX-2), lipoxygenases-12 and 15 (LOX-12, LOX-15) and cytochrome P450 oxygenases, all of them known to be involved in eicosanoid production from AA. Interestingly, COX-2 may even prefer eCBs over AA as natural substrates *in vivo*, producing prostaglandin ethanolamides/prostamides (PG-EAs) from AEA and prostaglandin-glycerol esters (PG-Gs) from 2-AG. Recent evidence suggests that these oxygenated derivatives of eCBs may have a biological activity of their own, but their impact on health and disease remains to be clarified (Hermanson *et al*., 2013).

FATTY ACID AMIDE HYDROLASE (FAAH)

As it has been mentioned, the effects of the ECS are mostly determined by the levels of eCBs in the cell. Because eCB availability profoundly depends on the activity of eCB-hydrolytic enzymes, the modulation of the expression and function of these enzymes provides a valuable tool to investigate the role of the ECS on a given process. As an approach to investigate the role of the ECS in mammary physiopathology, we focused our interest on the study of FAAH, the enzyme in charge of the degradation of AEA.

FAAH is an integral membrane enzyme that was first cloned in 1996 as a 63 kDa protein with oleamide hydrolase activity (Cravatt *et al*., 1996). It belongs to a large and diverse class of enzymes, mostly bacterial or fungal in origin, referred to as the amidase signature (AS) family. AS enzymes possess an unusual serine-serine-lysine catalytic triad, which functions to promote amide bond hydrolysis in a manner generally analogous to the serine-histidine-aspartic acid triad more commonly observed in serine hydrolases. Unlike other AS enzymes, which are usually soluble proteins, FAAH is an integral membrane enzyme. It crystallizes as a homodimer where a transmembrane hydrophobic domain anchors each monomer to the lipid bilayer with a parallel orientation. This domain (α18 and α19, amino acids 410–438) resides adjacent to the active site, suggesting that the enzyme may recruit its substrates directly from the lipid bilayer. However, the crystal structure of FAAH (Bracey *et al*., 2002) reveals a number of channels that appear to grant the enzyme simultaneous access to both the membrane and cytoplasmic compartments of the cell (McKinney *et al*., 2005) (**FIG. I8**).

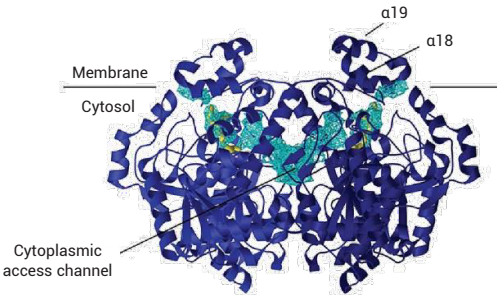

Figure I8. Crystal structure of the integral membrane protein FAAH modeled into a lipid bilayer. The enzyme is a homodimer assembled from 63-kD subunits. The inhibitor adduct MAP (yellow) is bound into the hydrophobic acyl chain-binding channel (light blue). The proposed membrane-binding domain of FAAH is also noted (α18–α19). Adapted from McKinney *et al*., 2005.

FAAH is the main enzyme in charge of physiologically terminating the action of the fatty acid amide (FAA) family of bioactive lipids, which can be divided into at least three chemical classes: *N*-acylethanolamines (NAEs) (e.g., AEA), fatty acid primary amides (e.g., oleamide) and *N*-acyl amino acids [e.g., *N*-acyl taurines (NATs)]. These FAAs play physiological roles as lipid neurotransmitters and autacoids and, except for AEA, lack affinity for CBRs, although some of their effects might be indirectly CBR-dependent. In examining the relative hydrolysis rates of

its substrates, it is evident that the rate of hydrolysis by FAAH increases with (i) greater degrees of unsaturation and (ii) unsaturation closer to the amide bond, which makes AEA a much better FAAH substrate than other FAAs with distinct acyl chain and head group preferences. This high affinity of FAAH for AEA underlies its rapid catabolism *in vivo*: in rodent brains, the half-life of AEA is less than five minutes (Boger *et al*., 2000).

Mice with a targeted disruption in the FAAH gene ($FAAH^{-/-}$ mice) are severely impaired in their ability to degrade FAAs and show hypersensitivity to the pharmacological effects of these lipids. FAAH loss also leads to highly elevated levels of endogenous FAAs in the nervous system and peripheral tissues that correlate with analgesic, anxiolytic, and anti-inflammatory phenotypes (Cravatt *et al*., 2001).

A second FAAH, termed FAAH-2, was later identified by Wei and colleagues (Wei *et al*., 2006). FAAH-2 shares 20 % sequence identity with the original FAAH and exhibits overlapping, but distinct tissue distribution [in breast tissue, FAAH is more abundant than FAAH-2 (Lonsdale *et al*., 2013)]. Both enzymes hydrolyze fatty acid primary amides at equivalent rates, whereas FAAH exhibits much greater activity with NAEs and NATs. Defining the rate of oleamide as one unit for both enzymes, the relative rates of hydrolysis of AEA for FAAH and FAAH-2 are 1.75 and 0.054, respectively. Remarkably, analysis of genome and gene expression databases revealed that the *FAAH-2* gene is present in primates, as well as in a variety of distantly related vertebrates, but not in murids (mice and rats). These results suggest differences in the enzymatic complexity of fatty acid amide catabolism across mammalian species (Wei *et al*., 2006).

THE ENDOCANNABINOID SYSTEM AND CANCER

ROLE OF THE ECS IN TUMOR GENERATION AND PROGRESSION

Alterations in the expression pattern of virtually every component of the ECS have been reported in several tumor types compared to their corresponding non-transformed tissue, and some of these alterations have been suggested to have prognostic significance. However, the conclusions drawn from these studies are correlative by nature rather than causal, and little experimental data on the role of the ECS in cancer is presently available. A descriptive overview of the reported alterations of the ECS in cancer and their functional meaning (when studied) will be done in the next sections, with a special focus on BC (**TABLE I1**).

ECS component	Type of contribution	Description	Reference
CB_1R, CB_2R	Expression in tumor vs. non-tumor tissue	↓ (CB_1R) and ↑ (CB_2R)	Caffarel *et al.*, 2006
	Association to clinical parameters	CB_1R decreases with tumor grade CB_2R increases with tumor grade	
CB_1R, CB_2R	Expression in tumor vs. non-tumor tissue	↓ (CB_1R) and ↑ (CB_2R)	Qamri *et al.*, 2009
CB_1R	Role in cancer pathogenesis	CB_1R promotes proliferation of BC cell lines *in vitro* and *in vivo*	Sarnataro *et al.*, 2006
CB_2R	Association to clinical parameters	Higher CB_2R in HER2+ subtype	Caffarel *et al.*, 2010
CB_2R	Association to clinical parameters	Higher CB_2R and poor patient prognosis in HER2+ patients	Pérez-Gómez *et al.*, 2015
	Role in cancer pathogenesis	CB_2R contributes to HER2 pro-oncogenic signaling in HER2+ patients	
GPR55	Association to clinical parameters	Higher GPR55 and higher tumor grade	Andradas *et al.*, 2011
	Role in cancer pathogenesis	GPR55 promotes BC cell proliferation	
GPR55	Association to clinical parameters	Higher GPR55 in TNBC / Higher GPR55 and poor patient prognosis	Andradas *et al.*, 2016
	Role in cancer pathogenesis	GPR55 promotes BC cell metastasis	
TRPV1	Role in cancer pathogenesis	TRPV1 controls BC cell proliferation	Vercellli *et al.*, 2014
TRPV2	Expression in tumor vs. non-tumor tissue	↑ (TNBC only)	Elbaz *et al.*, 2018
	Association to clinical parameters	Higher TRPV2 and higher relapse-free survival	
NAPE-PLD	Expression in tumor vs. non-tumor tissue	↑	Schmid *et al.*, 2002
MAGL	Association to clinical parameters	Higher MAGL and higher tumor grade	Gjerstorff *et al.*, 2006
MAGL	Expression in tumor vs. non-tumor tissue	↓	Sun *et al.*, 2013

Table I1. Summarized review of the available bibliography on the role of the ECS in BC. The studies are classified by the type of contribution they made to the field: 1) Description of the expression of an ECS component in tumor vs. non-tumor tissue; 2) Description of a relevant association between an ECS component and clinical parameters; 3) Description of a functional role of an ECS component in cancer pathogenesis.

(i) Cannabinoid receptors

Most of the research on the role of the ECS in cancer pathogenesis has focused on CB_1R and CB_2R, which generally appear upregulated in tumors when compared to their non-tumor counterpart. In the clinical setting, an association between high CBR expression and poor patient outcome has been demonstrated in different tumor entities. Additionally, some research has tried to elucidate whether CBR signaling has a role in cancer physiopathology and found that the inhibition of CBRs by pharmacological or genetic approaches most often reduces tumor growth and progression, while their overexpression can enhance predisposition to tumor development. Together, these observations support the fairly accepted view of CBRs as tumor promoters (Pisanti *et al*., 2013).

Regarding BC, Caffarel and colleagues provided the first direct evidence for the expression of CBRs in human breast tumors, where CB_1R and CB_2R mRNAs were initially found downregulated and upregulated, respectively, compared to noncancerous breast tissue. In addition, CB_1R decreased with tumor grade, while CB_2R increased (Caffarel *et al*., 2006).

Due to its moderate expression in BC, studies addressing the role of CB_1R in BC tumorigenesis have been scarce. Sarnataro and colleagues demonstrated that CB_1R is present in luminal and basal BC cell lines, and that the CB_1R selective antagonist rimonabant (SR141716) produces antiproliferative responses, suggesting a contribution of CB_1R to tumorigenesis (Sarnataro *et al*., 2006). More exhaustive work has been done regarding the role of CB_2R in breast tumors. Caffarel and colleagues first reported a significant association between CB_2R and HER2 expression in the HER2+ BC subtype (Caffarel *et al*., 2010), and shortly after, an oncogenic role was attributed to CB_2R as it was found to interact with HER2 forming heteromers and contributing to HER2 pro-oncogenic signaling (Pérez-Gómez *et al*., 2015). In a follow-up study, it was shown that these heteromers could be conveniently targeted for their disruption, leading to antitumor responses (Blasco-Benito *et al*., 2019).

The expression and function of other cannabinoid-related receptors have been also analyzed in BC. GPR55 is upregulated in higher grade vs. lower grade BC, is associated with TNBC, and promotes *in vitro* and *in vivo* cell proliferation (Andradas *et al*., 2011) and metastasis (Andradas *et al*., 2016). This receptor was later found to heterodimerize with CB_2R in BC cells (Moreno *et al*., 2014). Additionally, cell proliferation of the luminal cell line MCF7 was severely affected by treatment with TRPV1 agonists and antagonists (Vercelli *et al*., 2014), and TRPV2 expression was found to be higher in TNBC compared to normal tissue and to be associated with better prognosis and response to chemotherapy (Elbaz *et al*., 2018).

(ii) Endocannabinoids

Collectively, the currently available data regarding the levels of eCBs in cancer suggest that these fatty acid derivatives are upregulated in malignancies when compared to non-transformed tissue, reinforcing the idea that the ECS could play an oncogenic role (Pisanti *et al*., 2013). Regarding eCB-like substances, a recent study was able to find higher concentrations of circulating PEA and OEA in the plasma of cancer patients to be associated with higher number of metastases (Sailler *et al*., 2014).

Information concerning eCB levels in BC tissue specifically is limited. The only evidence to date comes from the first study reporting levels of NAEs and their precursors in human tumors, which demonstrated that the percentage of the AEA precursor, NAPE, was enhanced in BC compared to the adjacent non-tumor tissue (Schmid *et al*., 2002).

(iii) Endocannabinoid metabolic machinery

Except for a couple of studies analyzing the expression of NAPE-PLD, the majority of the evidence concerning the regulation of the endocannabinoid metabolic machinery in cancer tissue is mostly restricted to the main hydrolyzing enzymes, FAAH and MAGL. The expression of these enzymes has been found either upregulated or downregulated depending on the tumor type and their contribution to cancer progression is still unclear (Ramer *et al*., 2019).

Focusing on BC, the expression pattern of MAGL has been reported in two studies including human tumors, showing opposed expression patterns when compared to non-tumor tissue (Gjerstorff *et al*., 2006; Sun *et al*., 2013).

CLINICAL EXPLOITATION OF THE ECS IN CANCER

The ECS as a patient screening tool

While molecular classification of BC has been proven helpful to anticipate patient prognosis and guide therapeutic strategies, new screening tools are lacking that allow for a reliable identification of patients who are more likely to develop an aggressive form of the disease, show resistance to conventional therapies, or progress to metastasis. As it has been mentioned, the expression of several elements of the ECS has been found to be associated with clinical parameters such as overall survival (OS), relapse-free survival (RFS) and metastasis-free survival (MFS). Thus, the analysis of their expression in primary tumors may provide valuable prognostic information in order to support treatment decisions for oncologic patients.

The ECS a therapeutic target

It has been demonstrated that pharmacological activation of the ECS by exogenous cannabinoids produces therapeutic effects, and in fact, there are many countries in the world where cannabinoid-based drugs can be prescribed today for the symptomatic treatment of several pathologies (**BOX 3**). In the field of oncology, activation of the ECS has been extensively documented in the palliative setting, where cancer patients can benefit from the antiemetic properties of Marinol or Cesamet to prevent nausea and vomiting elicited by standard chemotherapy regimens, from Sativex for cancer-associated pain, or from other less controlled cannabis preparations for these symptoms and others associated with their diseases (lack of appetite, anxiety, sleep deprivation, etc.).

BOX 3 | **Cannabinoid-based drugs**

To date, four cannabinoid-based medicines have been approved by the American and European drug agencies (FDA and EMA, respectively). Marinol® (synthetic THC) and Cesamet® (synthetic THC analogue) are administered in oral capsules and were originally aimed at managing weight loss associated with wasting syndrome in patients with AIDS. Sativex® is an oromucosal spray with antispastic properties containing a 1:1 ratio of plant-derived THC and cannabidiol (CDB), a second, non-psychoactive cannabinoid that, when delivered together with THC, improves its tolerability. The fourth and most recently approved drug is Epidiolex®, made up entirely by highly purified CBD, which is indicated to attenuate convulsions of several forms of childhood epilepsy (Atance, 2017).

However, the potential of the ECS as a therapeutic target in oncology may not be restricted to the palliative effects. While the specific role of eCB signaling in tumorigenesis remains to be clarified, there is compelling evidence that pharmacological activation of the ECS leads to antitumor responses. Thus, a number of preclinical studies have found treatment with diverse CBR agonists (either plant-derived, endogenous and/or synthetic) to selectively exert antitumor effects in different models of cancer, ranging from cell cultures to xenografted and genetically engineered mice (Velasco *et al*., 2012).

The preclinical research accumulated during the last two decades pointing to the ECS as a therapeutic target for the management of cancer has led to the clinical study of cannabinoids as antitumoral agents. Thus, a phase Ib randomized, placebo-controlled clinical trial aimed at analyzing the safety and antitumor efficacy of Sativex has been recently completed. Patients with recurrent glioblastoma received temozolomide, the gold standard drug for this type of tumors, plus either placebo or Sativex. Patients in the Sativex group had a roughly double mean overall survival

than those in the placebo arm (22 months vs. 12 months, respectively), with 1-year survival rates of 83% vs. 44%, and 2-year survival rates of 50 % vs. 22 % (Twelves *et al.*, 2021).

Regarding BC, all the evidence on the antitumor effects of the activation of the ECS is restricted to the preclinical setting (**FIG. I9**). In fact, BC was one of the first cancer types where the activation of the ECS *in vitro* revealed antitumor actions. As early as two decades ago, De Petrocellis and colleagues showed that treatment with AEA produced a concentration-dependent inhibitory effect on the proliferation of MCF-7 and EFM-19 luminal cell lines through a CB_1R-like receptor-mediated

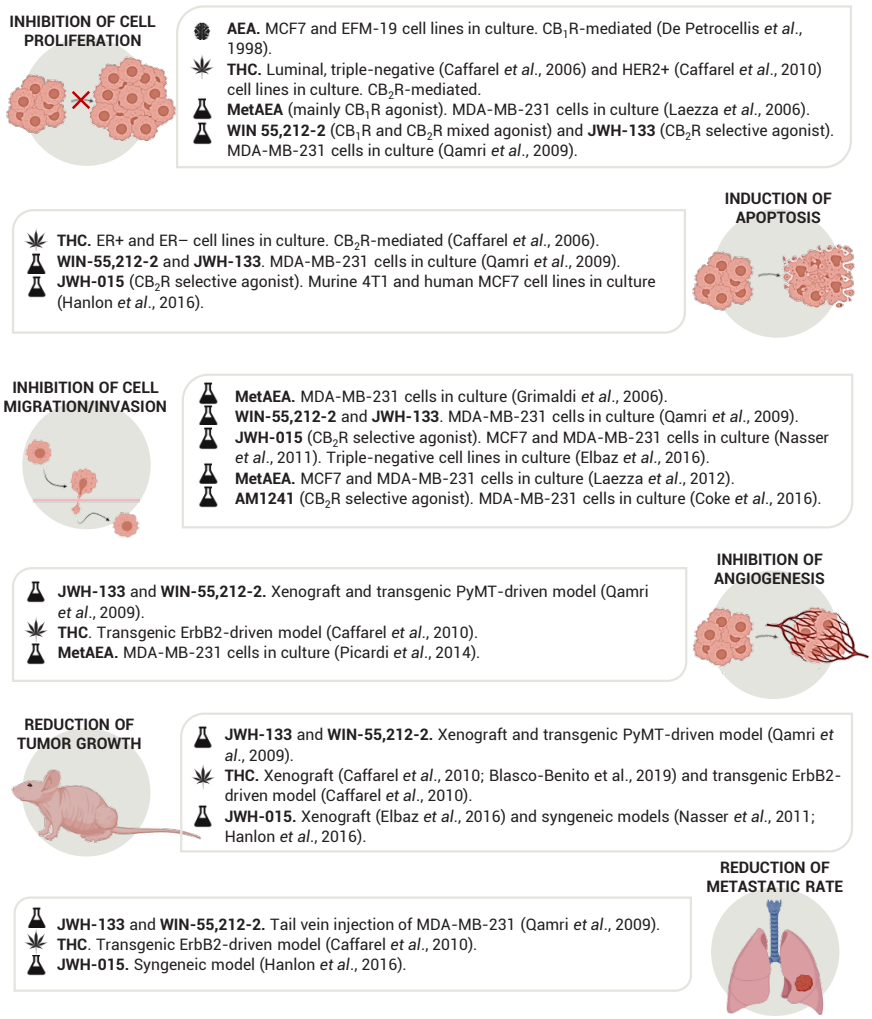

Figure I9. Summary of the main findings on the effect of the activation of the ECS on the hallmarks of cancer. The activation of the ECS was achieved by endogenous (brain icon), plant-derived (leaf icon) or synthetic cannabinoids (flask icon)

mechanism. AEA was shown to suppress PRLR synthesis and thus desensitize cells to the mitogenic effect of PRL, which is produced in high amounts by BC lines and has been proposed as major autacoid proliferative agent for these cells because of its capability of accelerating the G1/S transition of the cell mitotic cycle (De Petrocellis *et al*., 1998). A battery of plant-derived, endogenous, and synthetic cannabinoids has since proved to activate the ECS of BC cells and to inhibit (i) *in vitro* proliferation by blocking the progression through the cell cycle (Caffarel *et al*., 2006; Laezza *et al*., 2006; Qamri *et al*., 2009), as well as by inducing apoptosis (Caffarel *et al*., 2006; Hanlon *et al*., 2016); (ii) cell migration and invasion (Grimaldi *et al*., 2006; Qamri *et al*., 2009; Nasser *et al*., 2011; Coke *et al*., 2016; Elbaz *et al*., 2016); and (iii) the proangiogenic (Picardi *et al*., 2014) and the epithelial-to-mesenchymal transition (EMT)-like (Laezza *et al*., 2012) phenotype. Most of the aforementioned *in vitro* actions are reproduced in *in vivo* settings, where activation of the ECS with cannabinoids from varied sources have been shown to affect different aspects of breast tumorigenesis in xenograft-based (Qamri *et al*., 2009; Caffarel *et al*., 2010; Elbaz *et al*., 2016), syngeneic (Nasser *et al*., 2011; Hanlon *et al*., 2016) and genetic models of ErbB2-driven (Caffaret el al., 2010) and triple-negative (Qamri *et al*., 2009; Nasser *et al*., 2011) metastatic BC.

AIMS

Breast cancer (BC) is the most frequent malignancy worldwide and is curable in ~ 70–80 % of patients with early-stage, non-metastatic disease. However, advanced BC with distant organ metastases is considered incurable with currently available therapies. Therefore, there is a need for the development of new strategies for the treatment of advanced BC, especially those cases which progress to metastatic disease, as well as of new screening tools that allow for the identification of patients at a higher risk of suffering it. To that end, it is necessary to unravel the molecular mechanisms that govern mammary gland development and that are altered during tumoral processes in general and metastasis in particular. Because it is widely demonstrated that the endocannabinoid system (ECS) is implicated in the cellular processes that underlie the development of organs and tissues (proliferation, differentiation, and cell death), we decided to explore its role in the physiopathology of the mammary gland, as well as in the control of cancer cell biology. Specifically, and due to its main role in regulating the levels of endocannabinoids in the cell, we decided to focus our study on the anandamide-degrading enzyme, fatty acid amide hydrolase (FAAH).

In this context, we defined the following aims for this doctoral thesis:

- **Aim 1**. Analysis of the role of FAAH in the development of the adult mammary gland.
- **Aim 2**. Analysis of the role of FAAH in the generation, progression, and metastasis in BC.

MATERIALS & METHODS

ANALYSIS OF TRANSCRIPTOMIC DATA FROM PUBLIC DATASETS

The expression and prognostic value of FAAH and other elements of the endocannabinoid system (ECS) in non-transformed mammary gland and breast cancer (BC) were analyzed in publicly available datasets (properly referenced along the Results section) and plotted using GraphPad Prism software (San Diego, CA, US). In addition, some online tools designed to provide easy access to large amount of published annotated genomic data were used. Expression of *FAAH* and other metabolic enzymes from the ECS in molecular subtypes of BC was calculated using the BC Gene-Expression Miner v4.5 online dataset (http://bcgenex.centregauducheau.fr) (Jézéquel *et al*., 2021). Kaplan-Meier curves showing overall (OS) or metastasis-free survival (MFS) of BC according to *FAAH* and *MGLL* expression were obtained from Kaplan-Meier Plotter website (www.kmplot.com) (Györffy *et al*., 2010). Best threshold cutoffs were selected automatically by the program.

HUMAN SAMPLES

Human mammary gland sections from reduction mammoplasties were kindly given by Dr. Moreno-Bueno (MD Anderson Cancer Center, Madrid, Spain). Tissue microarrays (TMAs) were generated by taking 1 mm punches from a series of paraffin-embedded (donor) tissue blocks and transferring these tissue cores into a positionally encoded array in a recipient paraffin block. TMA #1 samples were donated by Dr. Wenners (University Hospital of Kiel, Germany) and included 617 breast tumor samples from cases operated in the University Hospitals of Kiel, Tübingen, or Freiburg between 1997 and 2010. TMA #2 included 276 pair-matched samples of luminal BC and were donated by Dr. Caffarel (Biodonostia Health Research Institute, San Sebastián, Spain). Complete histopathological information, date, and cause of death, as well as date of local and/or distant relapse were available for all the patients. All patients gave informed consent, and the study was authorized by the respective Hospital Ethics Committees.

CELL LINES AND CULTURE CONDITIONS

All cell lines were maintained at 37 °C in a humidified atmosphere of 5 % CO_2 and routinely tested for *Mycoplasma* spp. contamination. Prior to working with them, they were all authenticated by short tandem repeats (STR) profiling at the genomics core facility of "Alberto Sols" Biomedical Research Institute (Madrid, Spain). A detailed list of the cell lines used in this thesis is provided in **TABLE MM1**.

All cell media, hydrocortisone, and insulin were purchased from Sigma-Aldrich (St. Louis, MO, US). Fetal bovine serum (FBS) and epidermal growth factor (EGF) were

purchased from Gibco (Amarillo, TX, US). HEPES, L-glutamine and penicillin/streptomycin (P/S) mixture were purchased from Lonza (Basel, Switzerland).

Cell line	Cellular type	Species	Source	Complete medium
HC11	Mammary epithelium	Mouse	Kind donation by Dr. Castillo-Lluva (UCM, Madrid, Spain)	RPMI + 10 % FBS + 10 µg/mL insulin + 20 ng/mL EGF + 10 mM HEPES + 2 mM L-glutamine + 1 % P/S
MCF7	Breast carcinoma (Luminal A)	Human	ATCC	MEM + 10 % FBS + 10 µg/mL insulin + 1 % P/S
T-47D	Breast carcinoma (Luminal A)	Human	ATCC	RPMI + 10 % FBS + 10 µg/mL insulin + 1 % P/S
MDA-MB-361	Breast carcinoma (Luminal B)	Human	ATCC	Leibovitz's L-15 + 10 % FBS + 1 % P/S
BT-474	Breast carcinoma (Luminal B)	Human	ATCC	RPMI + 10 % FBS + 10 µg/mL insulin + 1 % P/S
HCC1954	Breast carcinoma (HER2+)	Human	ATCC	RPMI + 10 % FBS + 1 % P/S
SK-BR-3	Breast carcinoma (HER2+)	Human	ATCC	McCoy's + 10 % FBS + 1 % P/S
MDA-MB-231	Breast carcinoma (Basal-like)	Human	ATCC	DMEM + 10 % FBS + 1 % P/S
MDA-MB-231 (Lung-seeking)	Breast carcinoma (Basal-like)	Human	Kind donation by Dr. Moreno-Bueno	DMEM + 10 % FBS + 1 % P/S
SUM-159	Breast carcinoma (Basal-like)	Human	Kind donation by Dr. Moreno-Bueno	Ham's F-12 + **5** % FBS + 5 µg/mL insulin + 1 µg/mL hydrocortisone + 1 % P/S
HEK-293T	Embryonic kidney	Human	ATCC	DMEM + 10 % FBS + 1 % P/S

Table MM1. Source of origin and growth conditions of the cell lines used in this thesis. ATCC: American Type Culture Collection. RPMI: Roswell Park Memorial Institute. DMEM: Dulbecco's Modified Eagle Medium. MEM: Minimum Essential Medium. FBS: fetal bovine serum. EGF: epidermal growth factor. P/S: penicillin/streptomycin.

URB 597 and R-1 Methanandamide (metAEA) were purchased from Cayman Chemical (Ann Arbor, MI, US). BIA 10-2474 was purchased from Medchem Express (Monmouth Junction, NJ, US).

HC11 LACTOGENIC DIFFERENTIATION

The mammary epithelial cell line HC11 originates from mid-pregnancy BALB/c mice and resembles mammary stem cells in that they can differentiate in response to lactogenic stimuli. To induce their differentiation, subconfluent HC11 cells were trypsinized and seeded in complete medium at a density of 0.85 x 10^6 cells per well in 6-well plates. When they reached confluence (usually, overnight [O/N]), complete medium was changed to EGF-free medium and predifferentiated (or "competent") cells were obtained after 48 h of growth in this medium. To obtain completely differentiated cells, predifferentiated cells were then treated for additional 5 days with differentiation medium: EGF-free medium containing 1 µg/mL prolactin (PRL) (Sigma-Aldrich) and 100 nM dexamethasone (DXM) (Sigma-Aldrich). Differentiation medium was changed and added fresh at day 3. Differentiation was monitored by following the gradual increase in β-Casein expression by WB, for which an antibody against mouse whole milk was used (see the WB section). Band corresponding to β-Casein was identified according to Kumar and colleagues, who developed the β-Casein knockout mouse (Kumar *et al*., 1994).

CRISPR/CAS9-MEDIATED KNOCKOUT (KO)

FAAH knockout in T-47D cells was performed with a CRISPR/Cas9 kit from Origene (Rockville, MD, US). The kit provided one gRNA/Cas9 vector targeting a specific sequence in human FAAH (CCGCCACGAAGCAGGCC), one scramble (SCR)/Cas9 negative control and one linear donor DNA coding for a puromycin resistance cassette. Using the Amaxa™ HT Nucleofector™ (Lonza) and according to the protocol provided by the manufacturer for T-47D cell line, 1 x 10^6 cells were co-transfected with 1 µg of FAAH gRNA or SCR vector together with 1 µg of donor DNA. Cells were passaged for additional two weeks and then seeded at a low density in puromycin containing medium in 10 cm dishes. After puromycin selection (c: 0.5 µg/mL), cells were seeded at 5 % confluency and single colonies were isolated using cloning cylinders and transferred to 24-well plates. After monoclonal expansion, puromycin-resistant colonies were analyzed by genomic PCR, for which special primer pairs were designed (**TABLE MM2**). The totality of resistant clones of T-47D cells resulted to be heterozygous for the integration of the functional cassette and, out of them, just one clone showed protein knockdown by WB. This clone, hereafter referred to as "T-47D FAAH KO" was subsequently used to obtain the "T-47D rescue" by lentiviral delivery of human FAAH as described below.

Allele	Sense	Antisense
WT	GGCTGATCCAGTCCGGGTTT	TTGCCTGGGAGTCAGAGCGA
KO	CGGCTTCTACCACTTCGGCA	GCTCGGTGTTGCTGTGATCC

Table MM2. Primer pairs for FAAH genotyping in CRISPR/Cas9-mediated FAAH knockout. Wild type (WT) primers were designed to amplify a sequence inside the gRNA target region. Knockout (KO) primers were designed to amplify a sequence between FAAH1 and the donor cassette.

LENTIVIRAL DELIVERY OF EXPRESSION PLASMIDS

For lentiviral infection of HC11, T-47D and MDA-MB-231 cell lines, a second-generation packaging system was used. Commercial packaging and envelope plasmids [psPAX2 and pMD2.G, respectively, from Addgene (Watertown, MA, US)], as well as the pReceiver-Lv225 (Genecopoeia Rockville, MD, US), were kindly donated by Dr. Fernández-Piqueras lab ("Severo Ochoa" Centre for Molecular Biology, Madrid, Spain). EX-hFAAH-Lv225 transfer plasmid was home generated by subcloning human *FAAH* into the XhoI and BstbI sites of pReceiver-Lv225 (**FIG. MM1**) and then validated by Sanger sequencing at the genomics core facility of the UCM School of Biology. The empty (Ø) vector EX-NEG-Lv225 was used as negative control.

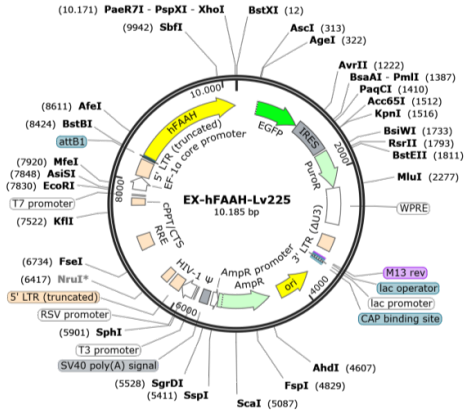

Figure MM1. Map of the viral transfer plasmid EX-hFAAH-Lv225. hFAAH was subcloned into the XhoI and BstbI sites of pReceiver-Lv225.

On day 1, HEK-293T cells were trypsinized and seeded in complete medium at a density of 3 x 10^6 cells/10 cm dish and cultured O/N at 37 °C and 5 % CO_2. On day 2, culture medium was replaced by antibiotic-free medium and cells were transfected 4 h later. For transfection, 6 µg of total DNA in a 1:2:3 ratio of pMD2.G:psPAX2:transfer plasmid were mixed in 750 µL of OptiMEM (Gibco) and then filtered through a 0.22 µm filter. 4 µg/µL DNA of polyethylenimine (PEI)

(Sigma-Aldrich) were added to the mix and incubated for 15' at room temperature (RT) and protected from light before being added to the cells. On day 3, cells to be infected were trypsinized and seeded in complete medium at a density of 750 x 10^3 cells/10 cm dish. Also, HEK293T supernatant was discarded and replaced with the culture medium of the cells to be infected. On day 4, which concurs with the peak of lentiviral particle production, HEK293T supernatant was harvested, centrifuged for 5' at 1000 rpm and filtered through a 0.45 µm filter to get rid of dead cells. Filtered supernatant of HEK293T cells supplemented with a freshly made solution of polybrene (Sigma-Aldrich) at a final concentration of 8 µg/mL was added to the cells to be infected. Cells were exposed to the lentiviral particles for 24 h and, on day 5, lentiviral supernatant was replaced with complete medium. Any material ever in contact with lentiviruses was safely inactivated in 50 % bleach before being discarded into biohazardous waste. Transduction efficiency was monitored by checking the expression of green fluorescent protein (GFP), which usually happened 48-72 h later.

The percentage of GFP+ cells was usually near 100 %, so antibiotic selection was not performed after the infection protocol. Interestingly, T47-D rescue cells maintained FAAH overexpression over cell passages, but MDA-MB-231 usually lost it after a few weeks (even under antibiotic pressure), and therefore experiments with this cell line were always performed in transient.

LIPIDOMICS

For sample preparation, cells were grown in 6 cm dishes, scraped off in 200 µL of ice-cold PBS and pipetted in Eppendorf tubes. They were centrifuged at 2000 x g for 10' at 4 °C, decanted, washed with PBS and centrifuged again. Pellets were immediately frozen in liquid nitrogen and stored at -80 °C. Lipid extraction and parallel quantification of endocannabinoids and endocannabinoid-like molecules was performed by the lipidomics unit of the *Universitätsmedizin* associated to the University of Mainz (Germany), in collaboration with Dr. Beat Lutz's research group.

RNA EXTRACTION AND REVERSE TRANSCRIPTION-PCR (RT-PCR)

RNA was isolated from cultured cells by scraping them off in Nucleozol (Macherey-Nagel, Allentown, PA, US) and following the extraction protocol suggested by the manufacturer. RNA concentration was measured with a Nanodrop™.

Reverse transcription (RT) was performed from 2-3 µg of RNA with the Transcriptor First Strand cDNA Synthesis Kit (Roche Life Science, Basel, Switzerland) using random hexamer primers. Two types of RT-PCR were performed:

• **End-point RT-PCR**. DreamTaq DNA Polymerase (Thermo Fisher Scientific, Waltham, MA, US) was used to co-amplify the human *FAAH* simultaneously with tata binding protein (*TBP*) gene as an internal control. cDNA was amplified with the primers from **TABLE MM3** and the following PCR conditions: initial denaturation at 95 °C for 1'; 35 cycles of denaturation at 95 °C for 1', annealing at 60 °C or 59 °C (for *FAAH* and *TBP*, respectively) for 1', and elongation at 72 °C for 1'. The final cycle was followed by extension at 72 °C for 7'. Results were visualized in a 1.5 % agarose gel.

• **Real-time quantitative RT-PCR (Q-PCR)**. Probe-based Q-PCR was performed in 384-well plates using the LightCycler® Multiplex DNA Master (Roche Life Science) and hybridization probes from the Universal ProbeLibrary Set (Roche Life Science). Specific Q-PCR primers were designed using the ProbeFinder Assay Design Software and are listed in **TABLE MM3**. Q-PCR was performed in a QuantStudio 7/12k Flex System (Applied Biosystems, Waltham, MA, US). *TBP* was routinely used as internal control for normalization, and the relative expression ratio of target/reference gene was calculated with the ΔΔCt method.

Gene	PCR type	Sense	Antisense
h*FAAH*	End-point	TGGGAAAGGCCTGG-GAAGTGAACA	GCCGCAGATGCCGCAGAA-GGAG
h*TBP*	End-point	CCCATGACTCCCAT-GACC	TTTACAACCAAGATTCACT-GTGG
h*CXCR4*	Quantitative	CTGTGAGCAGAGGGTC-CAG	ATGAATGTCCACCTCGCTTT
h*TBP*	Quantitative	CCCATGACTCCCAT-GACC	TTTACAACCAAGATTCACT-GTGG
m*Prlr*	Quantitative	TCCCTGGTATGG-CAGACTTT	AACATCTGCGATGCTCACCT
m*Cnr1*	Quantitative	GCACCTTCACGGTTCT-GG	GACTGCGGGAGTGAAGGAT
m*Cnr2*	Quantitative	CAGCTCTTGGGACCTAC-GTG	GGAGCTGTC-CCAGAAGACTG
m*Csn2*	Quantitative	GGTGAATCTCATGGGA-CAGC	TGACTGGATGCTGGAGT-GAA
m*Stat5a*	Quantitative	TTCCTGCGCCT-GTTTAGAAG	GCTCCTGACGGCTCTTGA
mCXCR4	Quantitative	TGGAACCGATCAGTGT-GAGT	GGGCAGGAAGATCCTATT-GA
mSDF1	Quantitative	CTGTGC-CCTTCAGATTGTTG	TAATTTCGGGTCAATGCACA
m*Tbp*	Quantitative	GGGGAGCTGTGATGT-GAAGT	CCAGGAAATAATTCTGGCT-CA
18S	Quantitative	CTCTAGAATTACCA-CAGTTATCCAA	AAATCAGTTATG-GTTCCTTTGGTC

Table MM3. Primers used for end-point RT-PCR and real-time quantitative (Q) RT-PCR.

PCR ARRAY

For analyzing the expression of a panel of functionally related genes, SYBR® Green-based Q-PCR was performed using the RT2 Profiler PCR Array System (Qiagen, Hilden, Germany) in accordance with the manufacturer's guidelines. Each assay was performed thrice, each one from a different biological replicate.

- RT² Profiler™ PCR Array Mouse Breast Cancer (Ref. no. PAMM-131Z).
- RT² Profiler™ PCR Array Human Tumor Metastasis (Ref. no PAHS-028Z).

RNA SEQUENCING (RNA-SEQ)

RNA from 6 cell samples (T-47D SCR, FAAH KO and rescue, in duplicate) was isolated as already described and resuspended in ultrapure water. Concentration and RNA integrity number > 7 were determined at the genomics core facility of UCM School of Biology, and 1 µg per sample was utilized for RNA-seq. Sequencing results were processed using the bioinformatics software Genome One (DREAMgenics S.L., Oviedo, Spain), certified with IVD/CE-marking.

PROTEIN EXTRACTION AND WESTERN BLOT (WB)

Cell lysis was usually performed on the cell culture dish and kept always at 4 °C. Cells were scraped off in RIPA buffer (0.1 % SDS, 0.5 % sodium deoxycholate, 1 % NP40, 150 mM NaCl, 50 mM Tris–HCl pH 8.0, in PBS) supplemented with protease (0.1 mM phenylmethylsulfonyl fluoride [PMSF], 2 µg/µL aprotinin and 2 µg/µL leupeptin) and phosphatase (1 mM sodium orthovanadate) inhibitors. Total protein content was calculated by using the Bradford assay and bovine serum albumin (BSA) as a protein standard. 25 µg of total protein were boiled for 5' at 95 °C in SDS-containing loading buffer and subsequently resolved by SDS-PAGE and transferred to PVDF membranes in a Trans-Blot® SD Semi-Dry Transfer Cell (Bio-Rad, Hercules, CA, US). Blocking was performed for 1 h at RT. Blocking solution was empirically determined depending on the primary antibody to be used, but, generally, 5 % w/v non-fat dry milk in TBST was used by default, and 5 % w/v BSA in TBST was used for antibodies against phosphorylated residues and for anti-milk. Primary antibodies were diluted in the blocking solution and membranes were incubated O/N at 4 °C. Membranes were then washed with TBST (3 x 10'), incubated for 1 h at RT with the corresponding secondary antibody and washed again before being developed with self-prepared ECL reagent (1.25 mM luminol, 0.2 mM p-coumaric acid, 100 mM Tris–HCl pH 8.5, in dH_2O). Densitometric analysis was performed with ImageJ™ software (Schneider *et al.*, 2012). Special mention has to be made for the WB protocol of GPCRs (CB_1R, CB_2R and CXCR4), where cell lysis was performed in 0.5 % DDM buffer (0.5 % n-dodecyl-b-d-maltoside, 140 mM

NaCl, 25 mM Tris-HCl pH 7.4, 2 mM EDTA, in dH_2O), 40 µg of total protein were loaded onto the gel, and samples were heated at 55 °C for 10'. A detailed list of the antibodies used for WB can be found in **TABLE MM4**.

Primary antibody	Reactivity	Host	Reference	Dilution
α-Tubulin	All	Mouse	Sigma-Aldrich #T9026	1:5000, TBST
β-Actin	All	Mouse	Sigma-Aldrich #A5441	1:5000, TBST
CB_1R	M, R	Guinea Pig	Frontier Institute #CB1-GP-Af530-1	1:500, Milk
CB_2R	H	Rabbit	Thermo-Fisher #PA1-744	1:1000, BSA
C-PARP	H	Rabbit	Cell Signaling Technology #9541	1:1000, Milk
CXCR4	M, R, H	Rabbit	Abcam #124824	1:500, Milk
FAAH	H, M	Rabbit	Abcam #ab128917	1:1000, TBST
Milk	M	Rabbit	Nordic-MUbio #RAM/TM	1:5000, BSA
pStat5	H, M	Rabbit	Cell Signaling Technology #9359	1:500, BSA
PRLR	M, R	Rabbit	Abcam #ab214303	1:1000, BSA
Oct4	M, H	Rabbit	Abcam #19857	1:1000, Milk
Sox2	H, M, R	Mouse	Abcam #ab75485	1:1000, Milk
STAT5	H, M, R	Rabbit	Cell Signaling Technology #94205	1:1000, Milk

Secondary antibody	Reactivity	Host	Reference	Dilution
HRP Mouse IgG	Mouse	Sheep	Cytiva Lifescience #NA931	1:10 000, TBST
HRP Rabbit IgG	Rabbit	Donkey	Cytiva Lifescience #NA934	1:10 000, TBST
HRP Guinea pig IgG	Guinea pig	Goat	Invitrogen #A18769	1:10 000, TBST

Table MM4. Antibodies used for WB analysis. Indicated are species reactivity, host species, commercial reference, and conditions of use. H: human; M: mouse; R: rat. Corporate headquarters: Frontier Institute (Glenroy, Australia); Cell Signaling Technology (Danvers, MA, US); Abcam (Cambridge, UK); Nordic-Mubio (Susteren, Netherlands); Cytiva Lifescience (Marlborough, MA, US); Invitrogen (Waltham, MA, US).

FLOW CYTOMETRY

Flow cytometry was used to analyze cell surface expression of CXCR4 in human BC cell lines and tumors from MMTV-neu mice.

Adherent cell lines were harvested using TrypLETM Express (Gibco). Cells were resuspended in FACS buffer (PBS + 1 % FBS + 1 % BSA + 0.02 % sodium azide) and distributed into individual wells of a U-bottom shape 96-well plate, which was kept on ice for subsequent experimental steps. The plate was centrifuged at 1000 rpm for 5' at 4 °C, supernatants decanted and cell pellets resuspended in 100 µL of primary antibody dilution in FACS buffer. Incubation with hCXCR4 primary antibody [R&D Systems (Minneapolis, MN, US) #MAB173] diluted 1:20 and then Alexa Fluor™ 647 Mouse IgG (Invitrogen #A-21235) diluted 1:200 were sequentially performed in agitation for 20' at 4 °C and protected from light. A washing step with FACS buffer was performed after each antibody incubation. Finally, cells were resuspended thoroughly in FACS buffer at a concentration of 1 x 10^6 cells/mL and transferred to polystyrene round-bottom tubes. 7-aminoactinomycin D (7-AAD) (Biolegend, San Diego, CA, US) was used as death cell marker and was added to all samples 15' before analysis.

In the case of breast tumors derived from MMTV-neu mice, a single cell solution was obtained from tumors after mechanical disaggregation followed by 2 h of enzymatic digestion in DMEM + 125 µg/mL collagenase (Sigma-Aldrich) at 37 °C. CXCR4 staining was performed as described above with already conjugated primary antibody Alexa Fluor™ 647 mCXCR4 (Biolegend #146503) diluted 1:100. Together with CXCR4, cell suspension was stained for biotinylated CD31 (Thermo Fisher Scientific #13-0311-82, diluted 1:200), CD45 (Thermo Fisher Scientific #13-0451-82, diluted 1:400) and TER119 (Thermo Fisher Scientific #13-5921-82, diluted 1:100) + PE Streptavidin (Biolegend #405203, diluted 1:300) to exclude endothelial and hematopoietic lineages (Lin+) from the analysis.

Data acquisition was performed in a FACSCalibur system (Becton Dickinson, Franklin Lakes, NJ, US). Compensation was applied according to single-stained controls of the same cell type. For data analysis, FlowJo™ software (Becton, Dickinson and Company, 2019) was used. Fluorescence minus one (FMOs) controls were used to set the blank for CXCR4 expression after exclusion of cell debris, nonviable cells, and (in the case of MMTV-neu-derived tumors) Lin^+ cells (**FIG. MM2**).

IMMUNOCYTOFLUORESCENCE AND PHALLOIDIN STAINING

75 x 10^3 cells/well for T-47D cells and 25 x 10^3 cells/well for MDA-MB-231 cells were seeded on 12 mm circular coverslips in 24-well plates and fixed the day after in 10 % formalin (20', 4 °C). For the study of epithelial-to-mesenchymal transition

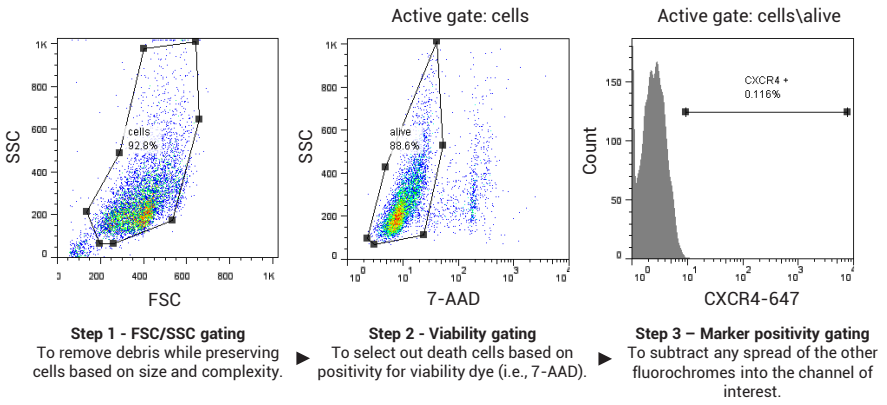

Figure MM2. Gating strategy for the flow cytometric analysis of cell membrane CXCR4 expression. Sequential gating to exclude cell debris and nonviable cells was performed on fluorescence minus one (FMO) control, a sample expressing all fluorochromes except for CXCR4-647. In the case of MMTV-neu-derived tumors, an extra gating step between 2 and 3 was included to exclude PE-expressing Lin^+ cells (not shown in the image).

(EMT) phenotype and Ki67, blocking was performed with 5 % goat serum in PBS + 0.25 % triton-X100 (Sigma-Aldrich) for 1 h at RT. Primary antibodies (**TABLE MM5**) were diluted in Antibody Diluent (Dako, Jena, Germany) and incubated O/N at 4 °C. Secondary antibodies (**TABLE MM5**) were diluted in blocking solution and incubated for 1.5 h at RT, protected from light. 1 µg/mL DAPI (Roche Life Science) for nuclei staining was added to the secondary antibody mix. 3 x 15' washes with PBS + 0.25 % triton were performed after each antibody incubation. For

Primary antibody	Reactivity	Host	Reference	Dilution
E-cadherin	H, M	Rabbit	Cell Signaling Technology #3195	1:200
Ki67	H	Rabbit	Epredia #RM-9106-S	1:400
Vimentin	H, M, R	Mouse	BD Biosciences #550513	1:200

Secondary antibody	Reactivity	Host	Reference	Dilution
Alexa Fluor™ 647 Mouse IgG	M	Goat	Invitrogen #A-21235	1:200
Alexa Fluor™ 647 Rabbit IgG	R	Goat	Invitrogen #A-21244	1:200

Table MM5. Antibodies used for immunofluorescence of adherent cell lines. To identify epithelial-to-mesenchymal (EMT) features, an epithelial marker (E-cadherin) and a mesenchymal marker (vimentin) were used. Phalloidin was also used to visualize filopodia and migrating structures. Indicated are species reactivity, host species, commercial reference, and conditions of use. H: human; M: mouse; R: rat. Corporate headquarters: Epredia (Portsmouth, NH, US).

visualization of the actin filaments, Alexa Fluor™ 647 Phalloidin (Thermo Fisher Scientific #A22287) diluted 1:40 in 1 % BSA in PBS was prepared and added to the fixed cells for 20' at RT, protected from light. Then they were washed 3 x 10' in PBS. Coverslips were mounted with Mowiol® mounting medium (Calbiochem, San Diego, CA, US). Fluorescence confocal images were acquired by using an Olympus FV1200.

IMMUNOHISTOCHEMISTRY

Paraffin-embedded tissue sections were de-waxed in the non-toxic xylene substitute isoparaffin H (Panreac, Darmstadt, Germany) for 20' at RT and hydrated by quick changes through serial ethanol baths (2 x 100 %; 2 x 96 %; 2 x 60 %; 5 x dH_2O). Antigen retrieval was performed by boiling in a water bath for 20' in sodium citrate buffer (10 mM Sodium citrate, 0.05 % Tween 20, pH 6.0, in dH_2O). Samples were subjected to 5 washes with dH_2O and 3 with washing buffer (NaCl 8.3 g/L, Tris 1.2 g/L; pH 7.4). From here, different procedures were followed depending on the immunodetection method:

- **Chromogenic.** Endogenous peroxidase activity was suppressed by incubation with 3 % H_2O_2 for 20' and protected from light. Blocking, primary (**TABLE MM6**) and secondary antibody incubations and immunodetection were performed with the ImmPRESS™ Polymer Detection kit (Vector, Burlingame, CA, US) following the manufacturer's instructions. Samples were finally counterstained with hematoxylin for 10', rinsed in running tap water for 30', dehydrated (2 x 60 %; 2 x 96 %; 3 x 100 %; 3 x isoparaffin H) and mounted in Eukitt® Quick-hardening mounting medium (Sigma-Aldrich).

- **Fluorescent.** Blocking was performed with 10 % goat serum in PBS, for 1 h at RT. Primary antibodies (TABLE MM6) were diluted in Antibody Diluent (Dako) and incubated O/N at 4 °C. Samples were rinsed 2 x 5' in PBS + 0.25 % triton and incubated with fluorescent secondary antibodies (**TABLE MM6**) and 1 µg/mL DAPI for 1 h at RT. Finally, they were mounted with Mowiol® mounting medium. Fluorescence confocal images were acquired by using an Olympus FV1200.

CELL VIABILITY ASSAY

Cells were seeded in complete medium into 24-well plates at a density of 15 x 10^3 cells/well for luminal cell lines and 10 x 10^3 cells/well for basal cell lines and cultured at 37 °C and 5 % CO_2. At each time point, the medium from the wells was aspirated and the remaining cells were stained with crystal violet solution (0.1 % crystal violet, 20 % methanol, in dH_2O) for 20' at RT. They were then intensively washed with tap water and left to dry out with the lid open. When plates from all

Primary antibody	Reactivity	Host	Reference	Dilution
CB_1R	M, R	Guinea Pig	Frontier Institute #CB1-GP-Af530-1	1:300
CK8	H, M	Rat	DHBS #531826	1:50
CK14	M, R, H	Rabbit	Abcam #ab181595	1:50
FAAH	H, M	Rabbit	Abcam #ab128917	1:100
PRLR	M, R	Rabbit	Abcam #ab214303	1:500
SMA	H, M	Mouse	DSHB #2289065	1:50

Secondary antibody	Reactivity	Host	Reference	Dilution
Alexa Fluor™ 488, 594 or 647 Mouse IgG	M	Goat	Invitrogen #A28175, #A-11032, #A-21235	1:200
Alexa Fluor™ 488, 594 or 647 Rabbit IgG	R	Goat	Invitrogen #A-11008, #A-11012, #A-21244	1:200
Alexa Fluor™ 488 or 647 Rat IgG	R	Goat	Invitrogen #A-11006, #A-21247	1:200
Alexa Fluor™ 488 Guinea Pig IgG	GP	Goat	Invitrogen #A-11073	1:200

Table MM6. Antibodies used for immunohistochemistry of paraffin-embedded tissue from human and mouse origin. Indicated are species reactivity, host species, commercial reference, and conditions of use. H: human; M: mouse; R: rat, GP: guinea pig. Corporate headquarters: Developmental Studies Hybridoma Bank (DSHB, Iowa, IA, US).

time points had been collected, the dyed crystals were solubilized in methanol and after 20' in agitation, the OD570 of each well was measured in a RT-6100 microplate reader (Rayto, Shenzhen, China) as an indirect readout for the number of viable cells in the culture.

TRANSWELL MIGRATION ASSAY

The migration potential of T-47D and MDA-MB-231 cells was evaluated using transwell inserts with 8.0 µm pore polyethylene terephthalate (PET) membranes (Corning, Corning, NY, US). Briefly, cells were serum-starved O/N and 50 x 10^3 were seeded in serum-free medium into the upper compartment of the insert while the lower compartment was filled with complete medium, 10 % FBS acting as chemoattractant. Cells were allowed to migrate across the membrane for 48 h (MDA-MB-231) or 72 h (T-47D). Then, non-migrating cells were gently removed from the upper side of the membrane with a cotton swab, and the remaining cells

were fixed with 10 % formalin (10', RT) and washed 3 x 15' with PBS before being stained with 1 µg/mL DAPI (10', RT). The membrane was again PBS washed 3 x 15', cut out with a scalpel and mounted in Mowiol medium. Cell migration was quantified by counting the nuclei on the whole membrane (T-47D) or in 5 random fields at 40 X magnification (MDA-MB-231) in a fluorescence microscope.

TRANSWELL INVASION ASSAY

The invasive potential of MDA-MB-231 cells was assessed *in vitro* by using transwell inserts with an 8.0 µm pore membrane coated with Matrigel® as a surrogate basement membrane (Corning). Since T-47D did not invade through commercial chambers, home-made invasion transwells were made by manually coating PET membrane inserts with 3 mg/mL Growth Factor Reduced (GFR) Matrigel® (Corning). Briefly, GFR Matrigel® was thawed on ice and diluted down to 3 mg/mL in ice-cold, serum-free RPMI. 60 µL were added to each insert and then, the plate was placed in the incubator at 37 °C for 30' before cell seeding. The protocol followed afterwards is identical to the one detailed for the transwell migration assay, endpoints included.

MAMMOSPHERE ASSAY

Mammosphere medium was prepared by supplementing phenol red-free DMEM/F12 (Gibco) with 1 X B27 minus vitamin A (Gibco), 20 ng/mL EGF, 20 ng/mL FGF, 2 µg/mL heparin (Sigma-Aldrich), 10 µg/mL insulin, 1 µg/mL hydrocortisone and 1 % penicillin/streptomycin.

T-47D cells were trypsinized at 60-70 % confluence, centrifuged and resuspended in phenol red-free DMEM/F12 for counting. They were then syringed three times using a 25 G syringe to ensure complete disaggregation. The presence of a single cell suspension was confirmed using a hemocytometer and the number of viable cells was calculated using trypan blue. Cells were plated at a density of 500 cells/well in 2 mL of mammosphere medium into ultra-low attachment 6-well plates (Corning). After 5 days in culture (37 °C, 5 % CO_2) without moving the plate, light microscopy at 40 X magnification was used to assess mammosphere formation. The presence of mammospheres was defined as dense and compact floating structures, greater than 40 µm and clearly distinguishable from loose aggregates of cells. Fields selected for quantification were those resulting from scanning the well from top to bottom twice, on either side of the vertical diameter.

In our hands, MDA-MB-231 cell line did not form mammospheres, as has been also reported by others (Iglesias *et al*., 2013; Berens *et al*., 2015).

ANIMALS

C57BL/6J FAAH $^{-/-}$ mice were kindly donated by Dr. Ben Cravatt's laboratory (Scripps Research Institute, La Jolla, CA, US). FVB/NJ MMTV-neu mice were kindly donated by Dr. Santos Mañes' laboratory (National Center for Biotechnology CNB-CSIC, Madrid, Spain).

All procedures involving animals were performed with the approval of the Complutense University Animal Experimentation Committee and Madrid Regional Government according to the European official regulations. Animals were housed in the animal facility of the UCM School of Biology, under a 12 h light-dark cycle, and were allowed to feed and drink *ad libitum*.

FAAH GENOTYPING

Animals were routinely genotyped for *Faah* according to an allelic-specific PCR method using the DreamTaq DNA Polymerase. Two PCR reactions were performed in parallel: primers P1 (TAACTAGGCAGTCTGACTCTAG) and P2 (ACTCAAGGTCAGCCTGAAACC) were used to amplify the WT allele, and primers P1 and P3 (TTTGTCACGTCCTGCACGACG) were used to amplify the FAAH KO allele. The PCR cycling conditions were as follows: initial denaturation at 94 °C for 3'; 27 cycles of denaturation at 94 °C for 1', annealing at 54 °C for 1', and elongation at 72 °C for 1'. The final cycle was followed by extension at 72 °C for 7'. A representative image of a genotyping result is shown in **FIG. MM3**.

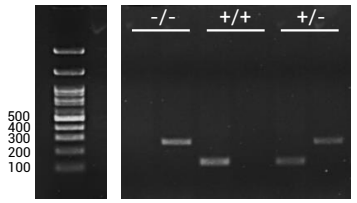

Figure MM3. 2 % agarose gel with all three possible FAAH genotypes.

MAMMARY GLAND DISSECTION

For studies during lactation, 12 to 18-week-old C57BL/6J FAAH $^{+/+}$ or FAAH $^{-/-}$ females were mated with wild type studs and allowed to litter. Tissue was harvested at lactation days 1, 5, 10 and 15. Pups were removed from the cage 2 h before mammary gland extraction to make sure that the differences between FAAH $^{+/+}$ and FAAH $^{-/-}$ littermates were not due to different sucking stimuli at the moment of dissection. Mice were euthanized by CO_2 inhalation, sprayed generously with ethanol 70 % and placed on its back with the four limbs spread. Using forceps, the

abdominal skin at the midline of the mouse was pulled up and a small incision was made while avoiding puncturing the abdominal or thoracic cavities. Starting from the incision, the skin was cut up to the neck and then manually peeled to the sides of the animal to expose mammary glands. Using forceps, the mammary gland of interest was lifted and the connective tissue between the gland and the skin was carefully cut with small sharp scissors. Integrity of pairs #1 and #5 was usually compromised after opening the skin and thus were never dissected. Pairs #2 and #3 were usually snap frozen and then used for RNA/protein extraction. Pair #4 was the preferred option for immunohistochemistry as it was easier to remove integrally, so it was spread over a 6 cm dish, fixed O/N in 10 % formalin and transferred to ethanol 50 %. Fixed mammary glands were then paraffin-embedded and sectioned at the Department of Medicine and Animal Surgery at UCM School of Veterinary, which also performed hematoxylin and eosin (H&E) staining.

GENERATION OF MMTV-NEU:FAAH $^{-/-}$ MICE AND SAMPLE COLLECTION

Generation of the congenic strain MMTV-neu:FAAH $^{-/-}$ was accomplished by mating MMTV-neu mice (The Jackson Laboratory, Bar Harbor, ME, US) with FAAH $^{-/-}$ mice. To transfer the FAAH line (with a C57BL/6J background) to the genetic background of the tumor prone animals (FVB/NJ), the descendants were backcrossed with MMTV-neu mice for 6 generations, using a marker-assisted selection protocol (MASP). Briefly, animals were genotyped for a set of 377 single nucleotide polymorphisms (SNPs) using the Mouse Low Density Linkage Panel from Illumina®. Selected breeders for the next generation were those with the highest percentage of FVB/NJ-linked SNPs. After 6 backcrosses, animals presented more than 99 % FVB/NJ background. FAAH $^{+/-}$ mice from this generation were then crossed between them to generate MMTV-neu:FAAH $^{-/-}$ and their corresponding control littermates (MMTV-neu:FAAH $^{+/+}$). A total of 64 MMTV-neu:FAAH $^{+/+}$ and 58 MMTV-neu:FAAH $^{-/-}$ female mice were analyzed. Females were palpated twice weekly for mammary gland nodules. As soon as tumors appeared, they were routinely measured with external caliper, and volume was calculated as $(4\pi/3)$ x $(\text{width}/2)^2$ x $(\text{length}/2)$. Animals were euthanized and mammary glands, breast tumors, and lungs were collected at T0: mammary gland before malignant transformation; T1: when the first tumor in each animal appeared; T2: 40 days after the appearance of the first tumor; and T3: 90 days after the appearance of the first tumor. After animal sacrifice, tumors were extracted and divided into four portions for 1) preparation of tissue sections for immunofluorescent staining [frozen in Tissue-Tek (Sakura Finetek Europe, Alphen aan den Rijn, Netherlands)], 2) preparation of tissue sections for H&E staining (fixed in 10 % formalin), 3) protein extraction (snap frozen), and 4) RNA isolation (snap frozen), and stored at -80 ºC until analysis (except formalin-fixed tumor fractions, that were kept at room temperature). Non-transformed mammary glands and lungs were fixed in 10 %

formalin O/N and changed to 50 % ethanol the day after. Macroscopic metastases in the lungs were visually assessed before tissue fixation and microscopic metastases were determined by subsequent H&E staining of fixed paraffin-embedded sections.

GENERATION OF XENOGRAFTS IN IMMUNOCOMPROMISED MICE

5-week-old athymic female mice (Charles Rivers Laboratories, Wilmington, MA, US) were housed in individually ventilated cages, fed with sterilized standard laboratory diet, and received sterile water ad libitum. After arrival, all mice were allowed to acclimate to the facility conditions for 1 week prior to experimentation.

Xenografts from T-47D cells

Subconfluent T-47D cells were collected, counted, and resuspended in PBS at a concentration of 100 x 10^6 cells/mL. An amount of 10 x 10^6 cells in a total volume of 200 µL (100 µL cell suspension + 100 µL GFR Matrigel®) were subcutaneously injected into the right flank of the mice. Drinking water of these mice was supplemented with 0.67 µg/mL 17β-estradiol (Sigma-Aldrich) from 1 week prior to inoculation until sacrificed. Fresh estradiol supplemented water was provided once a week. Tumors began to arise 4 weeks post inoculation and were monitored weekly for growth by measuring length and width with a digital caliper. Tumor volume was calculated as (4π/3) x (width/2)2 x (length/2). When tumors reached a volume > 1000 mm^3 (around 4 months post inoculation), mice were euthanized and tumors were excised.

Xenografts from MDA-MB-231 cells

Subconfluent MDA-MB-231 cells were collected, counted, and resuspended in PBS at a concentration of 50 x 10^6 cells/mL. An amount of 2.5 x 10^6 cells in a total volume of 50 µL were orthotopically inoculated into the right inguinal mammary fat pad of athymic mice. Tumors began to arise 2 weeks post inoculation and were monitored three times a week for growth by measuring length and width with a digital caliper. Tumor volume was calculated as $(4\pi/3) \times (width/2)^2 \times (length/2)$. When tumors reached a volume > 1000 mm^3 (around 1.5 months post inoculation), mice were euthanized and tumors were excised.

GENERATION OF LUNG METASTASIS IN IMMUNOCOMPROMISED MICE

Lung metastases were generated by injection of 5 x 10^5 lung-seeking MDA-MB-231 cells in 100 µL of PBS into the lateral tail vein of 6-week-old athymic female mice (Charles Rivers Laboratories). 6 weeks after cell injection, animals were euthanized and lungs were excised, fixed in 10 % formalin O/N, and changed to 50 % ethanol the day after. Fixed lungs were then paraffin-embedded at the Department of

Medicine and Animal Surgery at UCM School of Veterinary, which also determined the presence and severity of metastatic lesions.

STATISTICAL ANALYSES

The Pearson's chi-squared test was used for statistical analysis of the human samples included in the TMAs. Kaplan-Meier survival curves were statistically compared by the log-rank test. Unpaired, independent groups of 2 were analyzed by 2-tailed Student's t-test. A p value of less than 0.05 was considered statistically significant. Unless otherwise stated, data are expressed as mean ± SEM.

RESULTS

AIM 1 | ROLE OF FAAH IN ADULT MAMMARY GLAND DEVELOPMENT

EXPRESSION OF FAAH AND OTHER ELEMENTS OF THE ECS IN MAMMARY EPITHELIAL CELL POPULATIONS

In order to investigate the role of FAAH in the adult phase of mammary gland development, we first assessed its mRNA levels in mammary epithelial cells (MECs) from human samples through publicly available datasets. Microarray analyses on FACS sorted populations purified from reduction mammoplasties (Kannan *et al*., 2013) revealed that *FAAH* and *FAAH2* mRNA levels were significantly higher in the differentiated luminal subset ($EpCAM^+$ $CD49f^-$) than in the basal/mammary stem cell (MaSC) subset ($EpCAM^-$ $CD49f^+$), which is thought to contain both differentiated basal cells and bipotent MaSCs. In addition, differentiated luminal cells expressed higher *FAAH* mRNA levels than luminal progenitors ($EpCAM^+$ $CD49f^+$), although statistical significance was not reached in this case (**FIG. R1**).

Similar observations were made after the analysis of two additional studies involving gene expression profiling of human MEC subpopulations (Raouf *et al*., 2008; Lim *et al*., 2009) (**FIGs. R2A** and **R2B**): *FAAH* levels were the lowest in the basal/MaSC subset, increased in the luminal progenitor subset, and were the highest in the differentiated luminal subset. Through the use of a different combination of cell surface markers, one of these studies (Raouf *et al*., 2008) obtained further segregation of the basal/MaSC subset into basal and bipotent progenitor subsets separately, which allowed us to conclude that *FAAH* levels in differentiated basal cells and in bipotent MaSCs were equally low (**FIG. R2B**).

No significant differences between MEC populations were observed for the mRNA levels of other endocannabinoid (eCB)-synthesizing (*NAPE-PLD*, *DAGLA* and *DAGLB*) or eCB-degrading enzymes (*MGLL* and *NAAA*), except for *PTGS2,* which appears to be subjected to a regulation opposite to *FAAH* (it presents higher levels in the basal/MaSC compartment when compared with the luminal, and in the non-differentiated luminal cells when compared to their differentiated counterparts) (**FIG. R1**). Regarding cannabinoid receptors (CBRs) 1 and 2 (*CNR1* and *CNR2*, respectively) and other cannabinoid-related receptors that may be potentially engaged and activated by FAAH substrates (*GPR55*, *PPARA*, *PPARG* and *TRPV1*), mRNA levels of *CNR1*, *PPARA, PPARG* and *TRPV1* also showed differential expression between cell subsets, with levels of *CNR1* and *PPARA* being the highest in the basal/MaSC subset, and those of *PPARG* and *TRPV1* in the luminal subset (**FIG. R1**).

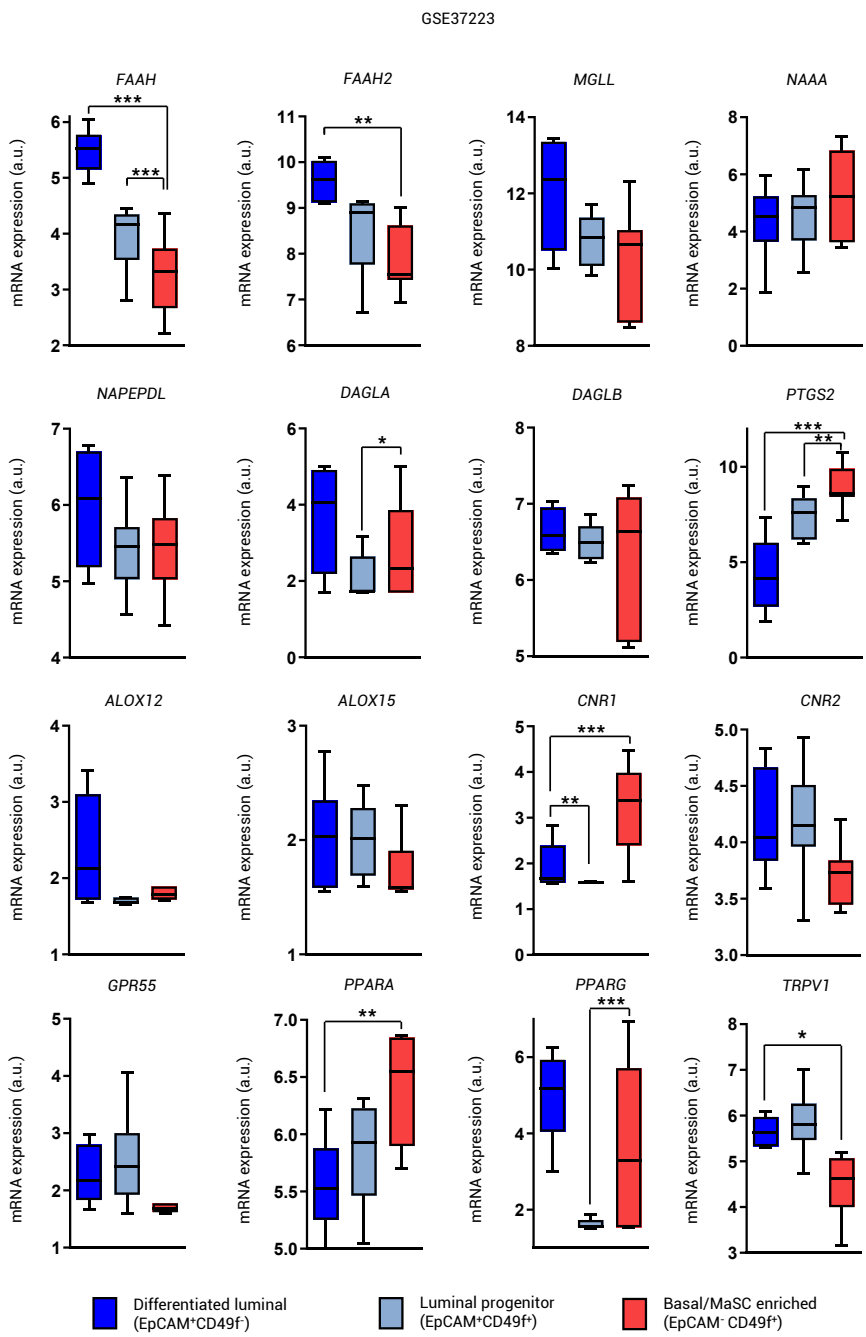

Figure R1. mRNA expression of the main components of the ECS in FACS-sorted human mammary gland cell populations. Data were obtained from the microarray dataset published by Kannan *et al.*, 2013 (study code GSE37223). Student's t-test: * $p < 0.05$, ** $p < 0.01$, *** $p < 0.001$.

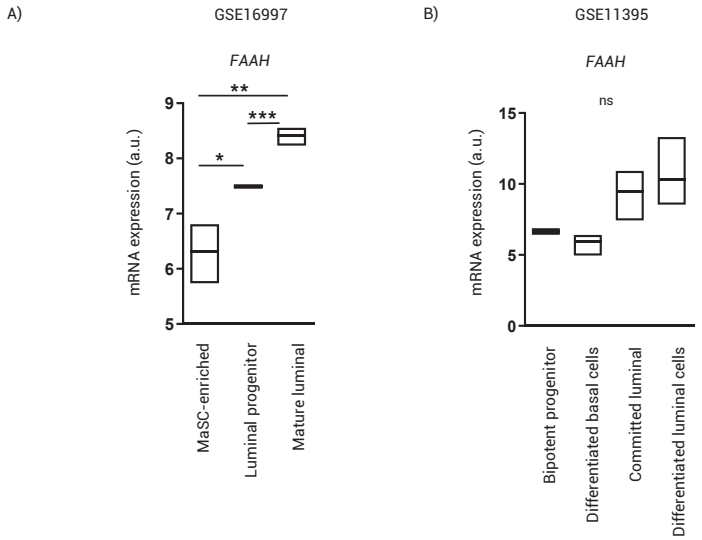

Figure R2. mRNA expression of human FAAH in FACS-sorted human mammary gland cell populations. A) Data were obtained from the microarray dataset published by Lim *et al*., 2009 (study code GSE16997). B) Data were obtained from microarray dataset published by Raouf *et al*., 2008 (study code GSE11395). Student's t-test: * $p < 0.05$, ** $p < 0.01$, *** $p < 0.001$.

To further confirm our observations pointing to an association between high FAAH expression and more differentiated phenotypes within the luminal lineage, we next studied FAAH and related proteins transcriptomes in a dataset containing single cell RNA-seq (scRNA-seq) profiling of mouse mammary gland from four adult developmental time points: nulliparous, mid gestation, lactation, and post involution (Bach *et al*., 2017) (**FIG. R3A**). Paralleling our observations in human tissue, *Faah* was predominantly expressed in clusters of differentiated luminal cells in nulliparous and post involution stages (C4 and C3, respectively), as well as in differentiated alveolar cells distinctive of the gestation and lactation stages (C8 and C11, respectively), while it was absent from basal (C12, C14) and MaSC (i.e., Procr+ cells, C15) clusters (**FIG. R3B**).

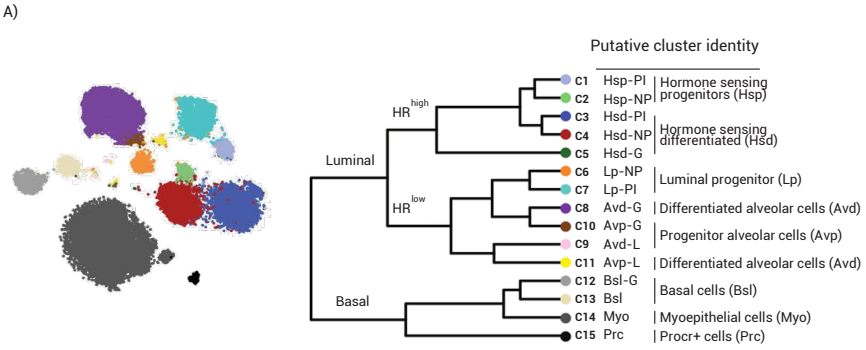

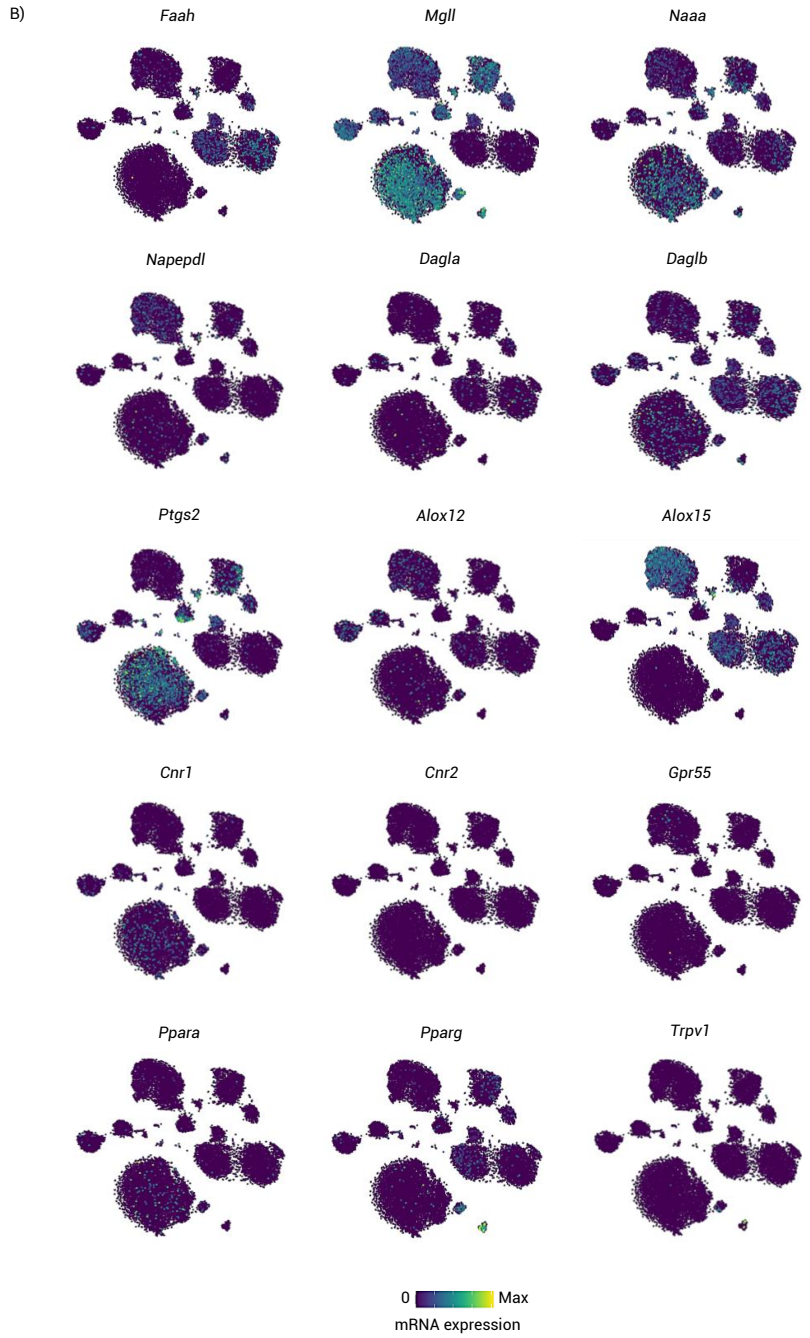

Figure R3. FAAH expression is restricted to differentiated luminal cell populations in all stages of adult mammary development. A) Putative cell clusters of mammary cell populations (depicted at the left and identified at the right) defined by scRNA-seq of the developing mammary gland of the mouse published by Bach *et al.*, 2017. B) t-SNEs plots representing mRNA expression of the main components of the ECS in cell clusters described in A). t-SNEs plots are colored by the normalized log-transformed expression of each of the genes.

Ptgs2 and *Mgll* showed an expression pattern complementary to that of *Faah* [i.e., they were predominant in C12 and C14 basal clusters and clusters with a luminal progenitor profile (C6, C7), while they were absent from C3 and C4 clusters of differentiated luminal cells, where *Faah* reached its highest]. mRNA levels of the rest of eCB-synthesizing and eCB-degrading enzymes showed a homogeneous distribution along all cell clusters except for *Alox15*, which was preferentially expressed in differentiated luminal clusters. As in the human samples, mRNAs of *Cnr1* and *Ppara* were found to be expressed mostly in clusters with a basal profile. Finally, *Pparg* showed a low expression in all clusters, and mRNAs of *Cnr2*, *Gpr55* and *Trpv1* receptors were barely detected in any stage of adult mammary gland development (**FIG. R3B**).

To further corroborate the information gathered from public databases, we performed immunofluorescence staining of FAAH and CB_1R proteins in human adult mammary gland samples (**FIG. R4**). Consistent with our previous results,

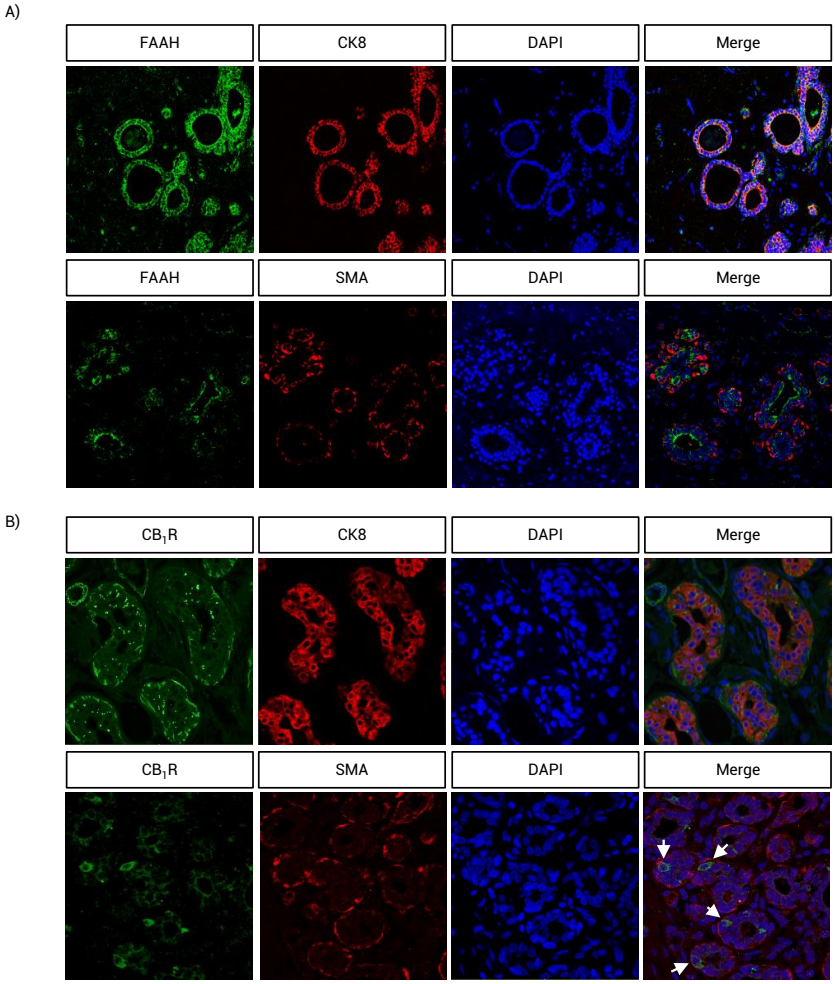

Figure R4. Expression of FAAH and CB_1R in the epithelial cell populations of the mammary duct. A) Immunofluorescence analysis of FAAH with cytokeratin 8 (CK8) as a luminal marker (upper panels) and with smooth muscle actin (SMA) as a basal marker (lower panels). Cell nuclei are stained in blue. B) Same as A) for CB_1R.

FAAH was found to colocalize exclusively with cytokeratin 8 (CK8) + luminal cells in the inner layer of the inactive lactiferous duct (**FIG. R4A**). Immunolabeling of CB_1R was more diffuse, displaying a dot pattern in the luminal layer of some but not all ducts, and being especially intense in isolated cells localized in an intermediate position between luminal and basal layers (**FIG. R4B**).

Together, these results support the notion that FAAH may be involved in the differentiation of luminal cells in the mammary gland.

PHARMACOLOGICAL INHIBITION OF FAAH HAMPERS LACTOGENIC DIFFERENTIATION OF MECS IN VITRO

To confirm the involvement of FAAH in the differentiation of luminal cells in the adult mammary gland, we next investigated its role in lactogenic differentiation, a crucial process that occurs when pregnancy is advanced to expand the ductal system and differentiate it to generate milk secretion sites. To this aim, we utilized HC11 cells, an immortalized MEC cell line harvested from a BALB/c mouse during pregnancy. Although immortalized, these cells retain their ability to undergo lactogenic differentiation in culture, including PRL-inducible expression of milk proteins (β-Casein) and formation of fluid-filled acini (Ball *et al*., 1988).

First, we differentiated HC11 cells from their stem-cell like state (i.e., undifferentiated) to their milk-producing state (i.e., differentiated), passing through an intermediate or "predifferentiated" state in which they become responsive to lactogenic stimuli (**FIG. R5A**). Differentiation was monitored by following the gradual increase in β-Casein expression by Western blot (WB). In line with our previous results, β-Casein increase (i.e., HC11 cell differentiation) was accompanied by a concomitant increase in FAAH expression (**FIG. R5B**).

To try to establish a cause-effect link between FAAH expression and HC11 differentiation, we next blocked FAAH activity by using the selective inhibitor URB 597 during the differentiation process. FAAH inhibition resulted in impaired lactogenic differentiation as determined by a decrease in β-Casein at the final stage of differentiation (**FIG. R5C**). These results were mimicked by using a different FAAH inhibitor (BIA 10-2474) (**FIG. R5D**), indicating that the catalytic activity of FAAH is required for the differentiation of HC11 cells. As expected, inhibition of FAAH with URB 597 resulted in an increase in the intracellular levels of its main substrates [i.e., anandamide (AEA) and other N-acylethanolamines (NAEs)] (**FIGs. R5E-H**), although only those of AEA reached statistical significance (**FIG. R5E**).

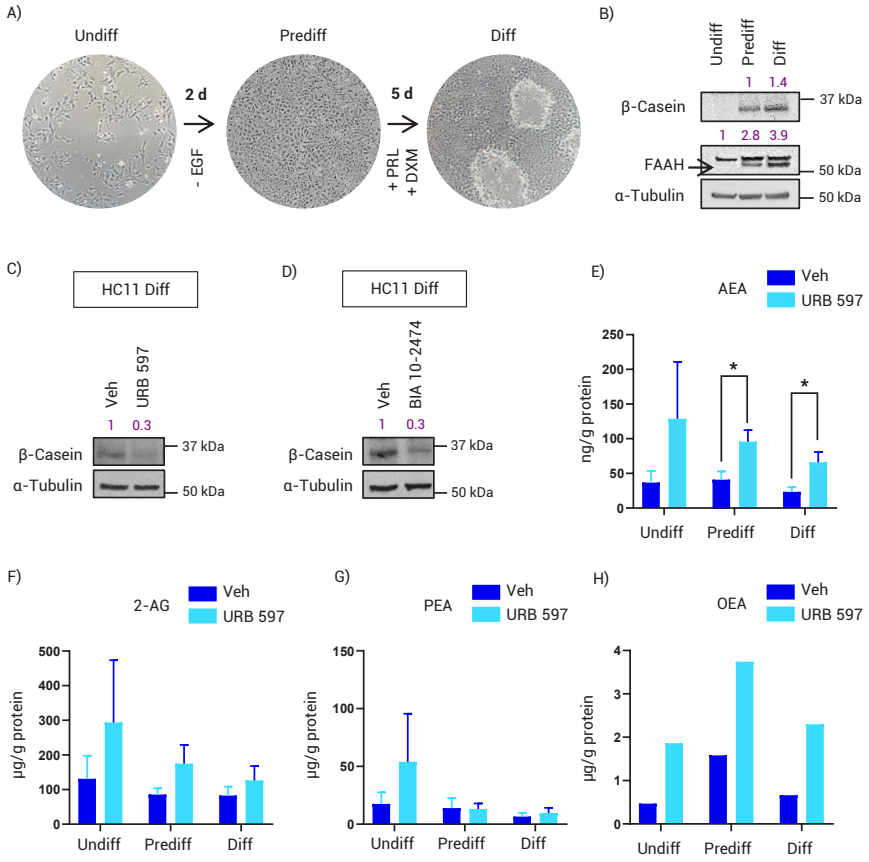

Figure R5. FAAH inhibition compromises HC11 differentiation. A) Schematic representation of the differentiation protocol of HC11 cells. B) Representative WB analysis of β-Casein and FAAH at the three differentiation points. Specific band for FAAH in HC11 cells was considered to be the lower one as revealed by WB analysis of the FAAH KO mouse. C) Representative WB analysis of β-Casein in HC11 cells after being differentiated in the presence of URB 597 at 5 µM. D) Same as C) for BIA 10-2474 at 5 µM. Densitometric values for all WBs after normalization against α-Tubulin and control condition are depicted in purple. E)-H) Levels of the main FAAH substrates normalized to protein content. AEA: anandamide (E); 2-AG: 2-arachidonoylglycerol (F); PEA: palmitoylethanolamide (G); OEA: oleoylethanolamide (H). Values represent mean ± SEM of three independent samples except for OEA, which could only be measured once. Student's t-test: * $p < 0.05$.

FAAH OVEREXPRESSION INDUCES LACTOGENIC SWITCH OF MECS IN VITRO

To further confirm that FAAH is involved in the differentiation process associated with the lactogenic switch, we overexpressed this enzyme in HC11 cells by using a retrovirus harboring *FAAH*. As shown in **FIG. R6A**, FAAH overexpression led to an increase in β-Casein and other milk proteins corresponding to molecular weights previously observed for lactoferrin and γ-Casein (with apparent molecular weights

of 80 and 25 kDa, respectively) (Boumahrou *et al*., 2011), even in those stages where exogenous PRL had not been added yet (i.e., undifferentiated and predifferentiated) (**FIG. R6A**). *FAAH* overexpression in the undifferentiated state of HC11 cells led to a downward trend on the endogenous levels of AEA and other NAEs that did not reach statistical significance (**FIGs. R6B-E**), but not 2-arachidonoylglycerol (2-AG) (**FIG. R6C**), and this effect that was lost in the predifferentiated and differentiated states, where endogenous FAAH levels are higher.

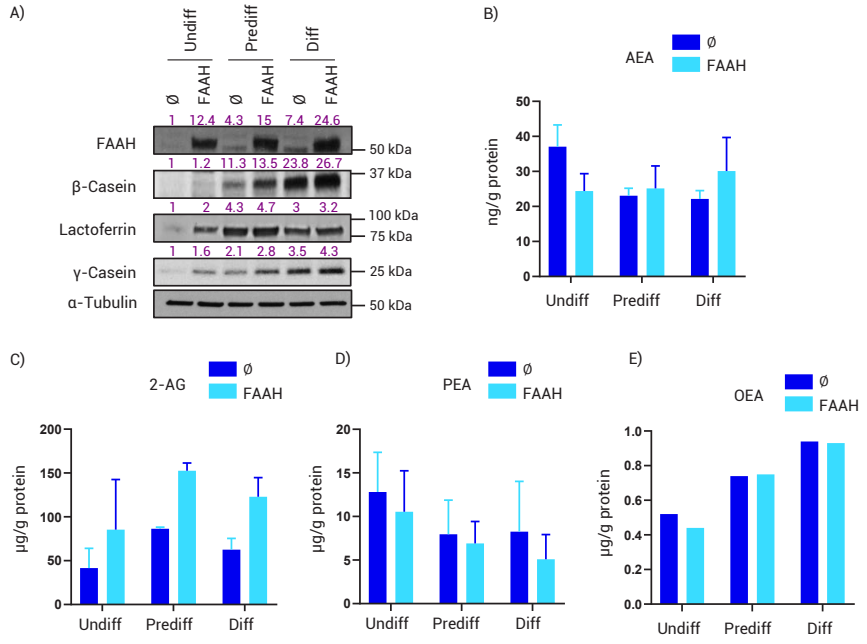

Figure R6. Constitutive FAAH expression in HC11 cells activates premature lactogenic differentiation. A) Representative WB analysis of β-Casein and other milk proteins during the complete differentiation of HC11 cells harboring an empty (Ø) or a FAAH overexpression vector. Densitometric values after normalization against α-Tubulin and control condition are depicted in purple. B)-E) Levels of the main FAAH substrates normalized to protein content. AEA: anandamide (B); 2-AG: 2-arachidonoylglycerol (C); PEA: palmitoylethanolamide (D); OEA: oleoylethanolamide (E). Values represent mean ± SEM of two independent samples except for OEA, which could only be measured once. Student's t-test: ns.

Collectively, the results obtained from the experiments modulating the activity and expression of FAAH support the idea that a high endogenous tone of its substrates, which is ultimately controlled by its activity, inhibits lactogenic differentiation in MECs.

FAAH MODULATES MEC DIFFERENTIATION THROUGH A CB_1R-MEDIATED MECHANISM

To unmask the primary molecular target of the lactogenic differentiation inhibition induced by FAAH substrates, we next blocked a battery of receptors that can be engaged and activated by these compounds. Differentiating HC11 cells were incubated with selective antagonists for CB_1R (SR141716, SR1), CB_2R (SR144528, SR2), PPARα (GW 6471) or PPARγ (GW 9662) in the presence of URB 597. Only SR1 completely prevented the downregulation of β-Casein triggered by URB 597 (**FIG. R7A**), indicating that CB_1R mediates the FAAH-controlled inhibition of MEC differentiation. A partial prevention of the downregulation of β-Casein by SR2 was also observed, suggesting CB_2R might be partly involved too. Of interest, SR1 not only prevented URB 597 effect on β-Casein levels, but increased them above those of the vehicle-treated cells (**FIG. R7A**). To better understand the importance of this observation, we treated HC11 cells during differentiation with SR1 in the absence of URB 597 and detected a concentration-dependent increase in β-Casein (**FIG. R7B**), suggesting that HC11 cells have an endogenous tone of FAAH substrates acting on CB_1R or constitutively active CB_1R that prevent them from undergoing complete differentiation. Finally, WB analysis of CB_1R in HC11 cells at different points of the differentiation process revealed that the expression of the receptor is downregulated

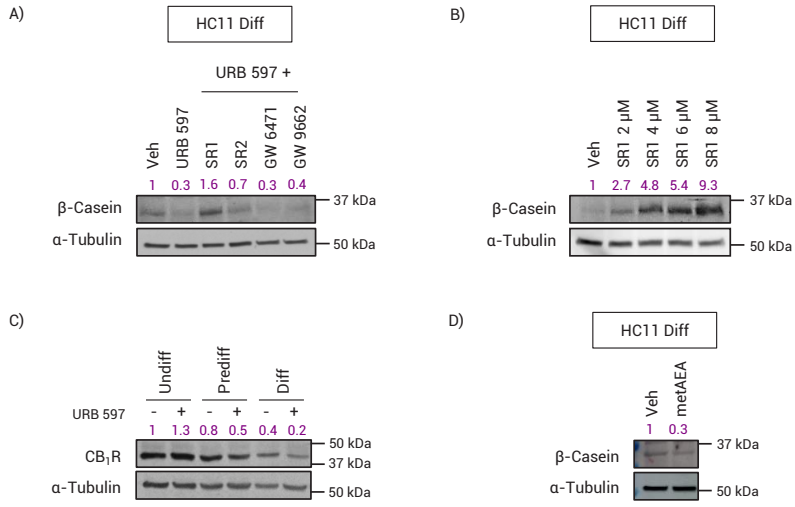

Figure R7. Activation of CB_1R blocks lactogenic differentiation of HC11 cells. A) Representative WB analysis of β-Casein in HC11 cells after being differentiated in the presence of URB 597 at 5 µM and selective receptor antagonists at 1 µM. B) Representative WB analysis of β-Casein in HC11 cells after being differentiated in the presence of increasing concentrations of the CB_1R selective antagonist SR1. C) Representative WB analysis of CB_1R during HC11 differentiation in the presence or absence of URB 597 at 5 µM. D) Representative WB analysis of β-Casein in HC11 cells after being differentiated in the presence of metAEA at 0.5 µM. Densitometric values after normalization against α-Tubulin and control condition are depicted in purple.

during differentiation (opposite to what happens with FAAH expression), which is more pronounced in the presence of URB 597, further supporting a role for a CB_1R tone in preventing HC11 differentiation (**FIG. R7C**).

Except for AEA, most endogenous NAEs do not bind to CB_1R. To examine whether this eCB was the responsible for the differentiation inhibiting effects described above, we challenged differentiating HC11 cells with metAEA, a non-hydrolysable AEA analogue. MetAEA phenocopied the effect of FAAH pharmacological inhibition (i.e., a downregulation of β-Casein), suggesting that endogenous AEA is responsible for the effects on differentiation found upon FAAH modulation (**FIG. R7D**).

GENETIC INACTIVATION OF FAAH DOWNREGULATES PRLR AND HINDERS LACTOGENESIS IN VIVO

HC11 differentiation closely resembles the part of mammalian lactogenesis that follows parturition (i.e., lactogenesis II), where alveolar MECs (aMECs) undergo terminal differentiation in response to PRL for milk synthesis and delivery. Since FAAH was found to be an important modulator of this process *in vitro*, we hypothesized that genetic inactivation of FAAH in the mammary gland would have deleterious effects over lactation in mice.

To test this hypothesis, we compared the mammary tissue of FAAH $^{+/+}$ and FAAH $^{-/-}$ females at different time points of lactation. Analysis of histological sections revealed similar grade of lobuloalveolar expansion in FAAH $^{-/-}$ and FAAH $^{+/+}$ littermates. However, alveoli from FAAH $^{-/-}$ mice were smaller and less distended, a difference that started being evident as soon as lactation day 5 (L5) and was maintained, at least, until lactation day 10 (L10) (**FIG. R8A**). Although the diameter of the alveoli in FAAH $^{-/-}$ animals was smaller, they contained similar numbers of epithelial cells than FAAH $^{+/+}$ mice, indicating a failure of the final stage of functional differentiation (Brisken *et al*., 1999). This was further supported by the observation that FAAH $^{-/-}$ mammary glands showed a (not statistically significant) dowregulation in mRNA levels of *Csn2* (encoding β-Casein) at the same time points (**FIG. R8B**), and of β-Casein protein at L5 and L15, although not L10 (**FIG. R8D**).

Given that PRLR activation is essential for PRL-mediated differentiation of aMECs, and that FAAH seems to control MEC differentiation, we analyzed whether there was any association between FAAH and PRLR levels. Analysis of the mammary tissue showed that FAAH $^{-/-}$ animals had a lower (although not statistically significant) expression of PRLR mRNA (**FIG. R8C**) and protein (**FIGs. R8D** and **R8E**) than their wild type littermates, suggesting that FAAH-deficient aMECs may not undergo complete differentiation because they exhibit partial resistance to PRL action. Consistent with this idea, URB 597 decreased the levels of the PRLR transcript in differentiated HC11 cells (**FIG. R8F**).

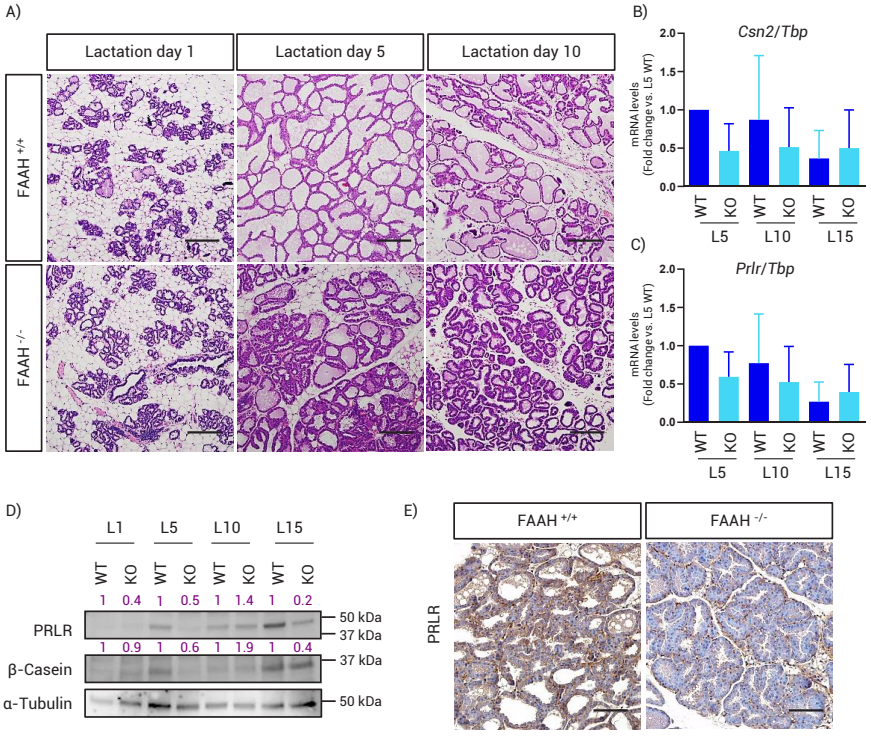

Figure R8. FAAH $^{-/-}$ mice show delayed mammary gland development during lactation associated to lower PRLR expression. A) H&E staining of mammary glands harvested at L1, L5 and L10. n = 2 mice per time point. Scale bar = 250 µm. B), C) qPCR analysis of *Csn2* (B) and *Prlr* (C) mRNA expression in whole tissue lysate of mammary glands harvested at L5, L10 and L15. Analysis at L1 could not be performed due to insufficient concentration of mRNA. Expression levels were normalized against *Tbp*. Data are shown as mean ± SEM from n = 2 mice per time point. Student's t-test: ns. D) Representative WB analysis of β-Casein and PRLR at L1, L5, L10 and L15. Densitometric values after normalization against α-Tubulin and WT condition for every time point are depicted in purple. E) IHC detection of PRLR in samples at L10. Scale bar = 100 µm. F) qPCR analysis of *Prlr* mRNA expression of HC11 cells after being differentiated in the presence of the FAAH inhibitor URB 597 at 5 µM. Expression levels were normalized against *Tbp*. Data are shown as mean ± SEM from at least 3 independent experiments. Student's t-test: * $p < 0.05$.

Together, our *in vitro* and *in vivo* results point to the existence of an eCB-mediated mechanism of lactogenic differentiation inhibition in MECs, which is driven by AEA activating CB_1R and relieved upon FAAH increase to allow cell specialization, that may cause PRLR-associated developmental defects in the mammary gland of FAAH $^{-/-}$ mice during lactation.

AIM 2 | ROLE OF FAAH IN BREAST CANCER

FAAH EXPRESSION IS ASSOCIATED WITH HIGHLY DIFFERENTIATED BC PHENOTYPES (LUMINAL SUBTYPE AND LOW HISTOLOGICAL GRADES)

Results presented in the first part of this thesis manuscript strongly support a role of FAAH in the control of MEC differentiation. Considering that 1) deregulation of cell fate (including differentiation decisions) is one of the main features of tumor cells and 2) other members of the ECS have been shown to be deregulated in cancer, we next aimed to explore the role of FAAH in breast cancer (BC).

First, we analyzed the expression of FAAH and other constituents of the eCB synthesis and degradation machinery in human samples *in silico*. For that, we used the BC gene-expression miner (bc-GenExMiner), a BC–associated online tool whose last version includes tumor transcriptomic data from published annotated microarrays (n = 10 716) and RNA-seq (n = 4712) (Jézéquel *et al.*, 2021). bc-GenExMiner revealed that, out of the examined genes, *FAAH* was the only one showing differential expression between BC subtypes. Thus, *FAAH* expression was higher in luminal tumors when compared to basal tumors (**FIG. R9A**). Similar results were observed when analyzing the METABRIC database, which includes genomic information from 2000 breast tumors and non-transformed controls (Curtis *et al.*, 2012) (**FIG. R9B**). Interestingly, *FAAH* levels in the non-transformed mammary gland were lower than those in luminal BC, but higher than those in basal BC, suggesting that FAAH variations during malignant transformation to BC may be highly dependent on the tumor subtype.

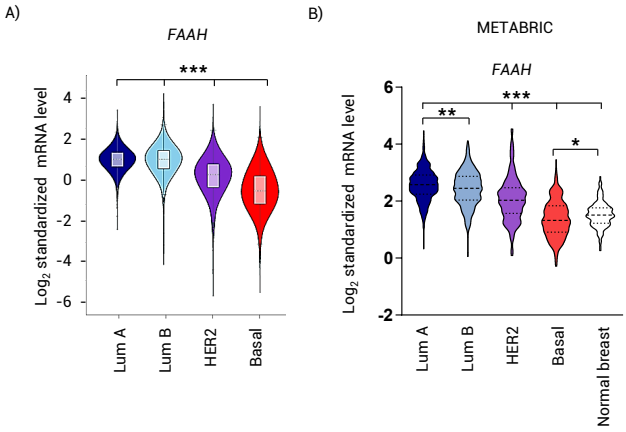

Figure R9. ***FAAH* expression is associated with the luminal BC subtype.** A) Relative *FAAH* mRNA expression in the different BC intrinsic subtypes according to the bc-GenEx-Miner v4.5 tool. Student's t-test: *** $p < 0.001$. B) Relative *FAAH* mRNA expression in BC intrinsic subtypes and normal breast tissue in the microarray dataset published by Curtis *et al.*, 2012 (study code METABRIC). Student's t-test: * $p < 0.05$, ** $p < 0.01$, *** $p < 0.001$.

No significant differences between BC subtypes were found regarding mRNA expression of other eCB-synthesizing (*NAPE-PLD*, *DAGLA* and *DAGLB*) or eCB-degrading enzymes (*MGLL*) (**FIG. R10**).

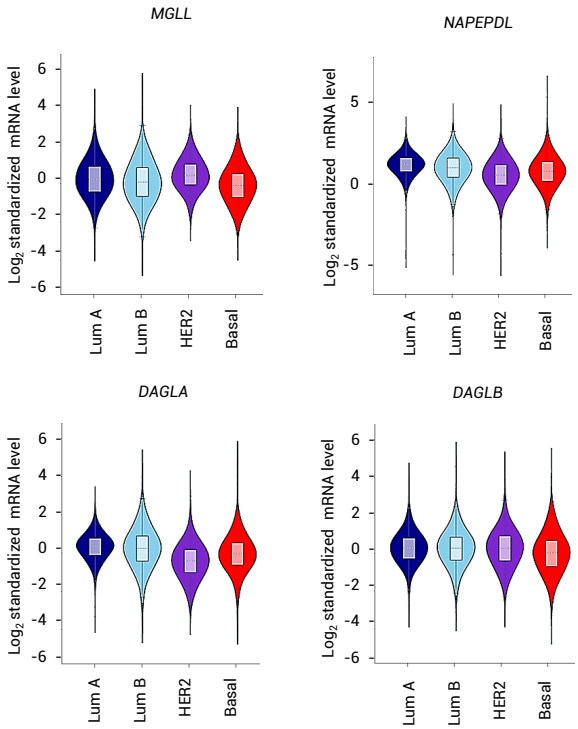

Figure R10. mRNA expression of other enzymes involved in the biosynthesis and degradation of eCBs is not associated with any BC subtype. Relative mRNA expression of eCB-synthesizing (*NAPEPLD*, *DAGLA*, *DAGLB*) and eCB-degrading (*MGLL*) enzymes other than FAAH in BC intrinsic subtypes according to the bc-GenEx-Miner v4.5 differential gene expression analysis. Student's t-test: ns.

We then analyzed FAAH protein expression in a series of human breast tumor samples (n = 617), included in different tissue microarrays (TMA), all here referred to as TMA #1. FAAH staining by IHC was scored as 0 (no staining), 1 (weak staining), 2 (moderate staining) or 3 (high staining) (**FIG. R11A**). FAAH expression was highly associated with the presence of hormone receptors (HR), mainly estrogen receptor (ER). Thus, 83 % of all ER+ samples expressed detectable levels of FAAH, while 85 % of the ER- (i.e., less differentiated tumors) had no-low FAAH expression (**FIG. R11B**). Conversely, most triple-negative (TN) tumors (86 %), which have less differentiated phenotypes when compared to HR+ tumors, expressed no-low FAAH (**FIG. R11B**). A moderate association between FAAH expression and HER2+ tumors was detected (**FIG. R11B**).

A)

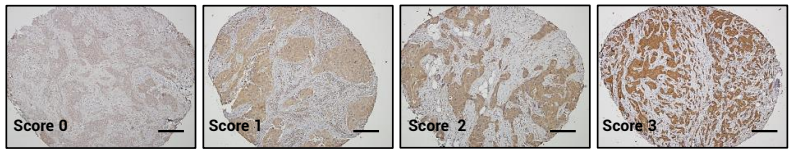

B)

		n	FAAH staining (Score) 0	1	2	3	p-value
Hormone receptor status	Positive	491	82 (17%)	198 (40%)	160 (33%)	51 (10%)	$2x10^{-7}$
	Negative	126	35 (28%)	73 (58%)	17 (13%)	1 (1%)	
Estrogen receptor status	Positive	466	78 (16%)	180 (39%)	157 (34%)	51 (11%)	$2x10^{-9}$
	Negative	142	39 (27%)	82 (58%)	20 (14%)	1 (1%)	
Progesterone receptor status	Positive	393	65 (17%)	163 (41%)	126 (32%)	39 (10%)	0.01
	Negative	215	53 (24%)	98 (46%)	51 (24%)	13 (6%)	
HER2 status	Positive	150	27 (18%)	79 (53%)	39 (26%)	5 (3%)	0.005
	Negative	350	69 (19%)	135 (39%)	108 (31%)	38 (11%)	
Triple negative status	Positive	47	20 (43%)	20 (43%)	6 (13%)	1 (2%)	$7x10^{-5}$
	Negative	450	76 (17%)	194 (43%)	140 (31%)	40 (9%)	
Grade	1	74	11 (15%)	24 (32%)	28 (38%)	11 (15%)	$7x10^{-4}$
	2	371	64 (17%)	154 (42%)	116 (31%)	37 (10%)	
	3	153	36 (23%)	81 (53%)	30 (20%)	6 (4%)	

Figure R11. FAAH expression is associated with HR+ status and negatively associated with basal/TNBC status in human breast tumors. A) Representative images showing FAAH expression scoring according to intensity staining in samples from TMA #1: scores 0, 1, 2, and 3 correspond to no, weak, moderate, and high staining, respectively. Scale bar = 500 μm. B) Association between FAAH expression and the molecular features of breast tumor samples included in TMA #1. The Pearson's chi-squared test was used for statistical analysis.

The association between FAAH expression and ER+ status suggests that FAAH might be regulated by ER signaling. In line with this idea, mRNA of *FAAH* was responsive to E_2 (**FIG. R12A**) and to ER silencing in luminal BC cell lines MCF7 and T-47D (Al Saleh *et al*.. 2011) (**FIG. R12B**).

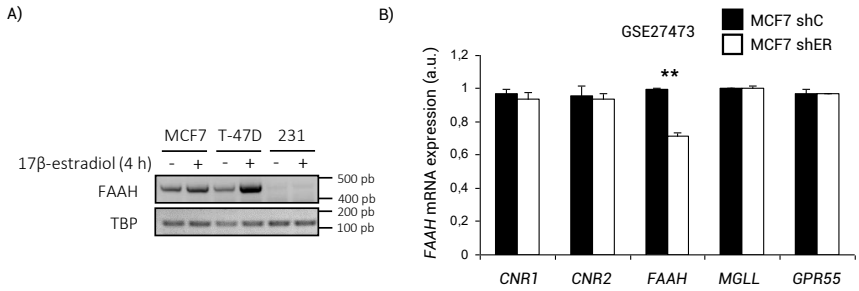

Figure R12. A) RT-PCR analysis of *FAAH* levels in luminal BC cell lines after treatment with 17β-estradiol at 10 nM. ER- cell line MDA-MB-231 was used as negative control. B) mRNA expression of several ECS components in ER-silenced MCF7 cells obtained from the microarray dataset by Al Saleh *et al*., 2010 (study code GSE27473). Student's t-test: ** $p < 0.01$.

Observations in human samples were confirmed at the mRNA level by bc-GenExMiner analysis. As shown in **FIG. R13**, *FAAH* mRNA expression was higher in HR+ tumors than in HR- tumors, and in non-TN or non-basal-like tumors vs. TN and basal-like tumors.

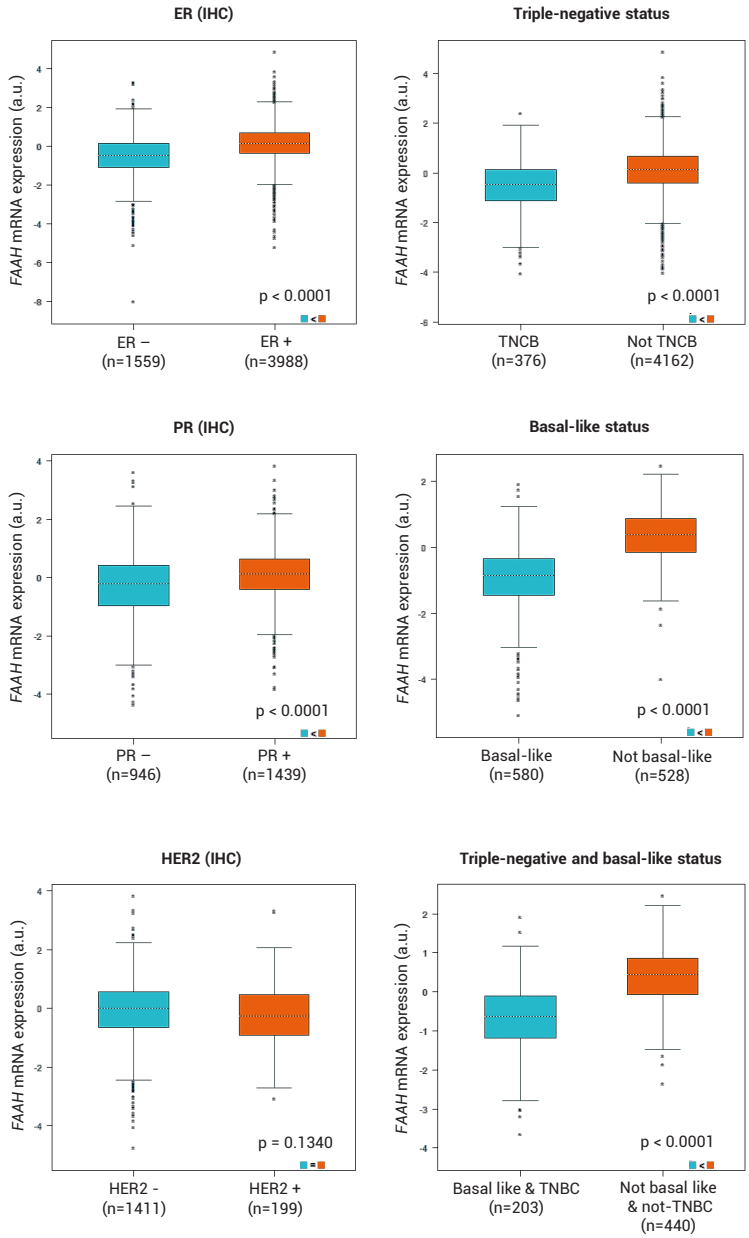

Figure R13. ***FAAH*** **mRNA expression is strongly associated with HR+ status and negatively associated with basal/TNBC status in human BC.** Relative *FAAH* mRNA expression in BC samples grouped by their HR or TN and basal-like status according to the bc-GenEx-Miner v4.5 differential gene expression analysis. Student's t-test p-values are shown.

In line with the observation that FAAH expression is associated with more differentiated tumor phenotypes, we also found an association between FAAH staining in TMA #1 and tumor histological grade. Thus, very few grade 3 (i.e., poorly differentiated) tumors expressed high levels of FAAH (4 %), and most of them expressed no-low FAAH (76 %). On the contrary, most (85 %) grade 1 (i.e., highly differentiated) tumors expressed detectable FAAH levels (**FIG. R11B**). Similar observations were made at the mRNA level in samples from METABRIC (Curtis *et al.*, 2012) (**FIG. R14A**) and Rosetta2002 (van de Vijver *et al.*, 2002) (**FIG. R14B**) databases, where lower FAAH expression was found in grade 3 tumors when compared to grades 1 or 2.

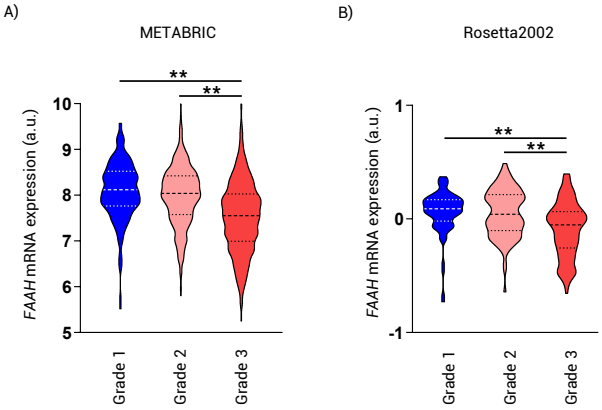

Figure R14. FAAH expression is associated with low histological grades. Relative *FAAH* mRNA expression in BC samples grouped by tumor grade obtained from the microarray dataset published by Curtis *et al.*, 2012 (study code METABRIC) (A) and van de Vijver *et al.*, 2002 (study code Rosetta2002) (B). Student's t-test: ** $p < 0.01$.

FAAH EXPRESSION IS ASSOCIATED WITH GOOD PATIENT PROGNOSIS IN BC

Since FAAH expression was associated with highly differentiated (i.e., less aggressive) BC phenotypes, we next aimed at investigating whether its levels in human tumors could provide prognostic patient information. We therefore analyzed potential associations between FAAH expression in samples included in TMA #1 and patient outcome. We found that patients with low FAAH expressing tumors (staining scores 0 and 1) had a higher probability to develop distant metastases (**FIG. R15A**) and significantly decreased overall survival rates (**FIG. R15B**) than those with high FAAH expression (scores 2 and 3). Similar observations were made when *FAAH* mRNA levels were analyzed in the Kaplan-Meier plotter (KM-Plotter) database (Győrffy *et al.*, 2021), which gathers gene expression data and survival information of 7830 BC patients downloaded from Gene Expression Omnibus (**FIGs. R15C** and **R15D**). These associations were not evident with the other eCB-degrading enzyme, MAGL (**FIGs. R15E** and **R15F**).

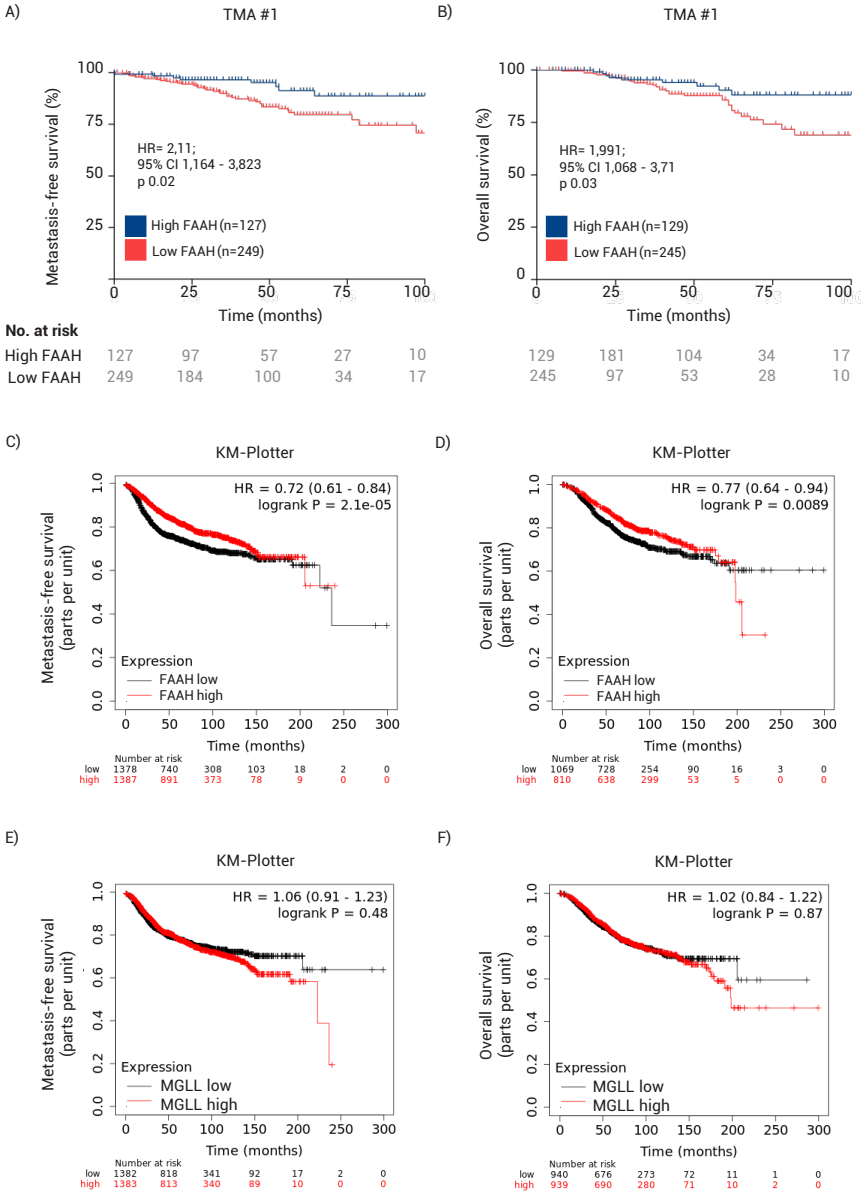

Figure R15. Low tumor FAAH (but not MAGL) expression is associated with poor patient prognosis. A), B) Kaplan-Meier curves for metastasis-free survival (A), and overall survival (B) in patients with high and low FAAH mRNA expression included in TMA #1. Survival curves were statistically compared by the logrank test. C), D) Kaplan-Meier curves for metastasis-free survival (C), and overall survival (D) in BC patients with high and low *FAAH* mRNA expression obtained from Győrffy *et al.*, 2021, through the KM-plotter (www.kmplot.com). E), F) Kaplan-Meier curves for metastasis-free survival (E), and overall survival (F) in BC patients with high and low *MGLL* expression, from the KM-plotter.

In further support of these observations, *FAAH* expression was found significantly higher in the group of tumors with a good prognosis signature according to the genetic classification established by van de Vijver and collaborators (van de Vijver *et al.*, 2002) (**FIG. R16**).

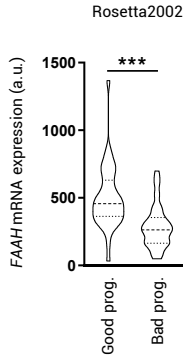

Figure R16. Relative *FAAH* mRNA expression in BC samples classified according to the prognosis signature established by van de Vijver et al., 2002 (study code Rosetta2002). Student's t-test: *** $p < 0.001$.

It is worth noticing that low *FAAH* expression was linked to BC metastasis to the lungs but not to brain or bone, according to the GSE2034 (Wang *et al.*, 2005) (**FIG. R17**) and Rosetta2002 (van de Vijver *et al.*, 2002) (**FIG. R18**) datasets.

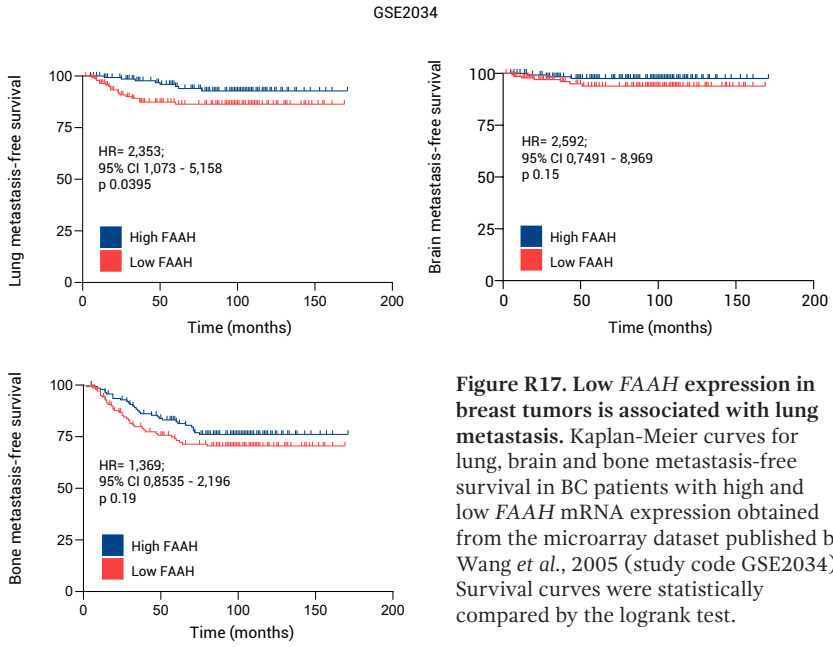

Figure R17. Low *FAAH* expression in breast tumors is associated with lung metastasis. Kaplan-Meier curves for lung, brain and bone metastasis-free survival in BC patients with high and low *FAAH* mRNA expression obtained from the microarray dataset published by Wang *et al.*, 2005 (study code GSE2034). Survival curves were statistically compared by the logrank test.

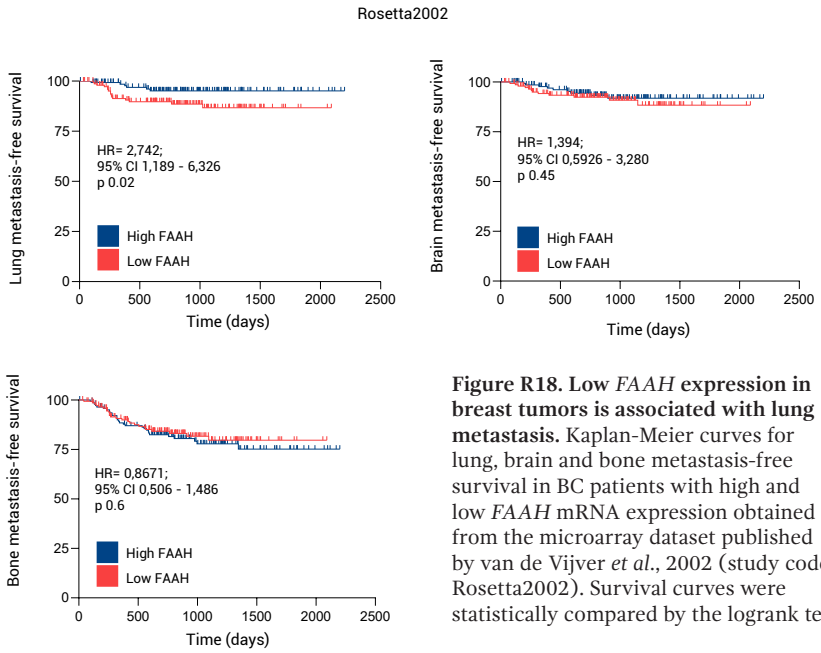

Figure R18. Low *FAAH* expression in breast tumors is associated with lung metastasis. Kaplan-Meier curves for lung, brain and bone metastasis-free survival in BC patients with high and low *FAAH* mRNA expression obtained from the microarray dataset published by van de Vijver *et al.*, 2002 (study code Rosetta2002). Survival curves were statistically compared by the logrank test.

In addition, FAAH expression was found significantly lower in the group of tumors expressing the lung metastasis signature (LMS) established by Minn and collaborators (Minn *et al.*, 2005) (**FIG. R19**).

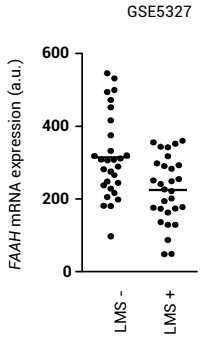

Figure R19. Relative *FAAH* mRNA expression in BC samples classified according to the lung metastasis signature (LMS) established by Minn *et al.*, 2005 (study code GSE5327). Student's t-test: *** $p < 0.001$.

Prognostic associations made from tumor data including all intrinsic subtypes may be biased considering that FAAH has a predominant expression in luminal BC, which is the BC subtype with greatest inherent survival rates. To rule out the possibility that our conclusions were affected by this limitation, we next analyzed FAAH protein expression in a second series of human breast tumor samples (TMA #2), containing the primary tumor and the matched lymph node metastasis of 276

non-treated patients with luminal BC. FAAH staining was scored as described in FIG. R11A and, as expected because of their luminal nature, was clearly detectable in most of the samples, with moderate-high signal in 65 % of them (**FIG. R20A**).

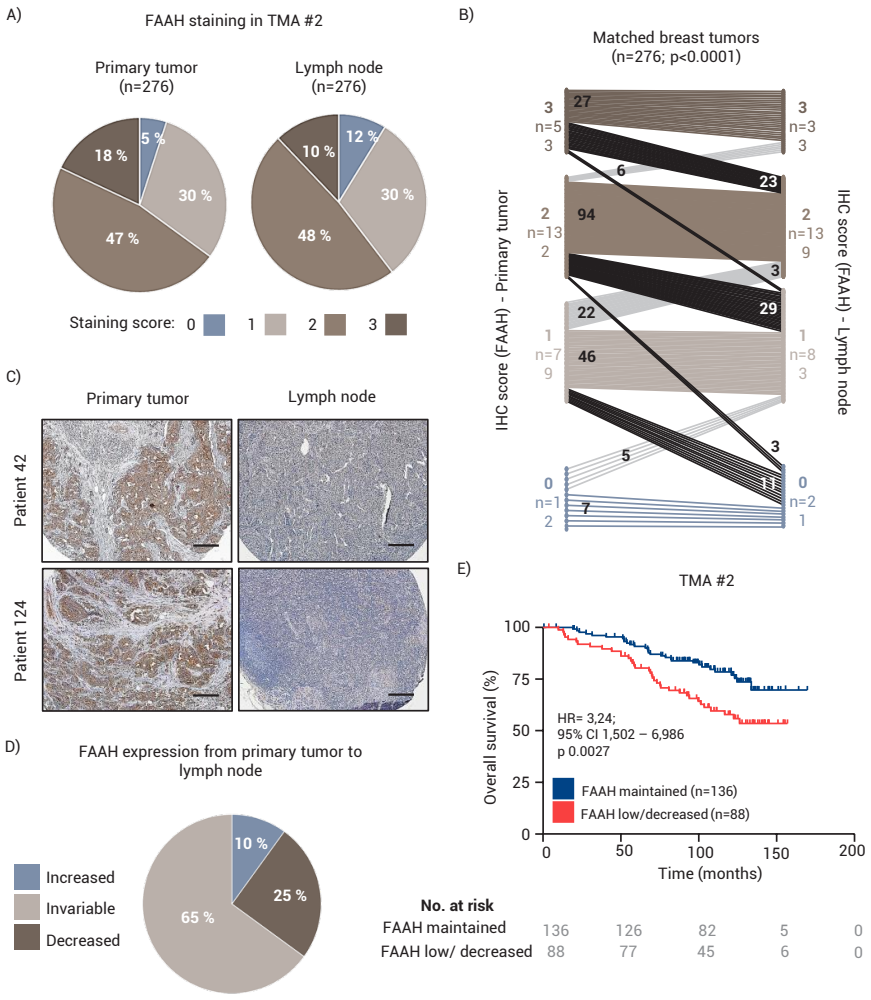

Figure R20. FAAH is frequently downregulated during metastatic progression in luminal BC. A) Pie charts representing FAAH expression (as determined by staining scoring) in samples of primary tumor and lymph node (LN) metastasis from patients included in TMA #2. B) Matched FAAH expression in samples of primary tumor and LN metastasis from patients included in TMA #2. p-value was calculated by paired two-tailed Student's t-test. C) Representative IHC images showing FAAH expression decrease in LN metastasis compared to primary tumor. Scale bar = 250 µm. D) Pie chart representing variations in FAAH expression from primary tumor to lymph node metastasis in TMA #2. E) Kaplan-Meier curve for overall survival from patients included in TMA #2. "FAAH maintained" group includes patients with high FAAH expression in primary tumor and lymph node metastasis. "FAAH low/decreased" includes patients with low FAAH expression in primary tumor and lymph node and patients with decreased FAAH expression in the lymph node compared to the primary tumor. Survival curves were statistically compared by the logrank test.

Our results show an overall decrease in FAAH expression in a significant proportion of the metastases when compared to the corresponding primary tumors (**FIG. R20B**). Specifically, 25 % of the pair-matched biopsies showed a decrease in FAAH in the metastatic sample vs. only 10 % of them showing an increase (**FIGs. R20C** and **R20D**). Additionally, patients with high FAAH expression in both the primary tumor and the lymph node metastasis ("FAAH maintained") exhibited higher probability of survival than those whose expression was either invariably low or decreased in the metastasis vs. the primary tumor ("FAAH low/lost") (**FIG. R20E**).

Together, these results point to a strong association between low FAAH expression and high tumor aggressiveness in BC. In further support of this idea, FAAH immunostaining was absent in breast tumor cells at the invasion front as well as in cells that have detached from the primary tumor (**FIG. R21**), which constitute the more invasive (and therefore aggressive) subpopulation of cancer cells.

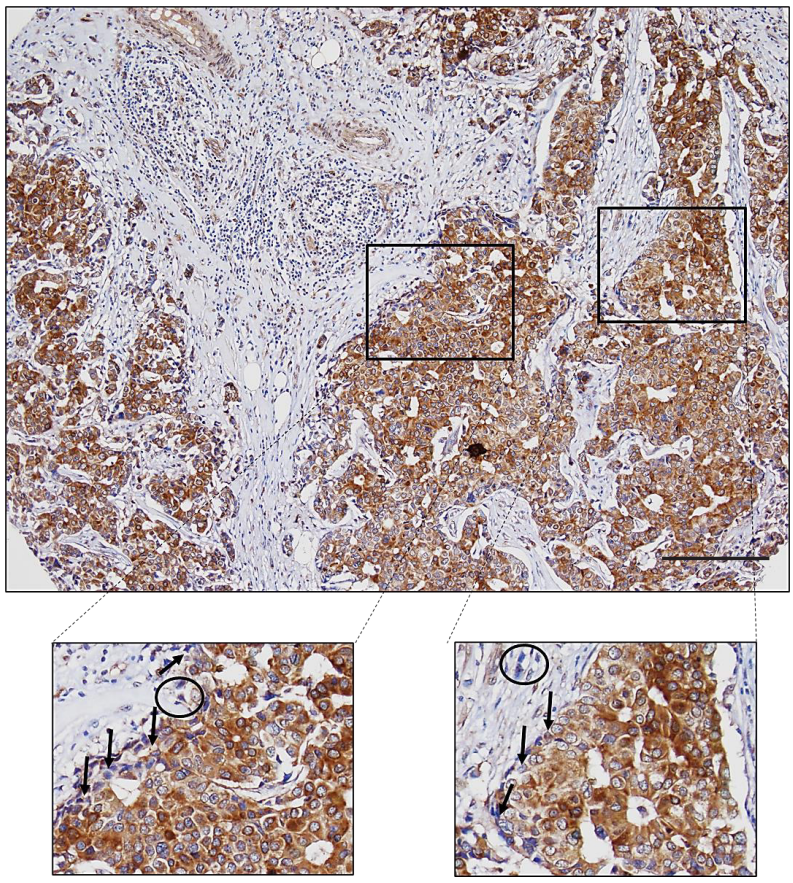

Figure R21. Representative image and detail magnification showing downregulation of FAAH staining in the cells from the invasion front in tumor samples from TMA #2. Scale bar = 250 μm.

GENETIC ABLATION OF FAAH PROMOTES BREAST TUMOR PROGRESSION IN MICE

To analyze whether there was a cause-and-effect link between FAAH expression and reduced BC aggressiveness, we modulated the expression of FAAH in a well-established animal model of metastatic BC: the MMTV-neu mouse. This mouse strain expresses the *Neu* oncogene (the rat ortholog of *HER2*), driven by the mouse mammary tumor virus (MMTV) promoter, and develops luminal-like breast tumors and lung metastases. MMTV-neu:FAAH $^{-/-}$ mice and their corresponding MMTV-neu:FAAH $^{+/+}$ littermates were generated by breeding MMTV-neu mice with FAAH $^{-/-}$ mice (see Methods) (**FIG. R22A**). Tumor generation and progression was then compared in the two genotypes at different time points: T0 (prelesion mammary gland), T1 (tumor onset), T2 (40 days after tumor onset) and T3 (90 days after tumor onset, culling point) (**FIG. R22B**).

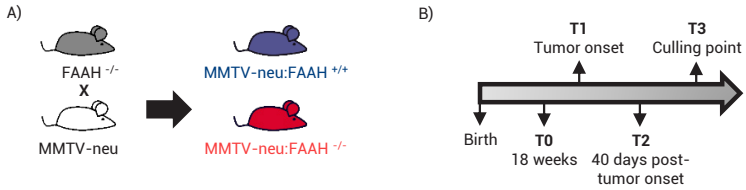

Figure R22. Experimental set up. A) MMTV-neu mice were bred with FAAH $^{-/-}$ mice (see Methods) to generate MMTV-neu:FAAH $^{+/+}$ and MMTV-neu:FAAH $^{-/-}$ littermates that were used to monitor tumorigenesis. B) 10-15 animals per genotype and time point were euthanized and tissue was harvested at four different time points.

Genetic inactivation of FAAH delayed tumor onset (**FIG. R23A**) but enhanced tumor growth rate (**FIG. R23B**), which was accompanied by increased levels of proliferating cell nuclear antigen (PCNA) in tumor cells (**FIG. R23C**).

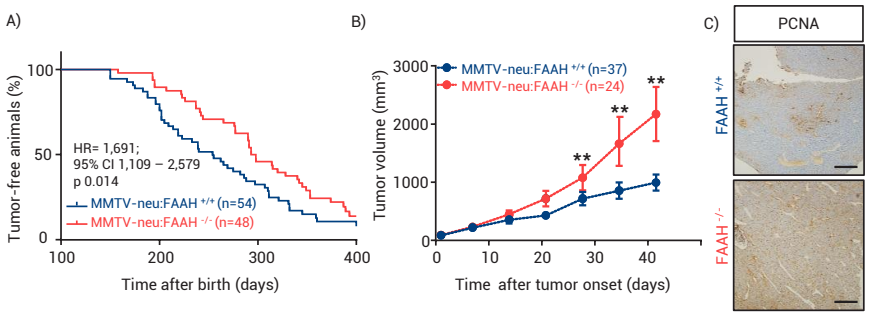

Figure R23 FAAH knock-out delays tumor onset but enhances tumor growth in a mouse model of spontaneous breast tumor formation. A) Kaplan-Meier curves for tumor onset. Results were analyzed by the logrank test. B) Tumor volume progression 50 days after first tumor arousal. Student's t-test: ** $p < 0.01$ vs. MMTV-neu:FAAH $^{+/+}$. C) Immunohistochemical analysis of proliferating cell nuclear antigen (PCNA) in tumors. Scale bar = 250 µm.

First, we observed that MMTV-neu:FAAH $^{-/-}$ mice grew tumors that had higher levels of AEA (but not 2-AG) than MMTV-neu:FAAH $^{+/+}$ animals, and that both genotypes had higher AEA levels in tumors than in their non-transformed counterpart tissues (i.e., T0) (**FIG. R24**).

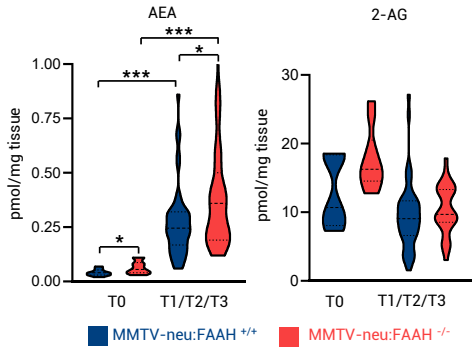

Figure R24. Analysis of anandamide (AEA) and 2-arachidonoylglycerol (2-AG) of tumors at different time points (T1, T2 and T3) and prelesion mammary glands (T0). Student's t-test: * $p < 0.05$, ** $p < 0.01$, *** $p < 0.001$.

Histological analysis of the generated tumors revealed that, at 18 weeks after birth (T0), most of the MMTV-neu:FAAH $^{-/-}$ females showed activated lymph nodes while MMTV-neu:FAAH $^{+/+}$ females showed normal histology (**FIG. R25**). Upon early tumor detection (T1), FAAH deficient animals showed solid high-grade carcinomas with moderate lymphatic invasion while the wild type littermates developed low grade adenocarcinomas with no lymphatic invasion (**FIG. R25**). In more advanced stages of tumor progression (T2 and T3), both groups developed solid carcinomas with necrotic areas. However, MMTV-neu:FAAH $^{-/-}$ mice showed evident signs of lymphatic invasion (**FIG. R25**), characteristic of more aggressive tumors.

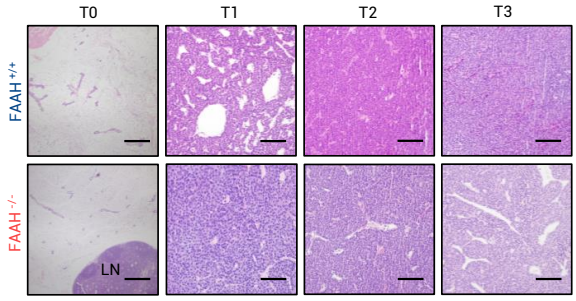

Figure R25. FAAH knock-out promotes the formation of higher grade tumors in MMTV-neu mice. A) Representative H&E images of the histology of the mammary gland before tumor onset (T0) and at different timepoints of tumor growth established in FIG. R22B. LN = lymph node. Scale bar = 250 μm.

At the molecular level, MMTV-neu:FAAH $^{+/+}$ mice showed a homogeneous luminal pattern (CK8 +), whereas MMTV-neu:FAAH $^{-/-}$ tumors consisted of different components with luminal (CK8 +) but mostly basal (CK14 +) identity (**FIG. R26**).

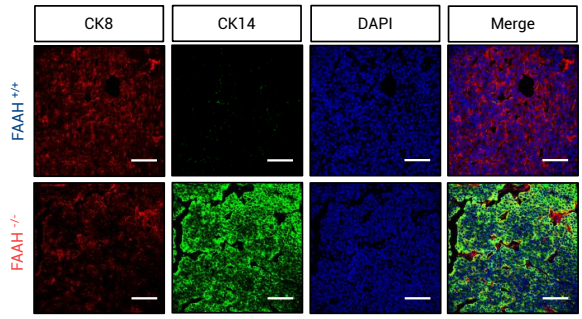

Figure R26. FAAH knock-out promotes the formation of more undifferentiated tumors in MMTV-neu mice. Immunofluorescence analysis of tumors for CK8 (red) and CK14 (green). Cell nuclei are stained in blue. Scale bar = 50 μm.

Finally, FAAH deficiency produced a remarkable increase in the lung metastasis rate (percentage of animals with metastases and number of metastasis per animal). Thus, while metastasis in MMTV-neu:FAAH $^{+/+}$ females was only evident at T3, MMTV-neu:FAAH $^{-/-}$ animals showed metastatic invasion as early as in T1, when the primary tumor had just begun to arise (**FIG. R27A**). Moreover, the number of metastases per animal was significantly higher in FAAH-deficient animals at T3 (**FIGs. R27B** and **R27C**).

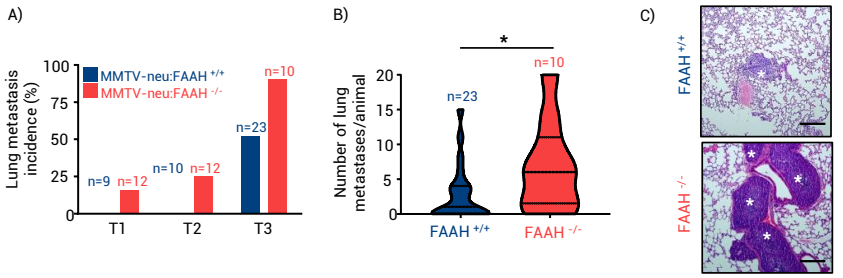

Figure R27. FAAH knock-out enhances lung metastasis rate in MMTV-neu mice. A) Percentage of animals with lung metastases at the time points established in FIG. R22B. B) Number of metastasis per animal at T3. Student's t-test: * $p < 0.05$. C) Representative pictures of lung metastases at T3. Scale bar = 250 μm.

To shed some light into the molecular mechanisms underlying the effect of FAAH on BC progression, we analyzed the expression of 84 BC associated genes in the MMTV-neu:FAAH $^{+/+}$ and $^{-/-}$ mice by means of a PCR array (**TABLE R1** and **FIG. R28**).

Gene	Log_2 KO vs. WT	p	Gene	Log_2 KO vs. WT	p
Abcb1a	0,807	0,262	*Jun*	-0,074	0,980
Abcg2	0,390	0,291	*Krt18*	-0,304	0,061
Adam23	1,287	0,080	*Krt19*	1,275	0,011
Akt1	-0,269	0,267	*Krt5*	2,302	0,010
Apc	0,124	0,371	*Krt8*	-0,304	0,382
Ar	-0,074	0,955	*Mapk1*	-0,014	0,945
Atm	-0,074	0,452	*Mapk3*	-0,218	0,138
Bad	-0,515	0,104	*Mapk8*	-0,074	0,501
Bcl2	-0,089	0,405	*Mgmt*	0,057	0,864
Birc5	0,000	0,971	*Mki67*	0,322	0,299
Brca1	0,390	0,112	*Mlh1*	-0,105	0,686
Brca2	0,986	0,131	*Mmp2*	0,465	0,284
Ccna1	0,322	0,542	*Mmp9*	-2,837	0,348
Ccnd1	-0,029	0,946	*Muc1*	-0,761	0,186
Ccnd2	0,848	0,005	*Myc*	0,189	0,627
Ccne1	0,227	0,548	*Nme1*	-0,340	0,141
Cdh1	-0,059	0,916	*Notch1*	0,000	0,921
Cdh13	0,748	0,225	*Nr3c1*	0,043	0,731
Cdk2	0,070	0,716	*Pgr*	1,036	0,269
Cdkn1a	0,014	0,987	*Plau*	0,275	0,171
Cdkn1c	0,084	0,570	*Prdm2*	0,202	0,091
Cdkn2a	0,014	0,711	*Pten*	0,227	0,209
Csf1	0,287	0,258	*Ptgs2*	-0,474	0,298
Cst6	-0,454	0,041	*Pycard*	-0,454	0,231
Ctnnb1	-0,234	0,154	*Rarb*	0,310	0,348
Ctsd	-0,434	0,250	*Rassf1*	-0,014	0,866
Egf	-0,889	0,174	*Rb1*	-0,322	0,121
Egfr	0,356	0,231	*Serpine1*	1,029	0,018
Erbb2	-0,286	0,256	*Sfn*	-0,252	0,530
Esr1	-0,737	0,020	*Sfrp1*	0,632	0,273
Esr2	-1,059	0,040	*Slc39a6*	0,098	0,399
Foxa1	2,602	0,173	*Slit2*	1,189	0,247
Gata3	0,043	0,676	*Snai2*	1,220	0,238
Gli1	0,766	0,482	*Src*	0,084	0,662
Grb7	0,057	0,778	*Tff3*	0,766	0,284
Gstp1	-0,556	0,244	*Tgfb1*	-1,152	0,382
Hic1	0,536	0,016	*Thbs1*	0,411	0,177
Id1	1,138	0,115	*Trp53*	0,275	0,224
Igf1	0,214	0,593	*Trp73*	1,714	0,265
Igf1r	0,367	0,316	*Twist1*	0,669	0,264
Igfbp3	-0,234	0,739	*Vegfa*	0,333	0,542
Il6	1,521	0,169	*Xbp1*	-0,578	0,088

Table R1. Complete list of genes included in the RT² Profiler PCR array of mouse BC performed on MMTV-neu:FAAH $^{+/+}$ and MMTV-neu:FAAH $^{-/-}$ mice. Relative expression depicted as log_2 fold change of MMTV-neu:FAAH $^{-/-}$ vs. MMTV-neu:FAAH $^{+/+}$ and the corresponding p-value of the t-test are reported within the table. p-values < 0.05 are highlighted in green. Each value is the result of the mean of n = 3 mice.

Supporting a role for FAAH in maintaining a differentiated, luminal tumor phenotype, the expression of both isoforms of ER (*Esr1* and *Esr2*) as well as PR (although this change was not statistical significant) was downregulated in tumors from MMTV-neu:FAAH $^{-/-}$ mice when compared to MMTV-neu:FAAH $^{+/+}$, while the basal marker CK5 (*Krt5*) was upregulated (**FIG. R28**). In addition, although most of the differences in gene expression observed in the PCR array did not reach statistical significance (**TABLE R1**), several genes known to be markers of poor prognosis in BC (*Twist1*, *Snai2*, *Adam23*, *Abcb1a*, *Id1*) showed an upward trend in their expression in MMTV-neu:FAAH $^{-/-}$ tumors, consistent with their more aggressive behavior (**FIG. R28**).

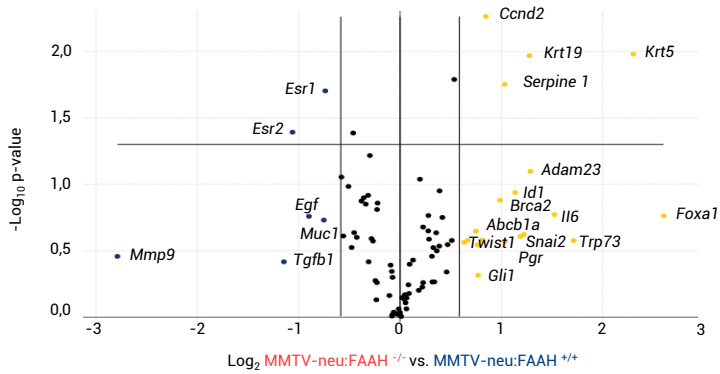

Figure R28. Volcano plot showing data of the RT² Profiler PCR array of mouse BC performed in MMTV-neu:FAAH $^{+/+}$ and $^{-/-}$ mice. The relative expression levels for each gene as $\log_2$ fold change of MMTV-neu:FAAH $^{-/-}$ vs. FAAH $^{+/+}$ are plotted against $-\log_{10}$ p-value. Upregulated and downregulated genes with a $\log_2$ fold change ≥ 0.58 (i.e., fold change ≥ 1.5) are depicted in yellow and blue, respectively, and statistically significant genes are over the horizontal line at $-\log_{10}$ p-value = 1.3 (i.e., p = 0.05). Each point is the result of the mean of n = 3 mice.

Collectively, these results reinforce the idea that FAAH plays a pivotal role in BC, specifically, inhibiting tumor progression.

FAAH KNOCK-OUT BESTOWS PRO-MIGRATORY AND PRO-INVASIVE PROPERTIES ON HUMAN BC CELLS IN VITRO AND IN VIVO

To better understand the role of FAAH in tumor progression, we performed a battery of experiments in cell models of BC. The analysis of *FAAH* mRNA expression in a panel of BC cell lines (Neve *et al*., 2006) revealed that, in line with our previous observations, the levels of this enzyme were higher in luminal than in basal cell lines, and in basal than in claudin-low cell lines (**FIG. R29A**). Similar results were obtained regarding FAAH protein expression, which was highly expressed in luminal cells and low/absent in basal and TN cells (**FIG. R29B**).

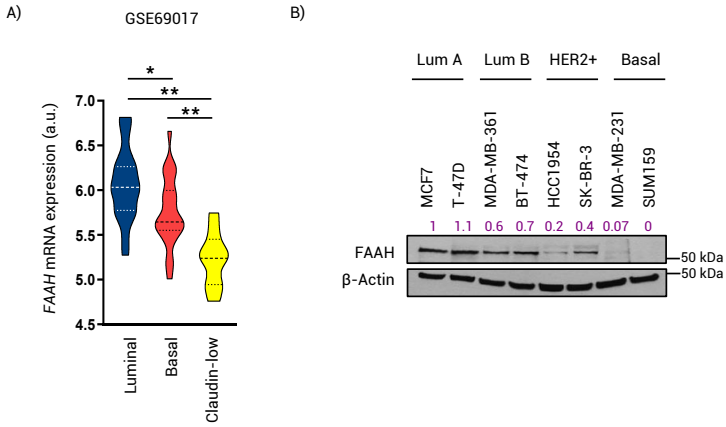

Figure R29. FAAH expression is high in luminal BC cell lines and low in basal and TNBC cell lines. A) *FAAH* mRNA expression in luminal, basal, and claudin-low BC cell lines obtained from the microarray dataset published by Neve *et al.*, 2006 (study code GSE69017). Student's t-test: * $p < 0.05$, ** $p < 0.01$. B) WB analysis of FAAH in a panel of human BC cell lines representative of the main intrinsic subtypes. Densitometric values after normalization against β-Actin and control condition are depicted in purple.

Based on these results, we decided to downregulate the expression of FAAH in a luminal A (highly FAAH expressing) cell line (T-47D) and to overexpress it in a basal (low FAAH expressing) cell line (MDA-MB-231), and analyze the functional impact of these modifications on cellular capabilities related to tumor progression.

First, we knocked-out (KO) *FAAH* in T-47D cells by using CRISPR-Cas9 technology (FAAH KO cell line), and then generated another T-47D-derived cell line by overexpressing FAAH in the FAAH KO cell line with a lentiviral vector (rescue cell line) (**FIG. R30A**). Visual analysis of the cell cultures revealed that, while parental (i.e., scrambled or SCR) T-47D cells had a cuboidal aspect and were densely packed in an ordered cobblestoned pattern, FAAH KO cells had a more fusiform morphology and appeared in disordered patterns, as found in less differentiated cultures or cultures that have undergone epithelial-to-mesenchymal transition (EMT). FAAH rescue cells recovered the morphology of parental T-47D cells (**FIG. R30B**).

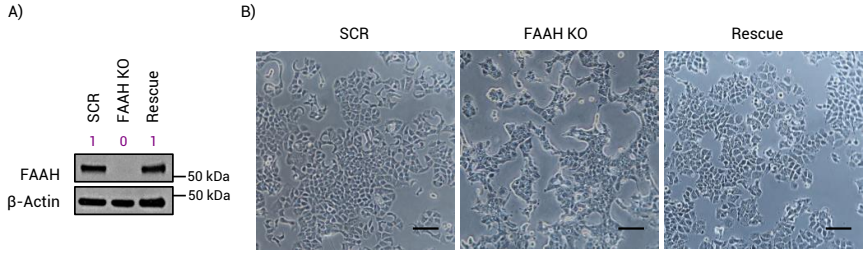

Figure R30. CRISPR-Cas9-mediated knock-out of FAAH in T-47D luminal BC cells. A) Representative WB analysis of FAAH in T-47D SCR, FAAH KO and rescue cells. Densitometric values after normalization against β-Actin and control condition are depicted in purple. B) Bright-field images showing morphologic variations of T-47D cell sublines. Scale bar = 100 μm.

Consistent with their morphology, T-47D FAAH KO cells expressed lower levels of epithelial markers (i.e., E-Cadherin) and higher levels of mesenchymal/progression (i.e., Vimentin) markers than parental and rescue sublines (**FIG. R31**).

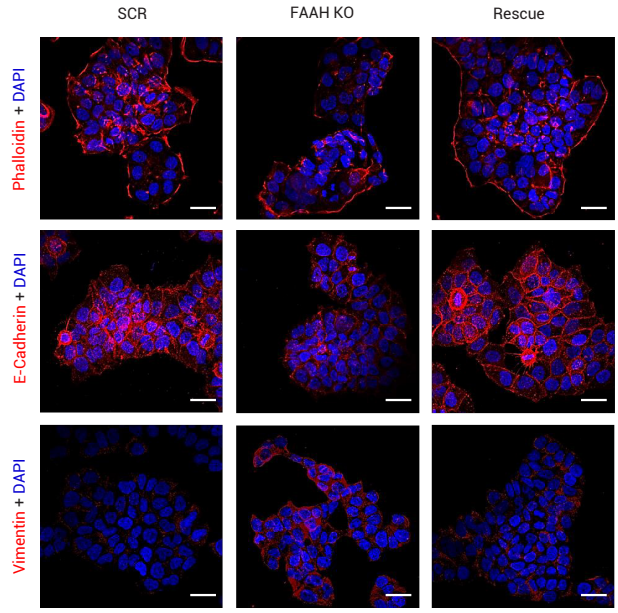

Figure R31. FAAH silencing promotes an epithelial-to-mesenchymal transition (EMT) phenotype in T-47D luminal BC cells. Inmmunofluorescence staining of cytoskeleton (phalloidin) and EMT markers (E-cadherin and Vimentin), in red, in T47D cells. Cell nuclei are in blue. Scale bar = 20 µm.

Lipid analyses of the cell lysates of the three T-47D sublines further confirmed the modulation of the levels (and therefore activity) of FAAH. Thus, the levels of AEA were increased in FAAH KO cells, and went back to normal in rescue cells (**FIG. R32A**). Similar results were observed for other FAAH substrates, but in this case statistical significance was not reached (**FIGs. R32B-D**).

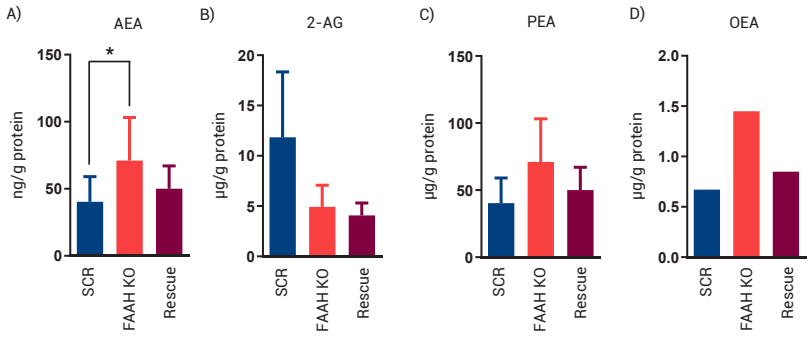

Figure R32. FAAH silencing increases AEA levels in T-47D luminal BC cells. A)-D) Analysis of the main FAAH substrates normalized to protein content. Bars represent mean ± SEM of three independent samples except for OEA, which could only be measured once. Student's t-test: * $p < 0.05$.

Intriguingly, FAAH knock-out in T-47D cells produced a decrease in the number of viable cells in the cultures, that was again rescued when FAAH was restored (**FIG. R33A**). This effect was probably due to a higher basal apoptosis rate rather than to a lower proliferation rate as suggested by the facts that FAAH KO cells presented higher levels of cleaved PARP (an indicator of executioner caspase activity) (**FIG. R33B**) and the same % of Ki67 positive cells (an endogenous proliferatition marker) (**FIG. R33C**).

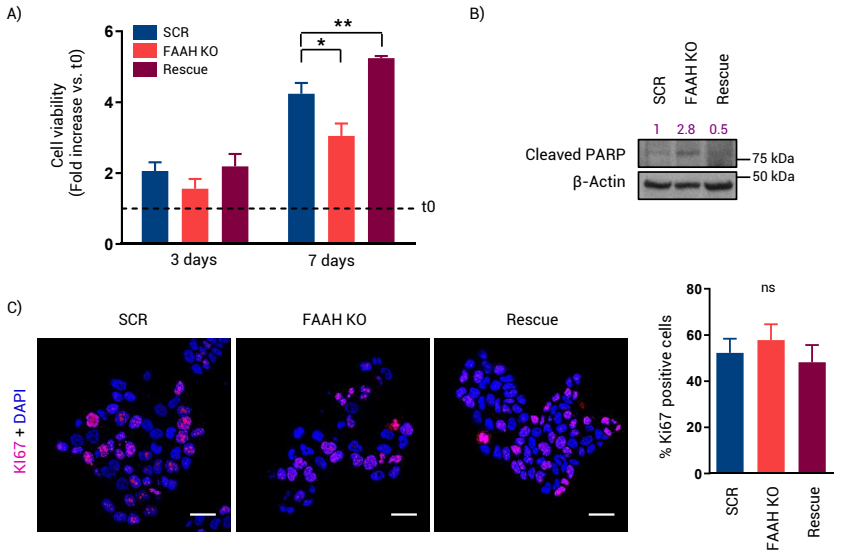

Figure R33. FAAH silencing increases basal apoptotic rate and impacts *in vitro* cell growth in T-47D luminal BC cells. A) Cell viability as measured by crystal violet assay. Student's t-test: * $p < 0.05$, ** $p > 0.01$. B) Representative WB analysis of the apoptotic death marker cleaved PARP. Densitometric values after normalization against β-Actin and control condition are depicted in purple. C) Representative images of the immunofluorescence analysis (left) and the corresponding quantification (right) of Ki67 proliferation marker. Cell nuclei are stained in blue. Scale bar = 50 µm.

FAAH KO cells also showed an increase in their migratory (**FIG. R34A**) and invasive capabilities (**FIG. R34B**), that was lost upon FAAH re-expression in the rescue cell line. In addition, FAAH KO resulted in more efficient mammosphere formation, a capability that was again lost upon FAAH rescue (**FIG. R34C**). Mammospheres are floating structures enriched in cancer stem cells (CSC) formed by some adherent BC cell lines when subjected to non-adherent conditions. Given their more undifferentiated phenotype, mammospheres express higher levels of pluripotency markers such as OCT4 and SOX2 (Simões *et al.*, 2011) (**FIG. R34D**). In line with our observations associating lower FAAH expression with undifferentiated cell states, we detected lower FAAH levels in mammospheres derived from parental T-47D cells than in their adherent, more differentiated counterparts (**FIG. R34D**).

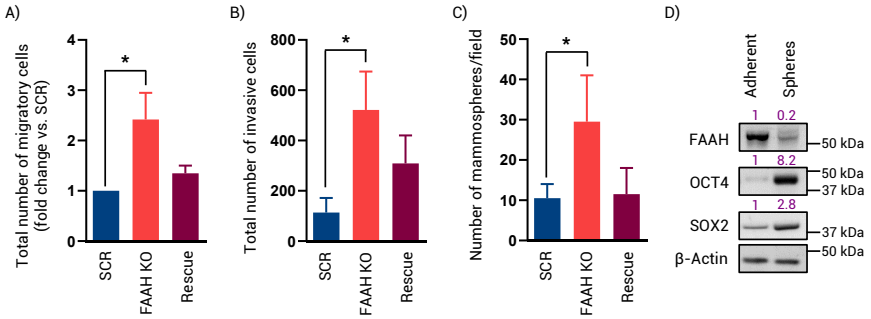

Figure R34. FAAH silencing enhaces the protumorigenic traits of T-47D luminal BC cells *in vitro*. A), B) Effects of FAAH silencing on T-47D cell migration (A) and invasion through matrigel (B) in Boyden chamber assay. Data are shown as mean ± SEM from at least 3 independent experiments. Student's t-test: * $p < 0.05$. C) Effects of FAAH modulation on mammosphere formation by T-47D cells. Student's t-test: * $p < 0.05$. D) WB analysis of FAAH and pluripotency markers (OCT4, SOX2) in a spheroid culture vs. an adherent culture of T-47D cells. Densitometric values after normalization against β-Actin and control condition are depicted in purple.

Finally, and in accordance with our *in vitro* results, the growth of T-47D-derived xenografts in immunocompromised mice was significantly enhanced in the absence of FAAH, an effect that was prevented by overexpression of FAAH in the rescue cell line (**FIG. R35A**). In addition, tumors derived from FAAH KO cells presented a more irregular and invasive aspect than those derived from the parental or the rescue cell line (**FIG. R35B**).

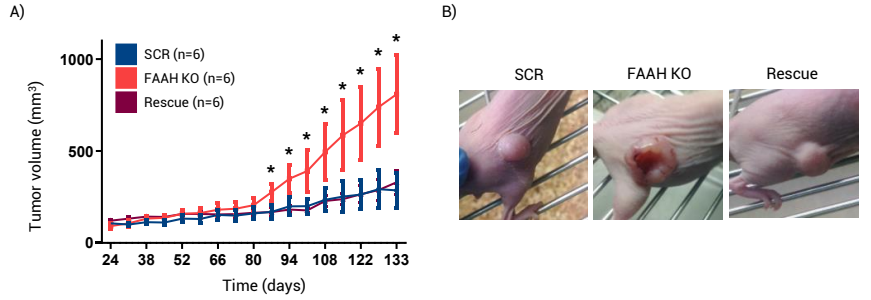

Figure R35. FAAH silencing in T-47D luminal BC cells enhaces tumor growth in a xenograft model. A) Effects of FAAH silencing on tumor growth in immunodeficient mice subcutaneously xenografted with the T-47D sublines. Student's t-test: * $p < 0.05$. B) Representative images of subcutaneous tumors from T-47D SCR, FAAH KO and rescue cells.

FAAH OVEREXPRESSION IMPAIRS PRO-ONCOGENIC FEATURES OF BC CELLS IN VITRO AND IN VIVO

To provide further support of the involvement of FAAH in the control of the pro-oncogenic features of BC, we next followed the opposite approach: overexpression of FAAH in basal (low FAAH expressing) MDA-MB-231 cells. A lentiviral system

carrying an empty (Ø) or a *FAAH* expression plasmid were used to generate MDA-MB-231 Ø and MDA-MB-231 FAAH sublines, respectively (**FIG. R36A**). Analysis of the cell lysates from MDA-MB-231-derived cell lines confirmed that FAAH overexpression resulted in a significant decreased in the intracellular levels of AEA (**FIG. R36B**). A similar trend was observed for other FAAH substrates, but statistical significance was not reached in those cases (**FIGs. R36C-E**).

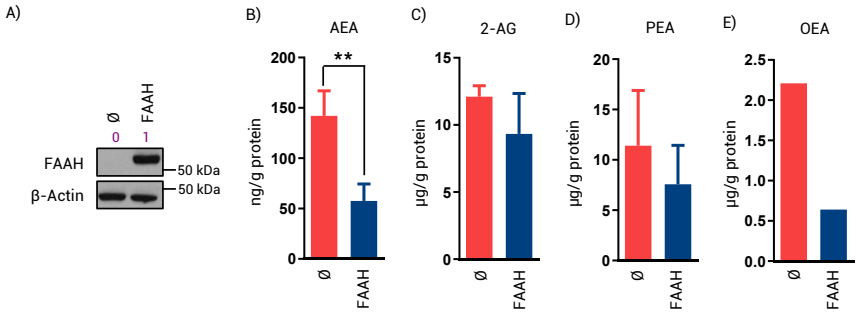

Figure R36. FAAH overexpression in MDA-MB-231 basal BC cells decreases AEA levels. A) Representative WB analysis of FAAH in parental and FAAH overexpressing MDA-MB-231 cells. Densitometric values after normalization against β-Actin and control condition are depicted in purple. B)-E) Analysis of the main FAAH substrates normalized to protein content. Values represent mean ± SEM of three independent samples except for OEA, which could only be measured once. Student's t-test: ** $p < 0.01$.

Further supporting the tumor suppressor activity of FAAH, MDA-MB-231 FAAH cells showed impaired proliferation (**FIG. R37A**) and a less migratory (**FIG. R37B**) and less invasive phenotype (**FIG. R37C**).

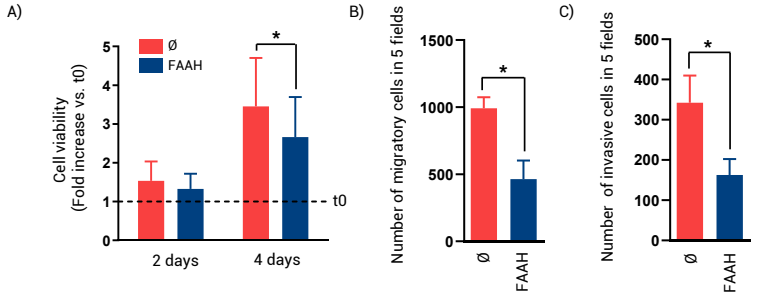

Figure R37. FAAH overexpression in MDA-MB-231 basal BC cells impairs *in vitro* tumorigenic traits. A) Cell viability as measured by crystal violet assay. Student's t-test: * $p < 0.05$. B), C) Effects of FAAH overexpression on MDA-MB-231 cell migration (B) and invasion through matrigel (C) in Boyden chamber assay. Data are shown as mean ± SEM from at least 3 independent experiments. Student's t-test: * $p < 0.05$.

Consistent with these observations, FAAH overexpression was also associated with an increased in epithelial markers and a decrease in mesenchymal/progression markers (**FIG. R38**).

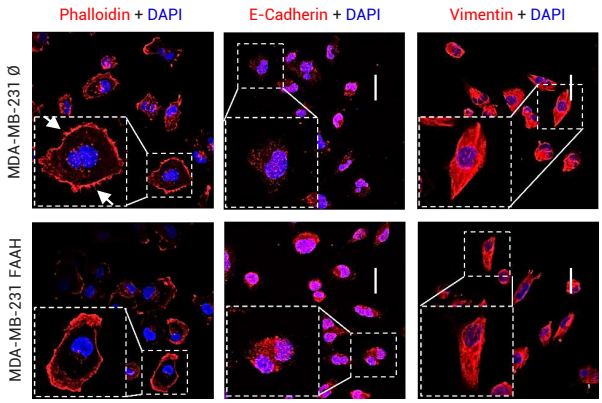

Figure R38. FAAH overexpression in MDA-MB-231 basal BC cells attenuates EMT phenotype. Inmmunofluorescence staining of cytoskeleton (phalloidin) and EMT markers (E-cadherin and Vimentin), in red, in T47D cells. Cell nuclei are in blue. White arrows point to filopodia of MDA-MB-231 Ø which are lost in MDA-MB-231 FAAH. Scale bar = 20 µm.

Tumor growth *in vivo* was also impaired upon FAAH overexpression in a xenograft-based model of BC (**FIG. R39A**). Notably, the tumors generated by MDA-MB-231 FAAH cells that reached the higher volumes were demonstrated to have silenced FAAH to some extent, as demonstrated by WB analysis (**FIG. R39B**), suggesting that the outcome (in terms of tumor growth) is highly dependent on FAAH activity, which strongly supports our hypothesis that FAAH blocks tumor progression.

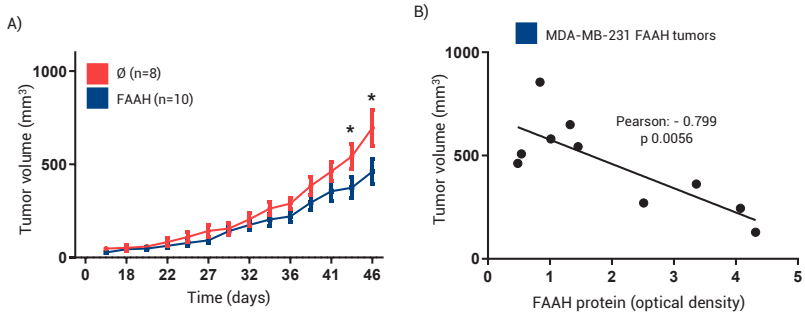

Figure R39. FAAH overexpression in MDA-MB-231 basal BC cells reduces tumor growth in a xenograft model. A) Effects of FAAH overexpression on tumor growth in immunodeficient mice orthotopically xenografted with the indicated MDA-MB-231 sublines. Student's t-test: * $p < 0.05$. B) Linear regression graph representing tumor size vs. FAAH protein levels in MDA-MB-231 FAAH tumors as determined by densitometric quantification of WB analysis. A negative correlation between both variables was found by calculating the Pearson's r.

Finally, MDA-MB-231 cells educated to metastasize to the lungs in which FAAH was overexpressed were much less efficient at generating lung metastases upon intravenous tail injections than control Ø cells (**FIGs. R40A** and **R40B**). Specifically, more than 40 % of the animals injected with MDA-MB-231 FAAH cells were metastasis-free (compared to only 8 % in the Ø group), and none of them reached score 3 of metastatic infiltration (compared to 15 % in the Ø group) (**FIG. R40B**).

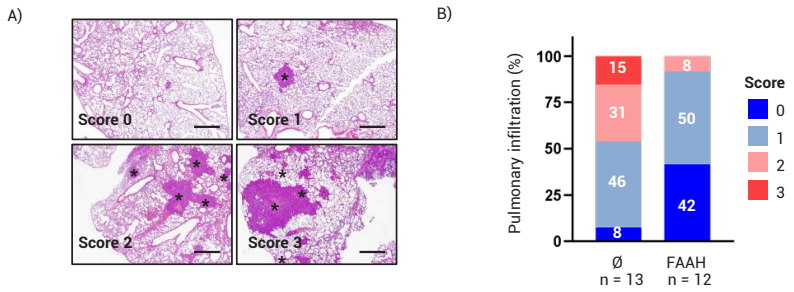

Figure R40. FAAH overexpression in MDA-MB-231 basal BC cells impairs lung metastasis. A) H&E images of lung histology showing representative scoring of metastatic damage (% of lung parenchyma invaded by cancer cells) after injection of MDA-MB-231 cells in the tail vein of athymic female mice. 0 = no metastasis; 1 = < 15 %; 2 = < 15-30 %; 3 = 30-60 %. Metastatic nodules are indicated by asterisks. Scale bar = 250 μm. B) Metastatic infiltration in the experiment described in A).

Collectively, these data show that FAAH overexpression impairs the pro-oncogenic features of human BC cell lines and, together with the results presented in the previous section, solidly demonstrate that FAAH controls the pro-oncogenic features of BC cells, behaving as a tumor suppressor.

MODULATION OF FAAH EXPRESSION ALTERS THE LEVELS OF METASTASIS-RELATED GENES

To try to unravel the molecular mechanisms responsible for FAAH—driven suppression of BC cell metastatic traits, we performed RNA-sequencing (RNA-seq) analysis in the three T-47D-derived cell lines (parental, FAAH KO and rescue). We identified 491 differentially expressed genes (DEGs) in the FAAH KO cells compared to the parental and rescue group (**FIG. R41A**), with a fold change >1.5 and statistical significance set at $p < 0.05$ (**FIG. R41B**). Some of the DEGs that are known to play important roles in BC progression have been highlighted in **FIG. R41B**.

To facilitate biological interpretation of the RNA-seq results, Gene Ontology (GO) (Mi *et al.*, 2019) and Kyoto Encyclopedia of Genes and Genomes (KEGG) (Kanehisa *et al.*, 2000) pathway enrichment analyses were subsequently conducted. GO analysis functionally categorized DEGs into three major categories: Cellular Component (CC) (**FIG. R41C** and **SUPPLEMENTARY TABLE 1**), Molecular Function (MF) (**SUPPLEMENTARY TABLE 2**), and Biological Process (BP) (**SUPPLEMENTARY TABLE 3**). Among these, information given by CC sub-ontology was of special interest for our study because it designates subcellular structures and macromolecular complexes which are known to be important for cell shape, motility, and invasivity. Consistent with their more mesenchymal and migratory phenotype, GO CC analysis showed that DEGs in T-47D FAAH KO cells belonged

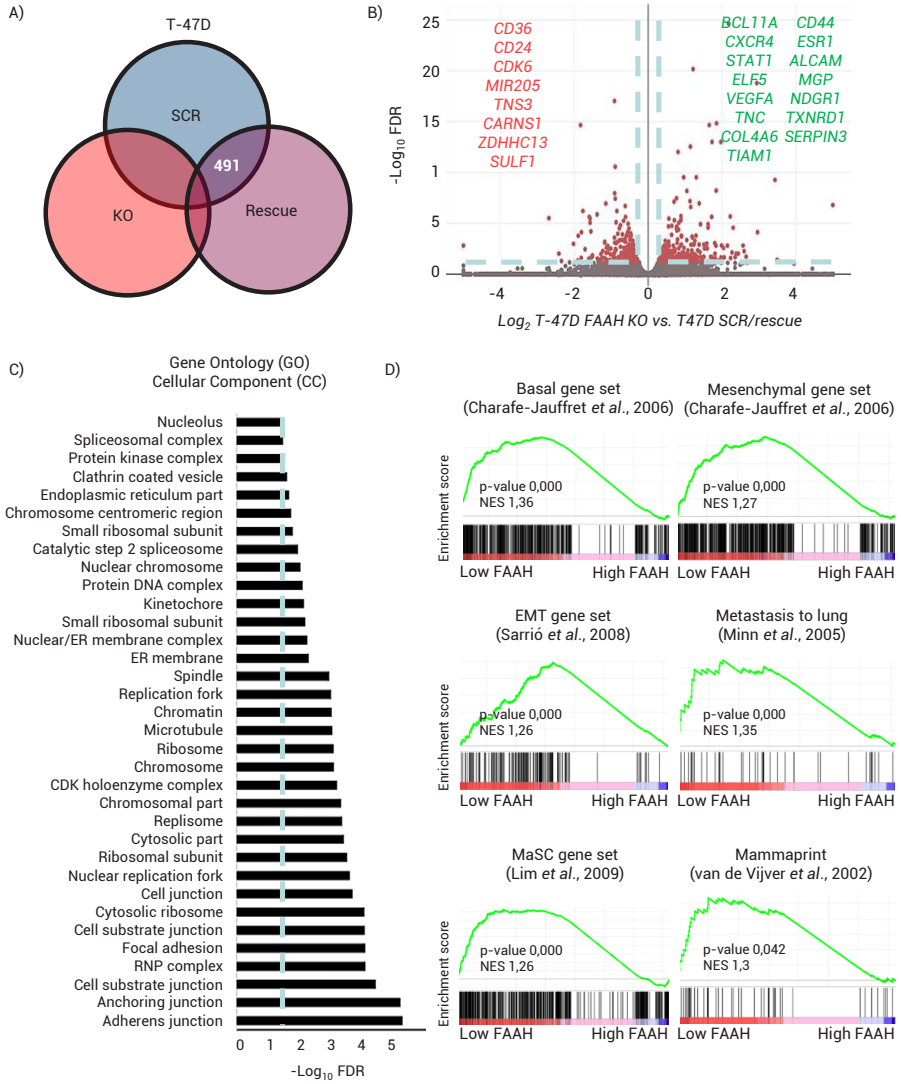

Figure R41. Genomic analyses identify transcriptional changes related to tumor invasion and metastasis in FAAH-modulated T-47D cells. A) Venn diagram summarizing the experimental design of the RNA-seq in FAAH-modulated T-47D cells. Differentially expressed genes (DEGs = 491) were those either upregulated or downregulated in T-47D FAAH KO compared to SCR and whose expression was recovered after FAAH re-expression (T-47D rescue). B) Volcano plot showing RNA-seq data. The relative expression levels for DEGs depicted as log2 fold change of T-47D FAAH KO vs. T47D SCR/rescue are plotted against FDR-adjusted p-value. Dashed blue lines establish inclusion cut-off values at -log10 FDR ≥ 1.3 (equivalent to FDR ≤ 0.05) and log2 fold change ≥ 0.58 (equivalent to fold change ≥ 1.5). Some relevant upregulated and downregulated DEGs are shown in green and red, respectively. C) Bar graph representing Gene Ontology (GO) Cellular Component (CC) analysis of RNA-seq data. DEGs in FAAH KO cells were enriched in 34 categories with a -log10 FDR ≥ 1.3. D) Gene set enrichment analyses (GSEA) of RNA-seq data. The green curve corresponds to the enrichment score, while the normalized enrichment score (NES) and the corresponding p-value are reported within each graph.

to categories involved in cell morphology, cell adhesion, directional cell migration, and extracellular matrix (ECM) reorganization (**FIG. R41C** and **SUPPLEMENTARY TABLE 1**), all of which have a critical function in tumor cell migration and invasion, and therefore in metastasis. KEGG pathway enrichment analysis further identified the signaling pathways that were most impacted upon FAAH knock out, among which we found the categories "ECM-receptor interaction" and "focal adhesion", in addition to specific signaling pathways involved specifically in BC progression (**SUPPLEMENTARY TABLE 4**).

Next, we performed gene set enrichment analyses (GSEA) (Subramanian *et al*., 2005) to determine whether there was an association between low FAAH expression and DEGs that are over-represented in phenotypes widely considered as highly aggressive. In support of our hypothesis, upregulated DEGs in T-47D FAAH KO cells were significantly enriched in basal and mesenchymal genes (Charafe-Jauffret *et al*., 2006), EMT genes (Sarrió *et al*., 2008), genes that mediate BC metastasis to lung (Minn *et al*., 2005), MaSC genes (Lim *et al*., 2009) and van de Vijver 70-gene signature (van de Vijver *et al*., 2002), which is clinically used to identify BC patients at greater risk of developing metastatic disease (**FIG. R41D**).

Finally, we analyzed the mRNA expression of a panel of 76 metastasis-associated genes included in a commercial PCR array in MDA-MB-231 parental cells and MDA-MB-231 cells overexpressing FAAH (**FIG. R42** and **TABLE R2**). Most of the genes included in the PCR array (92 %, 70 out of 76) appeared downregulated in MDA-MB-231 FAAH cells when compared to MDA-MB-231 Ø (**TABLE R2**). Among them, those with a well-established role in BC metastasis are depicted in **FIG. R42**.

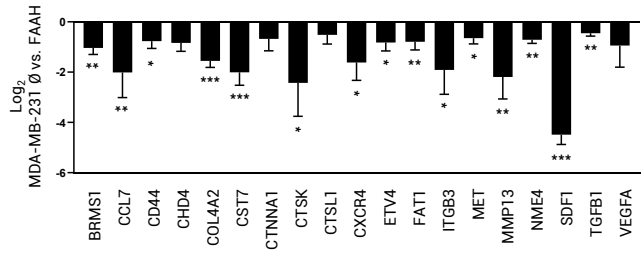

Figure R42. FAAH overexpression in MDA-MB-231 basal BC cells downregulates BC metastasis-associated genes. Bar graph showing results of the RT² Profiler PCR array of human tumor metastasis in FAAH-modulated MDA-MB-231 cells. Relative expression of significantly deregulated genes relevant in BC metastasis is depicted as $\log_2$ fold change of MDA-MB-231 FAAH vs. MDA-MB-231 Ø and represent mean ± SEM of three independent samples. Student's t-test: * $p < 0.05$, ** $p < 0.01$, *** $p < 0.001$.

These data together confirm that FAAH modulates the aggressiveness of BC cells by regulating the expression of invasion and metastasis-related genes.

Gene	Log_2 FAAH vs. Ø	p	Gene	Log_2 FAAH vs. Ø	p
APC	-0,934	0,000	*MET*	-0,649	0,014
BRMS1	-1,035	0,002	*METAP2*	-0,509	0,190
CCL7	-2,010	0,006	*MGAT5*	-1,007	0,084
CD44	-0,768	0,012	*MMP10*	-1,643	0,058
CD82	-0,116	0,440	*MMP13*	-2,191	0,009
CDH11	0,066	0,201	*MMP2*	-0,092	0,308
CHD4	-0,835	0,026	*MMP3*	-0,305	0,291
COL4A2	-1,555	0,000	*MTA1*	-0,626	0,011
CST7	-2,008	0,000	*MTSS1*	-0,219	0,229
CTBP1	-0,877	0,327	*MYC*	-0,360	0,086
CTNNA1	-0,680	0,091	*MYCL1*	-1,760	0,373
CTSK	-2,428	0,042	*NF2*	-1,016	0,088
CTSL1	-0,517	0,107	*NME1*	-0,064	0,428
CXCR2	-1,451	0,177	*NME4*	-0,715	0,001
CXCR4	-1,618	0,026	*NR4A3*	-1,411	0,196
DENR	-0,801	0,325	*PLAUR*	-0,636	0,007
EPHB2	-0,647	0,229	*PNN*	-0,658	0,096
ETV4	-0,820	0,012	*PTEN*	-1,198	0,151
EWSR1	0,185	0,277	*RB1*	-0,399	0,034
FAT1	-0,793	0,027	*RORB*	-2,465	0,006
FGFR4	-1,614	0,246	*RPSA*	-0,367	0,040
FLT4	-0,812	0,466	*SERPINE1*	-0,453	0,148
FN1	-1,161	0,063	*SET*	-0,185	0,344
FXYD5	-0,884	0,104	*SDF1*	-4,325	0,000
GNRH1	-2,619	0,011	*SMAD2*	-0,866	0,056
HGF	-2,680	0,009	*SMAD4*	-0,634	0,039
HPSE	-1,891	0,030	*SRC*	-1,675	0,083
HRAS	-0,780	0,277	*SSTR2*	-2,897	0,272
HTATIP2	-0,617	0,064	*SYK*	-0,590	0,254
IL18	-0,867	0,068	*TCF20*	-1,068	0,080
IL1B	-0,167	0,308	*TGFB1*	-0,455	0,004
ITGA7	-2,662	0,036	*TIMP2*	-0,639	0,023
ITGB3	-1,911	0,023	*TIMP3*	-0,975	0,020
KISS1	-0,063	0,449	*TIMP4*	-0,826	0,455
KISS1R	-0,741	0,240	*TNFSF10*	-0,681	0,277
KRAS	-1,651	0,037	*TP53*	-0,253	0,064
MCAM	-0,648	0,231	*TSHR*	-3,315	0,001
MDM2	-0,673	0,025	*VEGFA*	-0,944	0,147

Table R2. Complete list of genes included in the RT² Profiler PCR array of human tumor metastasis. Relative expression depicted as log_2 fold change of MDA-MB-231 FAAH vs. MDA-MB-231 Ø and the corresponding p-value of the t-test are reported within the table. p-values < 0.05 are highlighted in green. Each value represents the mean of n = 3 independent samples.

FUNCTIONAL IMPLICATION OF THE CXCR4-SDF1 AXIS IN FAAH-MEDIATED CONTROL OF BC METASTATIC TRAITS

Among all candidate genes that were significantly deregulated upon FAAH modulation in both T-47D and MDA-MB-231 cells, chemokine receptor *CXCR4* and its ligand *SDF1* were selected for functional validation due to their well-established role in lung-specific metastasis of BC (Müller et al., 2001).

The RNA-seq and PCR array results mentioned above revealed that *CXCR4* and *SDF1* levels were higher in cells with low FAAH levels (T-47D FAAH KO and MDA-MB-231 Ø) than in their FAAH-expressing counterparts (T-47D SCR/rescue and MDA-MB-231 FAAH, respectively) (**FIGs. R41B** and **R42**, respectively). In line with these observations, tumors generated by MMTV-neu:FAAH $^{-/-}$ animals expressed higher mRNA (**FIG. R43A**) and protein (**FIG. R43B**) levels of CXCR4 and SDF1 with respect to their MMTV-neu:FAAH $^{+/+}$ littermates, which is consistent with their more aggressive phenotype.

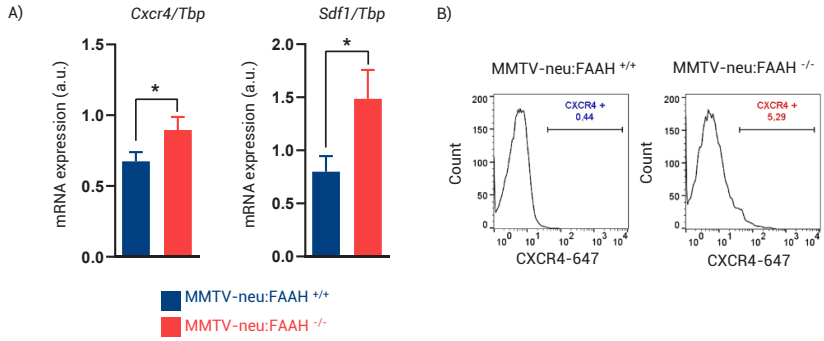

Figure R43. FAAH and CXCR4/SDF1 levels are inversely associated in BC cell lines and animal models of BC. A) qPCR analysis of *Cxcr4* and *Sdf1* mRNA expression in tumors derived from MMTV-neu:FAAH +/+ and MMTV-neu:FAAH -/- mice. Expression levels were normalized against *Tbp*. Data are shown as mean ± SEM from n = 6 mice. Student's t-test: * $p < 0.05$. B) Representative histograms of flow cytometric detection of cell membrane CXCR4 in tumors derived from MMTV-neu:FAAH +/+ and MMTV-neu:FAAH -/- mice. Cell count (y-axis) is plotted against fluorescence intensity (x-axis). Fluorescence-minus-one (FMO) controls were used to set the gate for CXCR4-647 positivity, and the percentage of CXCR4-positive cells is reported within each graph. 7-amino-actinomycin-D (7-AAD) was used for the exclusion of nonviable cells.

We next aimed to study whether there was a association between FAAH and CXCR4/SDF1 levels in human tumors. Supporting our previous results in cell and animal models, the analysis of 1904 BC tumors from public DNA microarrays (Curtis *et al.*, 2012) showed a strong negative association between *FAAH* and *CXCR4/SDF1* mRNA levels (**FIG. R44A**). In addition, GSEA analysis of the dataset published by Wang *et al.*, 2005, revealed an activation of the CXCR4 pathway (Schaefer *et al.*, 2009) in human BC tumors with low *FAAH* expression (**FIG. R44B**).

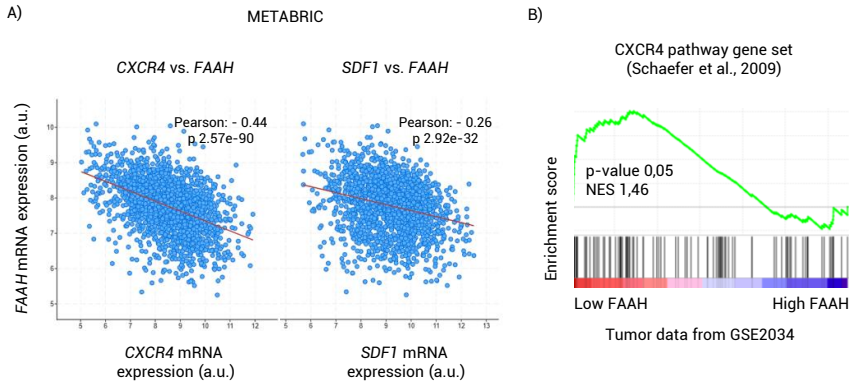

Figure R44. FAAH and *CXCR4/SDF1* levels are inversely associated in human tumors. A) Scatter plot showing inverse correlation between *FAAH* and *CXCR4* or *SDF1* mRNA expression of BC samples from public DNA microarrays (Curtis *et al*., 2012). Pearson's r and corresponding p-values are shown within the graph. B) GSEA of BC samples with low FAAH levels obtained from the dataset published by Wang *et al*., 2005 (study code GSE2034). Low FAAH tumors showed an activation of the CXCR4 pathway signature established by Schaefer *et al*., 2009.

To analyze the clinical relevance of these observations, we performed immunohistochemical analysis of CXCR4 expression in the human BC samples included in TMA #2 (i.e., paired-matched samples of luminal tumors and their lymph node metastasis) (**FIG. R45**). Higher levels of CXCR4 were associated with lower levels of FAAH (and vice versa) both in the primary tumors (**FIG. R45A**) and the lymph node metastases (**FIG. R45B**).

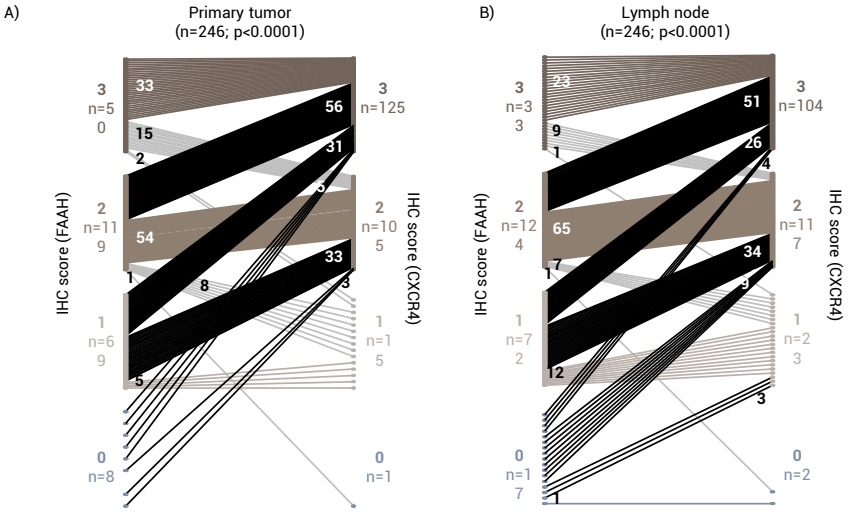

Figure R45. FAAH and CXCR4 levels are inversely associated in luminal breast tumors. A) CXCR4 expression (as determined by staining scoring) of samples in TMA #2 (primary tumor and lymph node metastasis separately). FAAH expression (already graphed in FIG. R20B) is again shown here to allow comparison with CXCR4 expression in the same sample. p-values were calculated by paired two-tailed Student's t-tests.

Of interest, the combination of FAAH and CXCR4 expression was a strong predictor of patient outcome. Thus, patients with FAAH high/CXCR4 low expression in their tumors had significantly higher overall survival than those with FAAH low/CXCR4 high expressing tumors (**Fig R46**).

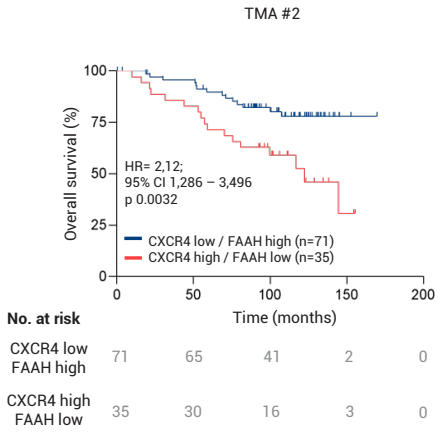

Figure R46. FAAH and CXCR4/SDF1 levels are inversely related in luminal breast tumor samples. Kaplan-Meier curves for overall survival of patients in TMA #2 with CXCR4 low/ FAAH high and CXCR4 high/FAAH low. Survival curves were statistically compared by the logrank test.

We then aimed to determine whether there was a causal link between FAAH modulation of the invasive phenotype and the regulation of the CXCR4-SDF1 signaling axis in T-47D and MDA-MB-231 cells. First, and by means of flow cytometry analyses, we confirmed that CXCR4 protein expression in the cell membrane of each cell line was the one qualitatively expected (i.e., lower in T-47D FAAH KO and MDA-MB-231 parental cells and higher in parental and rescue T-47D as well as in FAAH overexpressing MDA-MB-231) (**FIG. R47A**).

Next, CXCR4-mediated cell invasion was analyzed in these cells in the presence of SDF1 as chemoattractant. All three T-47D-derived cell lines were able to invade towards SDF1, although this effect was not statistically significant (**FIG. R47B**). Of interest, blockade of CXCR4 with the selective antagonist AMD3100 prevented SDF1-driven invasion only in T-47D FAAH KO cells, indicating that FAAH silencing is (at least partially) responsible of the CXCR4-mediated pro-invasive shift. In line with this idea, MDA-MB-231 FAAH cells (expressing lower levels of CXCR4) performed worse at SDF1-induced invasion assays and were less sensitive to treatment with AMD3100 in comparison to MDA-MB-231 Ø (**FIG. R47B**).

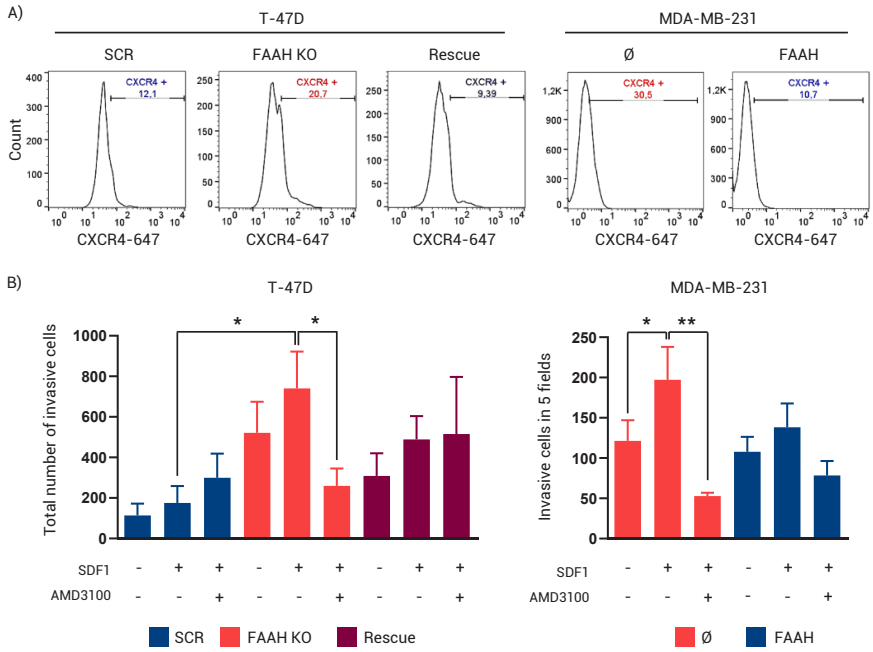

Figure R47. Involvement of the CXCR4-SDF1 axis in the control of the invasive phenotype of BC cells mediated by FAAH. A) Representative histograms of flow cytometric detection of cell membrane CXCR4 in FAAH-modulated T-47D and MDA-MB-231 cell lines. FMO controls were used to set the gate for CXCR4-647 positivity, and the percentage of CXCR4-positive cells is reported within each graph. 7-AAD was used for the exclusion of nonviable cells. B) Analysis of SDF1-induced chemotaxis and AMD3100 treatment on the invasive capacity of FAAH-modulated T-47D (left) and MDA-MB-231 (right) cells. SDF1 (50 nM) was added to the lower compartment of the Boyden chamber containing plain medium (as T-47D did not invade towards SDF1 alone, 10 % FBS was added as well). AMD3100 (20 μM) was added to the upper compartment after cell seeding. Invasive cells were stained with DAPI and counted manually all over the membrane (T-47D) or in 5 random fields (MDA-MB-231). Data are shown as mean ± SEM from 3 independent experiments. Student's t-test: * $p < 0.05$, ** $p < 0.01$.

Given that AEA was the FAAH substrate whose levels varied the most in response to FAAH modulation, we aimed to determine whether the AEA tone defined the invasive capacity of BC cell lines through the CXCR4-SDF1 axis. WB analysis of CXCR4 in T-47D cells revealed that metAEA was able to upregulate CXCR4 (**FIG. R48A**). This effect was mediated, at least in part, by the activation of CBRs, as it was partially prevented by co-incubation of the cells with the CB_1R- and CB_2R-selective antagonists SR1 and SR2, respectively (**FIG. R48A).** In Boyden chambers, treatment of T-47D cells with metAEA phenocopied FAAH KO cell invasive response. This effect was also prevented by SR1 and SR2, pointing to the involvement of CB_1R and CB_2R as targets of metAEA action. Finally, metAEA was also able to rescue the decreased in the invasion rate observed in MDA-MB-231 FAAH cells, although statistical significance was not reached (**FIG. R48B**).

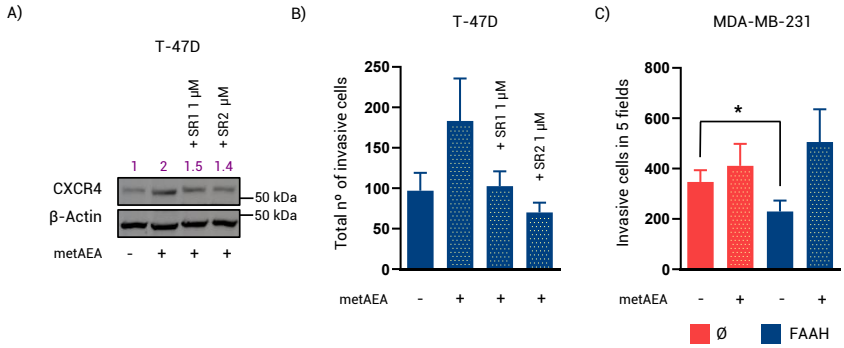

FIG. R48. metAEA enhances pro-tumorigenic features in human BC cell lines through a CBR-mediated mechanism. A) Representative WB analysis of CXCR4 of T-47D parental cells after being treated with metAEA (1 nM) and SR1 or SR2 (1 µM) for 24 hours. Antagonists were added to the cells 1 hour before metAEA. B) Effects of metAEA (1 nM) and SR1 or SR2 (1 µM) treatment on T-47D cell invasion in matrigel-coated Boyden chambers. Treatments were added to the upper compartment (antagonists 1 h before metAEA). C) Effects of metAEA (1 nM) (added to the upper compartment) on MDA-MB-231 cell invasion in matrigel-coated Boyden chambers.

These results uncover the importance of the CXCR4-SDF1 signaling axis in the role of FAAH-mediated control of BC cell metastatic traits, and suggest a role for endogenous AEA tone in the induction of protumorigenic phenotype in FAAH KO cells.

DISCUSSION

Breast cancer (BC) is the most frequently-diagnosed cancer and the leading cause of cancer-related death in women. Despite the improvement of early diagnosis and a growing progress in treatment strategies, there are still clinical challenges associated with the treatment of this pathology: innate or acquired resistance to conventional therapies, the side effects related to them, the lack of targeted therapies for triple-negative BC, and metastatic disease, which today is considered incurable (Harbeck *et al*., 2019). On the other hand, new patient screening tools are needed to be able to detect as soon as possible those patients with a more aggressive pathology or who will not respond to the available therapies, to adapt the treatment in each case. A better understanding of the molecular mechanisms that regulate the development of the mammary gland and that are deregulated during malignant transformation may give insight into the potential prevention and treatment of BC. In this regard, the expression of the endocannabinoid system (ECS) is altered in numerous types of tumors compared to non-transformed tissue, and this aberrant expression has been related to cancer prognosis and disease outcome (Fraguas-Sánchez *et al*., 2018). However, very little is yet known on the participation of this system in tumor onset, progression, and metastasis. Since the effects of the ECS on a given process are profoundly determined by the levels of endocannabinods (eCBs), in this thesis we focused our interest on one of the key enzymes in charge of the degradation of anandamide (AEA, one of the two eCBs). Specifically, we aimed at shedding light on the role of fatty acid amide hydrolase (FAAH) in the adult mammary gland development and in its potential deregulation in BC. First, we demonstrate that FAAH is a functional mediator of lactogenic differentiation in the adult mammary gland. Second, we describe that FAAH expression is highly associated to luminal breast tumors, where it is associated to a good patient prognosis. Finally, we show FAAH is an inhibitor of tumor progression and a negative regulator of lung-specific metastasis in BC.

ROLE OF FAAH IN ADULT MAMMARY GLAND DEVELOPMENT

The same molecular mechanisms that control normal mammary gland development and function can result in aberrant growth and cancer formation when they are disregulated. Thus, the identification of the signaling pathways and transcriptional regulators that control commitment of stem and progenitor cells to specific lineages in the mammary gland provides valuable insight to understand BC biology. As an initial approach to study the role of FAAH in BC, we began by studying its role in the developmental dynamics of the adult mammary gland.

FAAH expression in mammary epithelial cell hierarchy

A fundamental aspect in the development of any organ is the specification and maintenance of differentiated cell types arising from multipotent stem/progenitor

cells. Over the last decades, much work has been done to characterize the different populations of mammary epithelial cells (MECs) residing in the mammary gland. Fluorescence-activated cell sorting (FACS) together with the identification of several cell-surface markers has allowed to prospectively isolate three main subpopulations of MECs which are analogous in both mouse and human mammary glands. These are the basal/mammary stem cell (MaSC)-enriched (which contains mature basal cells and cells with bipotent MaSC activity), the committed luminal progenitors and the mature luminal subsets. In an attempt to establish gene signatures that most closely defined these populations, Lim and colleagues first identified a series of genes and pathways that were conserved in functionally equivalent subsets isolated from mouse and human. Here, FAAH was identified among the list of genes that showed consistent high expression in the mature luminal subset and low expression in the basal/MaSC-enriched subset (Lim *et al*., 2010). However, whether and how FAAH participates in the organization and identity of the mammary epithelial hierarchy was not investigated. In this thesis, we demonstrate that FAAH expression in the mouse and human mammary gland increases along luminal cell differentiation.

By analyzing multiple sources of transcriptomic data from MEC subpopulations of mouse and human origin, we gathered solid evidence that validated results by Lim and colleagues (i.e., FAAH expression is always higher in the mature luminal subset than in the basal/MaSC-enriched subset), and further observed that expression levels in the luminal progenitor subset were always in the middle of the other two. To date, molecular discrimination between mature basal cells and MaSCs remains a persistent problem in the field. While it has not yet been possible to isolate pure MaSCs fractions, the recent discovery of novel cell-surface markers followed by functional testing of regenerative capacity has led to further fractionation of putative MaSCs from the basal compartment. For example, Raouf and colleagues obtained highly purified populations of bipotent MaSCs from the $CD49f^{+}$ Mucin 1^{-} $CD133^{-}$ $CD10^{+}$ $THY1^{+}$ fraction of human mammary gland (Raouf *et al*., 2008). Analysis of their published data allowed us to verify that FAAH levels in both the MaSC and the mature basal subsets (separately) were equally low when compared to the luminal progenitor and mature luminal subsets. Regarding mouse mammary gland, scRNA-seq performed by Bach and colleagues (Bach *et al*., 2017) identified a basal cell cluster with high expression of protein C receptor ($Procr^{+}$ cells), which had been previously identified as a marker for multipotent MaSCs in mouse (Wang *et al*., 2015). FAAH expression in $Procr^{+}$ cells was practically null as well as in the other clusters with basal signature. Together, these observations support that FAAH is expressed in a highly-selective manner in the cells of the luminal lineage of the mammary gland, and that it increases in parallel to the grade of luminal cell commitment, suggesting that it plays a role in this process.

Role of FAAH in secretory differentiation of MECs *in vitro*

In line with the hypothesis that FAAH may be controlling luminal cell differentiation in the mammary gland, we provided evidence that pharmacological inhibition of FAAH (with URB 597 or with BIA 10-2474) significantly suppressed hormone-driven differentiation of the MEC line HC11 into milk-producing cells through a cannabinoid receptor 1 (CB_1R)-mediated mechanism. Treatment with the AEA analogue methanandamide (metAEA) later phenocopied the inhibitory effects of URB 597 over HC11 cell differentiation, suggesting that an upregulation of the endogenous levels of AEA triggered by FAAH inhibition might be responsible for the phenotype in the former case.

In the recent years, attention has been focused on the possible role of AEA and other eCBs in regulating cell differentiation, which might account for some physiopathological effects of these lipids (Galve-Roperh *et al*., 2013). For example, exogenous AEA is known to inhibit the differentiation of human keratinocytes (Paradisi *et al*., 2008) and neurons (Rueda *et al*., 2002) through CB_1R-mediated attenuation of cell type-specific differentiation pathways. Here, we demonstrated that HC11 cells that failed to undergo complete differentiation in the presence of metAEA/URB 597 expressed lower mRNA levels of prolactin receptor (PRLR), whose activation by prolactin (PRL) is the primary inducer of lactogenic gene expression. Suppression of PRLR levels by exogenous AEA in a CB_1R-dependent manner has been previously reported in BC cell lines EFM-19 and MCF7 (De Petrocellis *et al*., 1998), and a follow-up study next determined that this phenotype was mediated by inhibition of adenylyl cyclase (AC) and activation of mitogen-activated protein kinases (MAPKs), two well-recognized effectors of CB_1R signaling (Melck *et al*., 1999). Our results raise the possibility that a similar mechanism may be operating in differentiating MECs, so the reason for their defective differentiation when exposed to metAEA/URB 597 relies (at least partially) on reduced PRLR expression and a consequent inability to properly sense and respond to PRL. Further research involving drugs interfering with either cyclic adenosine monophosphate (cAMP) or MAPK signaling pathways may shed some light on the mechanisms that participate in the CB_1R-mediated inactivation of PRLR signaling triggered by metAEA/URB 597.

Several studies have demonstrated that PRL-mediated milk production through PRLR requires PRLR-mediated activation of the intracellular tyrosine kinase Janus kinase 2 (JAK2), which phosphorylates the transcription factor signal transducer and activator of transcription 5 (STAT5), an obligate transactivator of several milk protein-encoding genes, including *CSN2* (encoding β-Casein) (Hennighausen *et al*., 1997). In this work, the phosphorylation levels of JAK2 and STAT5A in HC11 cells differentiated in the presence of metAEA or URB 597 were studied, but no significant downregulation associated to lower PRLR expression was detected

(data not shown). In physiological conditions, JAK/STAT signaling is exquisitely controlled by a cohort of negative regulators: the suppressor of cytokine signaling (SOCS) family. SOCS proteins are direct transcriptional targets of STATs and negatively regulate the pathway, therefore signaling through the JAK/STAT pathway is normally of high intensity and short duration (Croker *et al.*, 2008). In HC11 cells, we have analyzed the consequences of our differentiation protocol (i.e., the cell status 5 days after PRL first addition), so we have probably missed the time window where activation levels of JAK2 and STAT5 reach their maximum, and consequently masked the effects that metAEA/URB 597 treatments may have on them. Hence, it would be ideal to work with two different time windows in the future: one to study the effect of the treatment on the immediate activation of the PRLR/JAK2/STAT5 axis (e.g., 15' after PRL addition) and another to study the effect of the treatment on the accumulation of milk proteins (5 d after PRL addition).

Importantly, treatment of differentiating HC11 cells with the CB_1R selective antagonist SR141716 (SR1) was sufficient to enhance cell-fate specification in a concentration-dependent fashion, pointing to either a ligand-independent constitutive activation of CB_1R or a basal endocannabinoid tone acting on CB_1R and actively inhibiting cell differentiation in MECs. Although the former cannot be ruled out, our results support the later hypothesis. Thus, constitutive activation of FAAH (accompanied by downregulation of its mains substrates) mimicked CB_1R antagonism, i.e., it promoted HC11 differentiation. Together, our observations support the existence of a basal CB_1R activity that prevents differentiation in luminal cells, ultimately controlled by FAAH activity, and possibly driven by an endogenous AEA tone, although prevention of the metAEA antidifferentiation effects by receptor blockade remains to be demonstrated (**FIG. D1**).

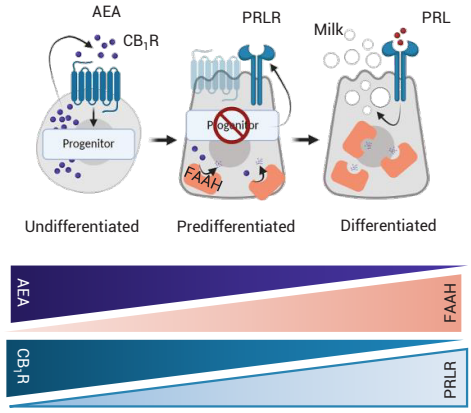

Figure D1. Schematic drawing of the proposed mechanism of the role of FAAH in MEC lactogenic differentiation *in vitro*. Low FAAH levels in undifferentiated cell states determine a high eCB tone (presumably composed by AEA) that inhibits cell differentiation through CB_1R. Increase of FAAH expression (accompanied by a decrease in AEA and in CB_1R expression) terminates eCB's inhibitory action and allows cell differentiation. Mechanistically, inhibition of MEC differentiation by the eCB tone might involve PRLR downregulation.

However, the contribution to inhibition of lactogenic differentiation of (i) FAAH substrates other than AEA that lack affinity for CB_1R as well as of (ii) other CB_1R agonists whose endogenous levels are not directly regulated by FAAH cannot be ruled out. Regarding the first, it is well-known that palmitoylethanolamide (PEA) and oleoylethanolamide (OEA) (also FAAH substrates) are able to downregulate the expression and activity of FAAH in BC cells (Bisogno *et al*., 1998; Di Marzo *et al*., 2001). It is thus tempting to speculate that, by downregulating FAAH, they could be further enhancing the anti-differentiation effects of AEA in MECs. Regarding the second, it is worth noticing that the levels of 2-arachidonoylglycerol (2-AG) in HC11 cells also suffered a notable (although not statistically significant) increase in response to URB 597. Although monoacylglycerol lipase (MAGL) is responsible for 85 % of 2-AG hydrolysis in the mouse brain, it can also be cleaved into glycerol and arachidonic acid by FAAH (Maccarrone *et al*., 2015). However, 2-AG levels did not decrease upon FAAH constitutive activation, so we concluded that it is probably not contributing to the FAAH-controlled eCB tone acting at CB_1R in HC11 cells.

Role of FAAH in adult mammary gland differentiation *in vivo*

The results we obtained in our cell culture models of differentiation were further confirmed in more complex and physiological settings, i.e., mice. Our data demonstrate that transgenic mice lacking FAAH show incomplete functional development of the mammary gland during lactation. Prior to parturition, approximately 30 % of the mouse mammary gland is still filled with adipocytes, but as lactation becomes established, the fat in the adipocytes is metabolized, the alveoli expand to completely fill the gland, and flattened epithelial cells in the process of secreting milk fat droplets are easily visible at higher magnification (Richert *et al*., 2000). From as soon as lactation day 5 (L5), the mammary gland of $FAAH^{+/+}$ mice was filled with distended lobuloalveoli containing milk proteins and lipids, while $FAAH^{-/-}$ mice alveoli were small and condensed, contained epithelial cells that were still cuboidal and expressed lower levels of the milk protein β-Casein at L5 and L15. Mammary glands of $FAAH^{-/-}$ mice also displayed lower expression of PRLR, which is crucial in the final stage of MEC secretory differentiation that takes place at parturition (Ormandy *et al*., 1997). These results are in line with our *in vitro* data suggesting that FAAH is involved in PRLR-dependent functional differentiation of luminal cells during lactogenesis in mice. However, a more detailed comparative characterization of the PRLR cascade as well as of other signaling pathways involved in the secretory phenotype of $FAAH^{-/-}$ and $FAAH^{+/+}$ mice is required in order to establish a molecular link between FAAH and MEC secretory differentiation *in vivo*.

Our *in vitro* data demonstrate that the eCB tone, which is ultimately modulated by FAAH, determine the cell fate of MECs through a CB_1R-mediated mechanism, suggesting that a similar regulation may take place *in vivo*. Notably, the expression patterns of FAAH and CB_1R in the mammary gland rarely overlap. As we have

reported, CB_1R mRNA is mostly expressed in cell populations with a basal/MaSC-enriched genetic profile. However, immunofluorescence of CB_1R in the human mammary gland reveals that it is not expressed by the basal layer of cells of the mammary duct. Instead, its expression is restricted to isolated cells which are part of the luminal layer but localize close to the basal compartment, and therefore could represent progenitor cells. Together with our *in vitro* results, these observations might uncover the existence of a cannabinoid-mediated regulatory mechanism of MEC commitment in the mammary gland, in which FAAH from luminal cells creates a local AEA tone which acts in a paracrine manner on CB_1R in bipotent progenitors and inhibits cell-fate specification. In this scenario, lack of FAAH during lactogenic differentiation would lead to an aberrantly high AEA tone which would ultimately impede MEC differentiation and secretory specialization. However, mechanistic studies involving acute administration of receptor antagonists at parturition and during lactation should be next performed to establish the precise metabolite(s) and receptor(s) implicated in the delayed mammary gland development observed in FAAH $^{-/-}$ mice. In the same line, histological and molecular characterization of the mammary gland of CB_1R $^{-/-}$ mice during lactation should shed some light on the implication of this receptor in FAAH-mediated regulation of lactogenesis *in vivo*.

With the onset of pregnancy, the hormonal milieu of the dam is altered causing sequential changes in gene expression that culminate in secretory activation and milk synthesis at or around birth. Because FAAH is abundantly expressed by many different cell types and tissues (Lonsdale *et al*., 2013) (**FIG. D2**), developmental failure in the postnatal mammary gland of FAAH $^{-/-}$ mice could be due to alterations in MECs but also in systemic hormones that act on MECs to orchestrate normal development and lactation (**FIG. D3**).

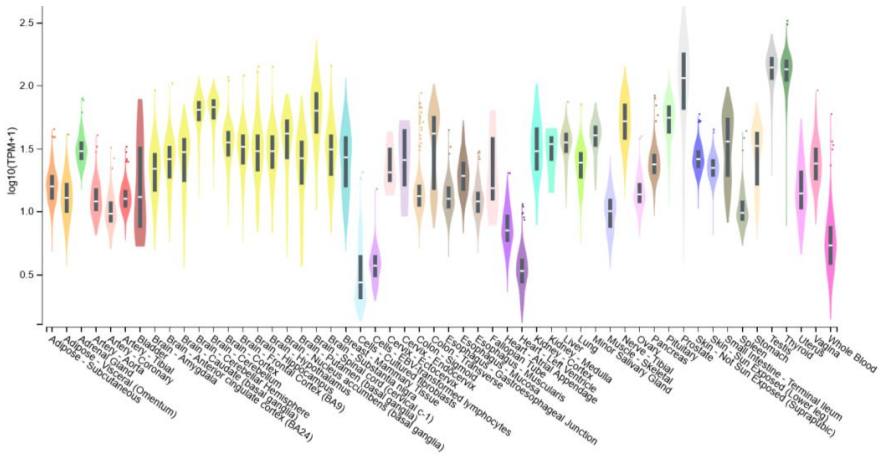

Figure D2. Bulk human tissue gene expression for FAAH. Source: The genotype-tissue expression (GTEx) project (Lonsdale *et al*., 2013).

In the hypothalamus and the anterior pituitary, AEA suppresses the release of gonadotropin-releasing hormone (GnRH) and luteinizing hormone (LH) -respectively-, which subsequently reduces circulating levels of estrogen (E) and progesterone (P) (Gorzalka *et al*., 2012). In addition, AEA impairs E_2-dependent human endometrium differentiation through the inhibition of aromatase (Almada *et al*., 2017). Lower levels of systemic E and P caused by an enhanced AEA tone in the FAAH $^{-/-}$ mouse could have an impact on ductal elongation (E), side branching (E, P) and alveologenesis (P) that take place during puberty and pregnancy, thus rendering an underdeveloped postpartum mammary gland even in the presence of a functional PRL/PRLR axis. However, whole-mount analysis of mammary glands from age-matched FAAH $^{+/+}$ and FAAH $^{-/-}$ virgin females showed that elongation of the ductal tree and ductal side branching from 4 to 10 weeks of age were similar (data not shown), and histological analysis of mammary glands at 1 day postpartum (L1) also revealed similar grade of lobuloalveolar development in both genotypes, suggesting the action of FAAH may be mostly restricted to PRL-driven differentiation of MECs into milk producing cells at parturition. In this regard, intraventricular AEA has also been shown to decrease plasma levels of PRL in male rats (Scorticati *et al*., 2003), which raises the possibility that FAAH $^{-/-}$ females are exposed to lower levels of circulating PRL that could compromise successful lactogenesis.

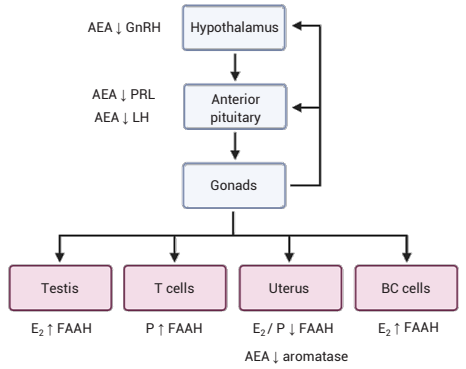

Figure D3. Summary of the bidirectional interactions of the AEA-FAAH system with the hypothalamic-pituitary-gonadal (HPG) axis. AEA suppresses release of GnRH from the hypothalamus (resulting in lower levels of circulating sex hormones) and of LH and PRL from the anterior pituitary. AEA also downregulates aromatase expression in human decidual cells. On the other hand, E_2 upregulates FAAH expression in the testis and in BC cells, and downregulates it in the uterus. P upregulates FAAH in T lymphocytes and downregulates it in the uterus. No interactions of other FAAH substrates with the HPG axis have been reported to date.

Transplantation experiments of FAAH $^{-/-}$ mammary epithelia into wild-type recipients (and vice-versa) would be helpful to study the relative contributions of local and systemic cues to lobuloalveolar development. In addition, selective ablation of FAAH from hormone-sensing MECs could be obtained by breeding

FAAH $^{flox/flox}$ mouse with a mouse expressing Cre recombinase under the control of hormonally-regulated promoters like the mouse mammary tumor virus (MMTV, which targets a heterogeneous group of progenitor cells) or the whey acidic protein (WAP, which targets alveolar progenitors) promoters (Wagner *et al*., 1997). Both approaches would be useful to elucidate whether the role of FAAH over PRL-dependent secretory differentiation of MECs is mammary cell autonomous or rather relies on endocrine signals.

Among the questions that remain to be answered in this thesis is determining the upstream regulators of FAAH that control its expression levels in differentiation contexts. In this regard, several hormones involved in the development of the mammary gland have been found to regulate FAAH expression through direct or indirect interaction with its promoter (**FIG. D3**). Research in human neuroblastoma cells (SY5Y) first identified estrogen and glucocorticoid response elements (EREs and GREs, respectively) in the *FAAH* promoter that regulated transcriptional activity independent of their ligand (Waleh *et al*., 2002). The discovery of EREs in the promoter sequence of *FAAH* was consistent with previous studies indicating that FAAH expression in the uterus was downregulated by sex hormones (Maccarrone *et al*., 2000). The opposite regulation has also been reported in mouse testis: estradiol (E_2) induced ERβ binding to ERE2/3 sites in the *Faah* promoter and activated transcription in primary mouse Sertoli cells (Grimaldi *et al*., 2012). In addition, there is evidence that P binds and regulates transcriptional activity of the *FAAH* gene in human T lymphocytes through the transcription factor Ikaros (Maccarrone *et al*., 2003). We have demonstrated in this thesis that treatment with estradiol (E_2) induces *FAAH* expression in BC cell lines MCF7 and T-47D. However, whether these observations are extensible to MECs is yet to be addressed. It is tempting to speculate that, given that FAAH acts as a driver of secretory differentiation in HC11 cells, the regulation of FAAH expression in MECs by systemic hormones may have physiological relevance for the success of mammary gland development *in vivo*. Follow-up studies may investigate in more detail the role of hormonal mediators as upstream regulators of FAAH in the mammary gland in order to clarify the biological significance of FAAH-mediated regulation of MEC lactogenic differentiation.

ROLE OF FAAH IN BREAST CANCER

There is increasing evidence that the numerous mechanisms that regulate cell differentiation during normal development are also involved in tumorigenesis. In BC, differentiation markers expressed by the primary tumor are routinely profiled to guide clinical decisions. Indeed, numerous studies have shown that the differentiation profile of tumors is associated with their metastatic potential (Kufe *et al*., 2003). Because results from the previous section revealed a role for FAAH in MEC differentiation in the mammary gland, we aimed to study the role of FAAH in BC.

FAAH promotes luminal BC phenotypes

The fact that the expression of some elements of the ECS have been found altered in some tumor malignancies compared with the tissues they derive from has posed the question whether this system plays a role in oncogenesis. In the specific case of FAAH, these alterations do not seem to follow a single trend and rather are highly tumor type-specific. For instance, in gliomas, the expression and activity of FAAH were lower when compared with normal brain tissue (Wu *et al*., 2012). In prostate cancer, however, FAAH had a higher expression than in normal tissue (Endsley *et al*., 2008), and this upregulation was later associated with poor patient outcome (Thors *et al*., 2010). In the case of pancreatic cancer, FAAH levels increased in transformed vs. non-transformed tissue, but higher levels in tumor samples were associated to a better patient prognosis (Michalski *et al*., 2008). However, neither the expression nor the function of FAAH had been studied in the context of mammary gland malignant transformation so far.

Bulk gene expression data has been traditionally helpful to analyze overall gene expression from a high amount of tissue samples, but it has the major limitation of not reflecting the individual contributions of the different cell populations and cellular states of the sampled tissue. In a similar way, bulk transcriptomes from cancer tissue often represent an amalgamation of very different tumor samples that, despite sharing the same anatomical origin, exhibit striking phenotypic diversity and clinical outcomes. Especially in the case of a highly heterogeneous diseases as BC, it is of paramount importance to recognize cell-type as well as tumor-type heterogeneity in order to understand the relevance of gene expression alterations for disease phenotypes, and therefore any comparison of bulk "transformed vs. non-transformed" breast tissue should be interpreted with caution. Here, we demonstrate that FAAH expression in both the non-transformed mammary gland and BC is positively associated to the luminal phenotype, hormone receptor (HR) + status, and high differentiation grade, while it is negatively associated with the basal phenotype, triple-negative (TN) status, and low differentiation grade. In essence, we provide compelling evidence that FAAH is a marker of the luminal gene signature in mammary physiopathology.

As it has been mentioned, BC is a group of heterogeneous diseases with substantial variations in both molecular and clinical characteristics. Though the intrinsic subtypes fall quite short of encompassing the full extent of BC diversity, in general, tumors that fall within the same subtype behave in similar ways and exhibit similar sensitivity to therapy. Therefore, dissecting how BC heterogeneity is originated is a fundamental question with important clinical implications (Skibinski & Kuperwasser, 2015). Comprehensive molecular profiles of BC subtypes have revealed significant differences in the mutational profiles of luminal-like and basal-like tumors, suggesting that many frequently mutated genes may act as drivers of

tumor phenotype in each case (Banerji *et al*., 2012; Koboldt *et al*., 2012; Shah *et al*., 2012). In this thesis, we show that FAAH plays an important role in determining a luminal phenotype in BC. For example, we observed that, when compared to MMTV-neu:FAAH $^{+/+}$ mice, MMTV-neu FAAH $^{-/-}$ animals generated higher grade, more proliferative tumors that displayed a cytokeratin (CK) staining pattern typical of basal-like BC (i.e., CK14 staining was predominant over CK8), suggesting that germline knockout of *FAAH* might predispose developing tumors of MMTV-neu mice to adopt a basal phenotype. Despite being driven by *Neu* oncogene (the rat ortholog of human *HER2*), tumors derived from MMTV-neu mice have a global gene expression profile that is more similar to the luminal A and B subtypes (Herschkowitz *et al*., 2007; Lim *et al*., 2010; Pfefferle *et al*., 2013; Hollern *et al*., 2014). Our results therefore suggest that the lack of FAAH switches the phenotypic identity of breast tumors from a basal to a luminal type.

The distinguishing features of luminal and basal-like BC cells have been traditionally explained by a cell-of-origin hypothesis, which establishes that tumor phenotype is determined by the nature of the precursor cell that receives the initial genetic insult. Thus, luminal and basal-like tumors are thought to arise from oncogenic mutations in the mature luminal cell and the luminal progenitor cell, respectively (Polyak *et al*., 2007). Because we have previously shown that FAAH is a driver of luminal cell differentiation in MECs in culture, germline inactivation of FAAH in MMTV-neu:FAAH $^{-/-}$ mice could lead to the accumulation of aberrant luminal progenitors in the preneoplastic mammary gland that increased predisposition to basal phenotype in case BC developed. Indeed, this has been reported before for *BRCA1* mutation carriers. Women with inherited mutations in the *BRCA1* gene have an increased risk of developing BC, but also exhibit a predisposition for the development of aggressive basal-like breast tumors. Due to the involvement of BRCA1 in the control of differentiation of MECs (Furuta *et al*., 2005), breast tissue from *BRCA1* mutation carriers harbors an expanded luminal progenitor population that shows factor-independent growth *in vitro* and that is thought to be the origin of *BRCA1*-associated basal tumors (Lim *et al*., 2009). Previous studies have suggested that tumorigenesis in parous and nulliparous MMTV-neu transgenics originate from a hormone-responsive, differentiating epithelial subtype within lobular units (Henry *et al*., 2004), which, as we have described, is the epithelial cell type where FAAH is expressed the most. By dictating progenitor cell fate in the normal mammary gland, FAAH could be involved in the determination of tumor phenotype in the MMTV-neu model (**FIG. D4A**).

On the other hand, the clonal expansion hypothesis (which coexists with the cell-of-origin hypothesis) establishes that tumor phenotype is not determined by the pre-existing differentiation state of the precursor cell, but rather by the nature of the initial and secondary mutations occurring in it (Polyak *et al*., 2007). In this context, genetic inactivation of FAAH would have led developing tumors in

MMTV-neu:FAAH $^{-/-}$ mice to adopt a basal phenotype regardless of the nature of the precursor cell (**FIG. D4B**). Future research involving a thorough analysis of the relative proportions of cell populations in breast tissue of FAAH $^{+/+}$ and FAAH $^{-/-}$ mice would be required to elucidate the precise way germline inactivation of FAAH of MMTV-neu:FAAH $^{-/-}$ mice contribute to the basal phenotype of the resulting tumors.

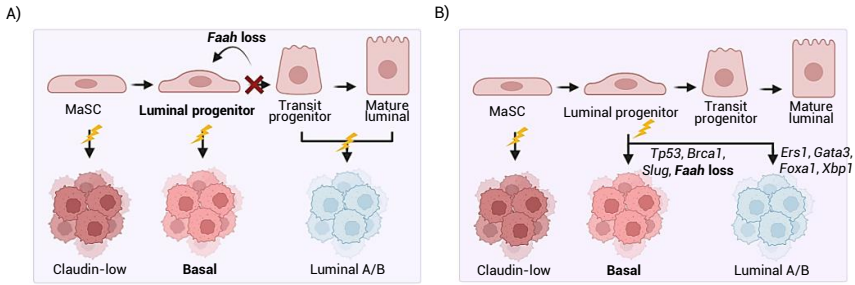

Figure D4. Schematic representation of the possible contributions of FAAH loss to the basal-like phenotype during spontaneous tumor formation according to the two models of BC heterogeneity. A) In the cell-of-origin model, each BC subtype originates from a different cell of origin and maintains its differentiation status during tumor progression. Here, loss of FAAH would lead to an accumulation of aberrant luminal progenitors in the mammary gland, thus increasing the target population for basal-like BC. B) In the clonal expansion model, both luminal and basal tumors arise from the luminal progenitor compartment, and the nature of the mutations determines the tumor phenotype. In the presence of a driver mutation, FAAH loss would lead the developing tumor to adopt a basal-like phenotype. Adapted from Skibinski & Kuperwasser, 2015.

Our results point to the possibility that FAAH might not only drive luminal type of BC during tumorigenesis, but also actively contribute to the maintenance of the differentiation state in the resulting tumor. Knockout of *FAAH* in the luminal BC line T-47D was sufficient to induce the dedifferentiation of the cells and re-acquisition of a molecular profile enriched in the basal, mesenchymal and MaSC signatures. T-47D FAAH KO cells also gained an epithelial-to-mesenchymal transition (EMT) phenotype, which preferentially occurs in undifferentiated, basal-like tumors (Sarrió *et al*., 2008). In the same line, FAAH overexpression downregulated EMT phenotype in the basal cell line MDA-MB-231. Pathologists have long recognized the intimate connection between tumor progression and its differentiation status. Well-differentiated tumors are generally less advanced and are associated with a better prognosis whereas poorly differentiated tumors are generally more aggressive and associated with a worse prognosis (Kufe *et al*., 2003). Accordingly, knockout of *FAAH* in T-47D cells was accompanied by an enhanced aggressive behavior (i.e., increased migration, invasion and mammosphere formation *in vitro*, and tumor growth *in vivo*), while overexpression of FAAH in the basal-like MDA-MB-231 cell line attenuated aggressive behavior (i.e., reduced proliferation, migration, and invasion *in vitro*, and tumor growth and metastasis *in vivo*).

Together, our findings reveal a previously unknown role of FAAH as a regulator in the specification and maintenance of BC luminal phenotype that, as will be discussed later, may have important implications for the treatment of basal-like BC.

FAAH acts as a lung metastasis suppressor in BC

Evidence gathered in this thesis also points to a causal role of FAAH in metastasis prevention in BC. Thus, genetic inactivation of FAAH in MMTV-neu mice increased the rate of spontaneous pulmonary metastases (higher percentage of animals with metastatic lesions, earlier onset and wider extension of metastatic nodules), while expression of FAAH in FAAH-negative, lung-seeking MDA-MB-231 cells (Minn *et al*., 2005) was sufficient to inhibit the formation of pulmonary metastases after tail-vein injection in immunocompromised mice.

In support of these results, we have demonstrated that FAAH levels in human tumors are negatively associated with the metastatic rate. Accordingly, and since metastasis accounts for 90 % of BC mortality, we also found an inverse association between FAAH expression and patient overall survival. In addition, we have shown that loss of FAAH expression is a frequent event during metastatic progression of luminal BC, and that this loss is associated to a worse clinical outcome. Together, these observations raise the possibility that intrinsic (already present in the primary tumor) or acquired (during metastatic progression) FAAH absence confers metastatic capability to BC cells that promotes the onset of tumor dissemination to distant organs. This is consistent with the observation that FAAH expression in luminal tumors is lost in the cells that are at the invasion front.

Mechanistically, we propose that FAAH blocks metastatic treats both in the primary tumor and during the dissemination process. Those relative to the primary tumor have been already discussed: FAAH has been identified as an important negative regulator of tumor features typical of poorly differentiated, basal-like tumors, which themselves constitute an inherent risk factor for metastatic development due to their aggressive tumor biology. Regarding those functions relative to the metastatic colonization *per se*, they are likely to be related to the direct or indirect regulation by FAAH of a number of genes that, playing or not a relevant role in primary tumor growth, actively participate in the escape, survival, and growth of the tumor cells in distant organs. Thus, FAAH overexpressing MDA-MB-231 cells, which displayed reduced ability to form metastasis in the lungs, were found to downregulate proteins involved in EMT induction [i.e., *MTA1* (Sen *et al*., 2014)], tumor cell migration [i.e., *TRPM7* (Middelbeek *et al*., 2012)], extracellular proteolysis and invasion [i.e., *ETV4, HPSE, PLAUR*, *SMAD4*, *TGFB1* (Yuan *et al*., 2014; Sun *et al*., 2017; Narayanaswamy *et al*., 2017; Wiercinska *et al*., 2011], interaction with the vasculature [i.e., *CD44*, *COL4A2* (McFarlane *et al*., 2015; JingSong *et al*., 2017)], evasion of the antitumor immunity [i.e., *CCL7*, *HGF* and its receptor *MET* (Liu *et al*., 2018; Kitamura *et al*., 2019)] and exosome-mediated organotropism [i.e., *ITGB3* (Fuentes *et al*., 2020)].

Of interest, the inverse association between FAAH levels in human tumors and the incidence of metastasis was exclusive to lung, but not to bone or brain metastasis. It is now well accepted that organotropic metastasis of BC is attributed to the acquisition, early in tumorigenesis, of specific gene expression signatures that endow tumor cells with metastatic abilities selective to certain sites (Weigelt *et al*., 2003). It is tempting to speculate that, in this case, the inverse association between FAAH expression and the incidence of lung metastasis may be related to the negative regulation by FAAH of the lung metastasis signature (LMS) established by Minn and colleagues (Minn *et al*., 2005) that we observed in T-47D cells. Unlike other metastatic signatures, which include genes known to play important functions in the host organ [for example, bone metastasis signature (Kang *et al*., 2003) encodes proteins able to alter the bone tissue environment to foster formation of osteolytic bone lesions], LMS is less specific to the lung microenvironment and rather promotes general features of aggressive growth and invasiveness in the tumor cells. Consistent with that, tumors enriched in the LMS predominantly express markers of clinically aggressive disease such as estrogen receptor (ER) negative status, a Rosetta-type poor prognosis signature (van't Veer *et al*., 2002) and a basal-like phenotype (Minn *et al*., 2005). Our data suggest that FAAH impairs both breast tumorigenicity and lung metastasis by blocking all those aggressive features.

Here, we provide evidence for the functional involvement of one of the members of the LMS signature, the chemokine receptor CXCR4, in the FAAH-mediated anti-metastatic phenotype. In BC, the SDF1-CXCR4 ligand-receptor interaction gives rise to actin polymerization and pseudopodia formation in tumor cells, leading to chemotactic migration towards SDF1-rich environments such as the lung (Müller *et al*., 2001). When secreted by endothelial cells, SDF1 interacts with CXCR4 in BC cells to stimulate transendothelial migration (Jin *et al*., 2012). In addition, SDF1 can be secreted by carcinoma-associated fibroblasts (CAFs) at the primary site and bind CXCR4 in BC cells to stimulate tumor growth (Orimo *et al*., 2005). Here, we have shown that both CXCR4 and SDF1 expression are inversely associated with that of FAAH in mouse and human tumors and that, in BC cell lines, FAAH regulates CXCR4 expression and CXCR4-dependent capacity to transmigrate through a matrigel membrane towards SDF1-containing medium. Although regulation of lung metastasis by FAAH in BC probably relies on multiple signaling routes, these results strongly support an involvement of CXCR4-SDF1 signaling in FAAH-mediated antimetastatic behavior and justify further research on the significance of the FAAH-CXCR4 axis in metastasis formation *in vivo*.

Role of eCBs on tumor and metastasis suppressing actions of FAAH

The identification of the molecular mediators of FAAH activity, either upstream or downstream, remains an important goal to understand its diverse roles in BC. Regarding the later, our results strongly suggest the participation of AEA in the

control of the antitumorigenic properties of FAAH. Thus, treatment of T-47D cells with methanandamide (metAEA) phenocopied FAAH silencing in enhancing their invasive potential and CXCR4 levels through a cannabinoid receptor (CBR)-mediated mechanism.

Over the last decades, several authors have detected higher levels of AEA in tumor tissue (gliomas, meningiomas, pituitary adenomas, prostate, colon, and endometrial cancer) than in the tissues they derive from (Fraguas-Sánchez *et al.*, 2018). In patients with metastasis, plasma levels of AEA were higher than in patients with no metastases (Sailler *et al.*, 2014). However, studies aimed at unraveling the role of endogenous AEA in cancer have been scarce. Here, we provide evidence that activation of CBRs by low concentrations of metAEA (in the nM range) in BC cell lines (mimicking FAAH loss) drives protumorigenic responses through CBR activation, and support the hypothesis of the existence of an endogenous AEA tone that may underlie tumor progression in BC.

Initially, this hypothesis may be in contradiction to a large number of studies describing the actions of AEA or AEA analogues in the inhibition of BC cell proliferation (De Petrocellis *et al.*, 1998), migration (Grimaldi *et al.*, 2006), EMT induction (Laezza *et al.*, 2012) and angiogenesis (Picardi *et al.*, 2014) that, together, contribute to the widely accepted view that pharmacological activation of the ECS produces antitumor responses. However, the antitumor effects described in the studies mentioned above displayed EC_{50} values within the micromolar range (1-10 μM), which are unlikely to be achieved *in vivo*. We and others (Bisogno *et al.*, 1998) have previously demonstrated that AEA is expressed at picomolar levels in BC cells (**FIG. D5**). Therefore, we firmly believe that the use of concentrations in the low nanomolar range such as the ones used in this thesis (i.e., 1 nM) are more appropriate to study the role of the endogenous AEA tone in BC.

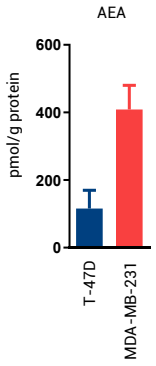

Figure D5. Endogenous AEA levels in T-47D and MDA-MB-231 cell lines normalized to protein content. Lipidomics were performed in whole cell lysates coming from one 6 cm plate with 1 x 10^6 cells, which contains approximately 100 μg of protein. Student's t-test: ns.

The biphasic effect of AEA as well as of other cannabinoids has been reported before. MetAEA and AEA (respectively) are able to inhibit the proliferation of prostate (Sánchez *et al.*, 2003) and gastric (Miyato *et al.*, 2009) cancer cell lines

when used at micromolar concentrations, while at nanomolar concentrations, they activate mitogenic signal transduction pathways through CBR-mediated mechanisms. Despite the inhibitory effect on migration reported at higher doses, AEA is also able to stimulate the migration of epithelial cells with EC50 values of 39.9 ± 3.7 nM (Song *et al*., 2000). Similarly, several lines of evidence show that THC at submicromolar concentrations exerts protumoral instead of antitumoral actions in breast (McKallip *et al*., 2005), lung (Zhu *et al*., 2000), and brain tumors (Hart *et al*., 2004). Although the pleiotropic actions of cannabinoids on CBRs have long been acknowledged, there is still no consensus on the molecular basis of their concentration-dependent effects. It is generally believed that, when cannabinoids are administered in high concentrations, they can take over the endocannabinoid signaling for longer time periods, leading to downstream biological responses that might greatly differ from the activation by lower concentrations or by the endogenous eCB tone, which is subjected to a tight temporal and spatial regulation. For example, the fact that AEA at low doses exhibits 'excitatory' rather than 'inhibitory' actions in several behavioral tests has been explained by a CB_1R-mediated activation of adenylyl cyclase via a G_s protein, instead of the more typical G_i-mediated inhibition of the enzyme (Glass & Felder, 1997). On the other hand, it is known that some G-protein independent actions of cannabinoids rely on the prolonged activation of downstream routes which otherwise would mediate the opposite effects on cell fate. This is the case of ERK pathway, whose activation generally leads to cell proliferation but, when subjected to a prolonged activation, can lead to cell death. This is the molecular basis of THC-mediated cycle arrest and cell death in glioma cells, which originates from a prolonged activation of ERK cascade caused by *de novo* ceramide synthesis (Galve-Roperh *et al*., 2000). A biphasic effect on CBRs in cancer cells is thus possible, triggering proliferative responses when activated locally at nanomolar concentrations (either exogenously or by the eCB tone) and antiproliferative responses when activated by exogenous cannabinoids at micromolar concentrations.

Although the role of an endogenous AEA tone in tumor progression has not ever been studied in BC, there are some examples in the literature where an enhancement of the endogenous AEA levels by FAAH inhibitors leads to antitumor responses in other cancer models (Jaiswal *et al*., 2021). Further investigations on the signaling pathways involved in the oncogenic actions of the AEA tone in BC are necessary in order to explain the differences between our results and theirs.

The effects of metAEA in T-47D cells were prevented by the use of CB_1R- and CB_2R-selective antagonists, implying that CBRs participate in the protumorigenic actions of metAEA and might operate similarly in mediating the actions of a hypothetic protumorigenic endogenous AEA tone. During malignant transformation of the mammary gland, there is a switch between CB_1R and CB_2R expression. CB_1R levels are higher in the mammary gland than in BC, and in tumor samples, its expression

decreases with tumor grade. Conversely, CB_2R expression is absent in the non-transformed mammary tissue, and it increases in BC, where it is most expressed in the HER2+ subtype (Caffarel *et al*., 2006). This expression pattern suggests the possibility that each receptor controls different functions in BC cells. In the studies mentioned above, the authors frequently attributed the antitumor action of FAAH inhibitors to the antiproliferative effects of AEA at CB_1R (Jaiswal *et al*., 2021). It could be hypothesized that endogenous AEA in BC inhibits tumor cell proliferation through CB_1R, but promotes other tumorigenic features through CB_2R, which has indeed recently been shown to act as a pro-oncogenic factor in HER2+ BC (Pérez-Gómez *et al*., 2015). That would explain the fact that, despite driving mostly tumor-promoting events, FAAH silencing in T-47D cells decreased cell proliferation *in vitro,* while the increase of the AEA tone after FAAH overexpression in MDA-MB-231 did not result in increased cell proliferation, possibly because in this cell line there is no (or very low) CB_1R to mediate such response (**FIG. D6**). This hypothesis is also consistent with MMTV-neu:FAAH $^{-/-}$ mice showing delayed tumor onset (probably due to a predominant CB_1R activity in the mammary gland inhibiting cell proliferation), but enhanced growth once the tumor is established (due to CB_2R becoming the predominant CBR after malignant transformation and favoring oncogenic signaling). Of interest, and in line with this idea, one of the very few studies published to date on the role of the ECS in cancer that involves genetic models of CBR inactivation (apart from Pérez-Gómez *et al*., 2015) reveals CB_1R and CB_2R exert opposite effects on hepatocarcinogenesis (Suk *et al*., 2019).

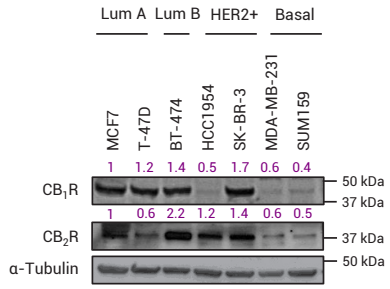

Figure D6. Western blot analysis of CB_1R and CB_2R in a panel of human BC cell lines representative of the main intrinsic subtypes. Densitometric values after normalization against α-Tubulin and control condition are depicted in purple.

The inverse association between FAAH and tumor progression in BC could also involve the activation of receptors other than CBRs by AEA, as well as by other FAAH substrates. For instance, metAEA promoted tumor growth in murine lung cancer by a CBR-independent pathway associated with the upregulation of COX-2 and prostaglandin E_2 (PGE_2) production (Gardner *et al*., 2003), both of which are well-known risk factors in BC (Reader *et al*., 2011). Interestingly, in our hands, FAAH modulation in MECs as well as in BC lines usually preceded changes in COX-

2 expression in the opposite direction of FAAH (data not shown), suggesting that FAAH and COX-2 might be subjected to opposite regulations in the mammary gland. Regarding cannabinoid-related receptors, AEA is able to bind and activate PPARγ, whose overexpression in the mammary tissue of transgenic mice accelerates BC progression (Saez *et al*., 2004). Additionally, inhibition of FAAH confers increased stem cell migration via PPARα (Wollank *et al*., 2015), which is not activated by AEA but by PEA and OEA, whose levels are also upregulated in T-47D FAAH KO cells. Of note, low concentrations of OEA (0.01-1 μM) promoted melanoma cell migration whereas high concentrations (2-100 μM) inhibited it (Sailler *et al*., 2014), evoking the concentration-dependent effects of AEA on cancer cells. Future research should investigate the relative contributions of CBRs and non-CBRs to the protumorigenic actions in BC cells here ascribed for FAAH substrates.

We also consider the possibility that genetic blockade of FAAH might simply divert degradation of AEA and other FAAH substrates towards compensatory catabolic pathways able to promote oncogenic functions. For example, AEA can be efficiently oxygenated by COX-2 to generate prostaglandin ethanolamides (PG-EAs), whose role in cancer has just begun to be studied. In squamous carcinoma and melanoma, treatment with 15-deoxy $\Delta^{12,14}$-prostaglandin J_2-ethanolamide (15d-PMJ_2) induced tumor cell proliferation or cell death when used at concentrations below and over 1 μM, respectively (Ladin *et al*., 2017). Additionally, FAAH silencing could lead to the upregulation of MAGL to take over 2-AG degradation. Overexpression of MAGL has been observed in aggressive human cancer cells and primary tumors, where it regulates a fatty acid network enriched in oncogenic signaling lipids that promotes migration, invasion, survival, and *in vivo* tumor growth (Nomura *et al*., 2010). In BC, higher levels of MAGL were found in ductal breast tumors vs. less malignant medullary breast tumors (Gjerstorff *et al*., 2006). T47-D FAAH KO cells displayed lower levels of 2-AG and an upward trend on *MGLL* mRNA expression (data not shown), thus raising the possibility that an oncogenic fatty acid network driven by a higher MAGL activity in these cells is supporting cancer pathogenesis.

TRANSLATIONAL IMPLICATIONS OF THIS WORK

As a result of this doctoral thesis, it can be concluded that the AEA-hydrolyzing enzyme FAAH plays essential roles both in the adult mammary gland and in BC. Specifically, we have demonstrated that FAAH promotes cellular differentiation in both physiological and pathological contexts, which may have therapeutic implications at several levels. As it has been already discussed, the findings on the role of FAAH in MEC differentiation in the mammary gland provide valuable insights into the role of FAAH in BC, but they also have translational relevance on their own. Inadequate milk production affects many women after giving birth, but the molecular determinants underlying lactational failure are still poorly understood

(Olsen & Gordon, 1990; Kent *et al*., 2012). The identification of physiological barriers for lactation would allow to develop novel interventions to support lactation success and provide health benefit across two generations, and thus merits further attention in the future. On the other hand, we have demonstrated that FAAH plays a similar role in BC (it promotes specification to more differentiated, less aggressive tumor types and blocks lung metastasis to the lung), which holds important implications regarding the use of FAAH as a patient screening tool and as a therapeutic target in BC.

FAAH as a BC patient screening tool

This doctoral thesis supports that FAAH may be a robust prognostic indicator in BC. Our studies link high FAAH expression in breast tumors with a better overall patient survival (OS). This association was found when analyzing datasets containing tumors from all BC intrinsic subtypes, but also when analyzing datasets with luminal tumors only, thus confirming that the value of FAAH as a prognostic marker is independent from its association with the luminal subtype, which inherently carries a better OS.

Two of the main survival-affecting events in BC are development of metastatic disease and distant recurrence after initially successful treatment (Harbeck *et al*., 2019). A proper classification of BC tumors into metastasis-prone and unlikely-to-metastasize is considered a key issue in BC research since it allows to personalize disease management. On the other hand, and although some genomic tests have been developed that estimate the risk of recurrence, there is a further need for prognostic tools able to foresee the risk of relapse in an accurate and precise manner, especially if the relapse occurs in distant organs (Tabor *et al*., 2020). Here, we demonstrate that high FAAH levels are associated with higher metastasis-free survival (MFS) and relapse-free survival (RFS), and propose that FAAH is a favorable prognostic marker that might provide additional discriminatory power to the currently available tools in assessing the risk of metastatic disease and relapse.

Although this thesis does not directly address the validity of FAAH as a marker with predictive significance in BC, our results open up new perspectives for investigating the use of FAAH as a predictive tool. It is tempting to speculate that higher risk of relapse in patients with lower FAAH levels could be explained by FAAH loss providing tumor cells with resistance mechanisms to escape primary treatments. For instance, one could speculate that the interrelation between FAAH and ER signaling might underlie some of the mechanisms driving tamoxifen resistance (Ali *et al*., 2016). On the other hand, and based on the demonstrated role of FAAH in the differentiation of MECs and breast tumors, FAAH loss would be expected to increase the number of cancer stem cells (CSCs) in the tumor, a subpopulation of long-lived cells with stem-like features that sustain tumor growth and exhibit chemotherapy resistance (Batlle *et al*., 2017). In addition, genetic inactivation of

FAAH in BC precedes higher immune infiltration in the tumor, which could create a microenvironment enriched for the expression of immune checkpoint genes and thus increase susceptibility to immune checkpoint blockade strategies (Bertucci *et al*., 2021). Future research is needed to validate these hypothesis and determine how FAAH activity impacts the response of BC to certain treatments.

FAAH as a therapeutic target in BC

Collectively, our results show that FAAH is a critical regulator of tumor differentiation and lung metastasis, and therefore, it might have potential as a therapeutic target in BC.

Over the last years, FAAH has attracted considerable attention in the preclinical and clinical community due to the promising pharmacological properties of FAAH inhibitors in pain, anxiety and trauma-related disorders (Van Egmond *et al*., 2021). However, research on FAAH was brought to a screeching halt after a phase I trial with one of these compounds (BIA-10-2474) led to one fatality and several patients with neurological alterations (Kerbrat *et al*., 2016). Later studies determined this unfortunate event was unrelated to FAAH blockade, but instead to the promiscuity of BIA-10-2474 molecule which, apart from FAAH, inhibited several other lipases that were not targeted by other FAAH inhibitors (Van Esbroeck *et al*., 2017).

Nevertheless, evidence gathered in this doctoral thesis point to the possibility that BC patients would not benefit from FAAH inhibition, but instead, from an upregulation of FAAH expression and/or activity in the tumor cells. Unfortunately, introducing FAAH into the tumor cells possesses several limitations as a therapeutic strategy. Despite the significant improvements made in the recent years, cancer gene therapy is in its infancy and still needs to overcome several hurdles related to the delivery and the optimal expression of the therapeutic genes (Das *et al*., 2015). A more rational approach to bring FAAH upregulation closer to the clinic would be to identify upstream regulators that increased its expression or activity. Recently, the first compound ever reported that stimulates the activity of a FAAH protein was isolated from *Arabidopsis thaliana*, thus providing a novel tool to downregulate the endogenous NAE tone in the cell (Khan *et al*., 2017).

Setting aside the current limitations to implement FAAH stimulating therapies, it is important to keep in mind that, due to its aggressive tumor biology and the lack of selective therapeutic targets, basal-like BC remains an unmet clinical challenge. Pharmacologic strategies for triggering the switch from basal-like to a luminal subtype would profit the clinical therapy of basal-like BC patients. Abundant studies are currently in progress trying to use differentiation agents such as all-trans retinoic acid (Li *et al*., 2011), miR-100 (Petrelli *et al*., 2015) and histone deacetylase inhibitors (Witt *et al*., 2017) in BC. miR-100, for example, induces a basal-to-luminal switch that boost basal-like BC cells response to hormonal therapy through

the expression of ER. Although the upregulation of luminal-specific genes in MDA-MB-231 basal cells upon FAAH overexpression remains to be demonstrated, they showed a reduction in their invasive capability, EMT phenotype and tumor growth *in vivo*, suggesting that FAAH is capable of inducing less differentiated BC cells to acquire phenotypic characteristics of more differentiated or luminal cells, and therefore could represent a valid candidate for differentiation therapy. In addition, because FAAH upregulation in MDA-MB-231 cells was able to reduce lung metastasis, elevating the expression or activity of FAAH in the primary tumor may prove useful for reducing the chances of developing metastasis in BC.

In summary, and in view of the antitumoral and antimetastatic properties of FAAH described herein, it would be worth continuing research on the signaling pathways regulated by this protein in the context of BC, that may provide new grounds for the design of new strategies and tools for the management of this pathology.

CONCLUSIONS

The data obtained in this doctoral thesis allow delineating the following conclusions:

1. FAAH expression in the mammary gland is restricted to the luminal lineage of the mammary epithelial cell (MEC) hierarchy, where it increases along luminal cell differentiation.

2. FAAH is a driver of lactogenic differentiation *in vitro* (by downregulating the endocannabinoid tone and its activity at CB_1R) and *in vivo (*it is necessary for complete mammary gland differentiation).

3. FAAH expression is associated with the luminal subtype of breast cancer (BC), and a better patient prognosis, so it offers the potential to be used as a biomarker with prognostic value.

4. FAAH is a driver of tumor cell differentiation in BC cells (it promotes the acquisition and maintenance of a luminal-like, less aggressive phenotype) and a suppressor of lung metastasis, and therefore, it offers the potential to be used as a therapeutic target in BC.

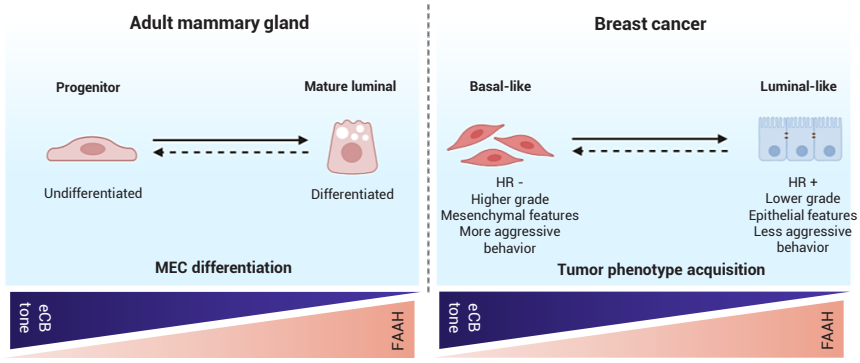

Figure D7. Graphical abstract on the role of FAAH in mammary physiopathology. FAAH is a key factor in determining the biological characteristics of mammary luminal epithelial cells and BCs with a luminal phenotype.

REFERENCES

Ablett, M. P., O'Brien, C. S., Sims, A. H., Farnie, G., & Clarke, R. B. (2014). A differential role for CXCR4 in the regulation of normal versus malignant breast stem cell activity. Oncotarget, 5(3), 599.

Al Saleh, S., Al Mulla, F., & Luqmani, Y. A. (2011). Estrogen receptor silencing induces epithelial to mesenchymal transition in human breast cancer cells. PloS one, 6(6), e20610.

Ali, S., Rasool, M., Chaoudhry, H., Pushparaj, P. N., Jha, P., Hafiz, A., ... & Jamal, M. S. (2016). Molecular mechanisms and mode of tamoxifen resistance in breast cancer. Bioinformation, 12(3), 135.

Almada, M., Oliveira, A., Amaral, C., Fernandes, P. A., Ramos, M. J., Fonseca, B., ... & Teixeira, N. (2019). Anandamide targets aromatase: a breakthrough on human decidualization. Biochimica et Biophysica Acta (BBA)-Molecular and Cell Biology of Lipids, 1864(12), 158512.

Anderson, S. M., Rudolph, M. C., McManaman, J. L., & Neville, M. C. (2007). Key stages in mammary gland development. Secretory activation in the mammary gland: it's not just about milk protein synthesis! Breast Cancer Research, 9(1), 204.

Andradas, C., Blasco-Benito, S., Castillo-Lluva, S., Dillenburg-Pilla, P., Diez-Alarcia, R., Juanes-García, A., ... & Sánchez, C. (2016). Activation of the orphan receptor GPR55 by lysophosphatidylinositol promotes metastasis in triple-negative breast cancer. Oncotarget, 7(30), 47565.

Andradas, C., Caffarel, M. M., Perez-Gomez, E., Salazar, M., Lorente, M., Velasco, G., ... & Sánchez, C. (2011). The orphan G protein-coupled receptor GPR55 promotes cancer cell proliferation via ERK. Oncogene, 30(2), 245-252.

Anstine, L. J., & Keri, R. (2019). A new view of the mammary epithelial hierarchy and its implications for breast cancer initiation and metastasis. J. Cancer Met. Treat., in press. Invited review.

Asselin-Labat, M. L., Vaillant, F., Sheridan, J. M., Pal, B., Wu, D., Simpson, E. R., ... & Visvader, J. E. (2010). Control of mammary stem cell function by steroid hormone signalling. Nature, 465(7299), 798-802.

Atance, J. A. R. (2017). Efectos terapéuticos de los cannabinoides. Especiales.

Bach, K., Pensa, S., Grzelak, M., Hadfield, J., Adams, D. J., Marioni, J. C., & Khaled, W. T. (2017). Differentiation dynamics of mammary epithelial cells revealed by single-cell RNA sequencing. Nature communications, 8(1), 1-11.

Bachelder, R. E., Wendt, M. A., & Mercurio, A. M. (2002). Vascular endothelial growth factor promotes breast carcinoma invasion in an autocrine manner by regulating the chemokine receptor CXCR4. Cancer research, 62(24), 7203-7206.

Badowska-Kozakiewicz, A. M., & Budzik, M. P. (2016). Immunohistochemical characteristics of basal-like breast cancer. Contemporary Oncology, 20(6), 436.

Ball, R. K., Friis, R. R., Schoenenberger, C. A., Doppler, W., & Groner, B. (1988). Prolactin regulation of beta-casein gene expression and of a cytosolic 120-kd protein in a cloned mouse mammary epithelial cell line. The EMBO journal, 7(7), 2089-2095.

Banerji, S., Cibulskis, K., Rangel-Escareno, C., Brown, K. K., Carter, S. L., Frederick, A. M., ... & Meyerson, M. (2012). Sequence analysis of mutations and translocations across breast cancer subtypes. Nature, 486(7403), 405-409.

Barash, I., & Reichenstein, M. (2002). Real-time imaging of β-lactoglobulin-targeted luciferase activity in the mammary glands of transgenic mice. Molecular reproduction and development, 61(1), 42-48.

Batlle, E., & Clevers, H. (2017). Cancer stem cells revisited. Nature medicine, 23(10), 1124-1134.

Berens, E. B., Holy, J. M., Riegel, A. T., & Wellstein, A. (2015). A cancer cell spheroid assay to assess invasion in a 3D setting. JoVE (Journal of Visualized Experiments), (105), e53409.

Bertucci, F., Boudin, L., Finetti, P., Van Berckelaer, C., Van Dam, P., Dirix, L., ... & Mamessier, E. (2021). Immune landscape of inflammatory breast cancer suggests vulnerability to immune checkpoint inhibitors. Oncoimmunology, 10(1), 1929724.

Bisogno, T., Katayama, K., Melck, D., Ueda, N., De Petrocellis, L., Yamamoto, S., & Di Marzo, V. (1998). Biosynthesis and degradation of bioactive fatty acid amides in human breast cancer and rat pheochromocytoma cells: implications for cell proliferation and differentiation. European journal of Biochemistry, 254(3), 634-642.

Blasco-Benito, S., Moreno, E., Seijo-Vila, M., Tundidor, I., Andradas, C., Caffarel, M. M., ... & Hernández, L. (2019). Therapeutic targeting of HER2–CB2R heteromers in HER2-positive breast cancer. Proceedings of the National Academy of Sciences, 116(9), 3863-3872.

Bloom, H. J. G., & Richardson, W. W. (1957). Histological grading and prognosis in breast cancer: a study of 1409 cases of which 359 have been followed for 15 years. British journal of cancer, 11(3), 359.

Boger, D. L., Fecik, R. A., Patterson, J. E., Miyauchi, H., Patricelli, M. P., & Cravatt, B. F. (2000). Fatty acid amide hydrolase substrate specificity. Bioorganic & medicinal chemistry letters, 10(23), 2613-2616.

Bos, P. D., Zhang, X. H. F., Nadal, C., Shu, W., Gomis, R. R., Nguyen, D. X., ... & Massagué, J. (2009). Genes that mediate breast cancer metastasis to the brain. Nature, 459(7249), 1005-1009.

Boumahrou, N., Bevilacqua, C., Beauvallet, C., Miranda, G., Andrei, S., Rebours, E., ... & Martin, P. (2011). Evolution of major milk proteins in Mus musculus and Mus spretus mouse species: a genoproteomic analysis. BMC genomics, 12(1), 1-13.

Bracey, M. H., Hanson, M. A., Masuda, K. R., Stevens, R. C., & Cravatt, B. F. (2002). Structural adaptations in a membrane enzyme that terminates endocannabinoid signaling. Science, 298(5599), 1793-1796.

Brisken, C., Kaur, S., Chavarria, T. E., Binart, N., Sutherland, R. L., Weinberg, R. A., ... & Ormandy, C. J. (1999). Prolactin controls mammary gland development via direct and indirect mechanisms. Developmental biology, 210(1), 96-106.

Brown, A. J. (2007). Novel cannabinoid receptors. British journal of pharmacology, 152(5), 567-575.

Caffarel, M. M., Andradas, C., Mira, E., Pérez-Gómez, E., Cerutti, C., Moreno-Bueno, G., ... & Guzmán, M. (2010). Cannabinoids reduce ErbB2-driven breast cancer progression through Akt inhibition. Molecular cancer, 9(1), 196.

Caffarel, M. M., Andradas, C., Pérez-Gómez, E., Guzmán, M., & Sánchez, C. (2012). Cannabinoids: a new hope for breast cancer therapy?. Cancer treatment reviews, 38(7), 911-918.

Caffarel, M. M., Sarrió, D., Palacios, J., Guzmán, M., & Sánchez, C. (2006). Δ9-tetrahydrocannabinol inhibits cell cycle progression in human breast cancer cells through Cdc2 regulation. Cancer research, 66(13), 6615-6621.

Caffarel, M. M., Zaragoza, R., Pensa, S., Li, J., Green, A. R., & Watson, C. J. (2012). Constitutive activation of JAK2 in mammary epithelium elevates Stat5 signalling, promotes alveologenesis and resistance to cell death, and contributes to tumourigenesis. Cell Death & Differentiation, 19(3), 511-522.

Charafe-Jauffret, E., Ginestier, C., Monville, F., Finetti, P., Adelaïde, J., Cervera, N., ... & Bertucci, F. (2006). Gene expression profiling of breast cell lines identifies potential new basal markers. Oncogene, 25(15), 2273-2284.

Chen, W., Hoffmann, A. D., Liu, H., & Liu, X. (2018). Organotropism: new insights into molecular mechanisms of breast cancer metastasis. NPJ precision oncology, 2(1), 1-12.

Coke, C. J., Scarlett, K. A., Chetram, M. A., Jones, K. J., Sandifer, B. J., Davis, A. S., ... & Hinton, C. V. (2016). Simultaneous activation of induced heterodimerization between CXCR4 chemokine receptor and cannabinoid receptor 2 (CB2) reveals a mechanism for regulation of tumor progression. Journal of Biological Chemistry, 291(19), 9991-10005.

Cravatt, B. F., Demarest, K., Patricelli, M. P., Bracey, M. H., Giang, D. K., Martin, B. R., & Lichtman, A. H. (2001). Supersensitivity to anandamide and enhanced endogenous cannabinoid signaling in mice lacking fatty acid amide hydrolase. Proceedings of the National Academy of Sciences, 98(16), 9371-9376.

Cravatt, B. F., Giang, D. K., Mayfield, S. P., Boger, D. L., Lerner, R. A., & Gilula, N. B. (1996). Molecular characterization of an enzyme that degrades neuromodulatory fatty-acid amides. Nature, 384(6604), 83-87.

Croker, B. A., Kiu, H., & Nicholson, S. E. (2008, August). SOCS regulation of the JAK/STAT signalling pathway. In Seminars in cell & developmental biology (Vol. 19, No. 4, pp. 414-422). Academic Press.

Curtis, C., Shah, S. P., Chin, S. F., Turashvili, G., Rueda, O. M., Dunning, M. J., ... & Aparicio, S. (2012). The genomic and transcriptomic architecture of 2,000 breast tumours reveals novel subgroups. Nature, 486(7403), 346-352.

Das, S. K., Menezes, M. E., Bhatia, S., Wang, X. Y., Emdad, L., Sarkar, D., & Fisher, P. B. (2015). Gene therapies for cancer: strategies, challenges and successes. Journal of cellular physiology, 230(2), 259-271.

De Petrocellis, L., & Di Marzo, V. (2010). Non-CB 1, non-CB 2 receptors for endocannabinoids, plant cannabinoids, and synthetic cannabimimetics: Focus on G-protein-coupled receptors and transient receptor potential channels. Journal of Neuroimmune Pharmacology, 5(1), 103-121.

De Petrocellis, L., Melck, D., Palmisano, A., Bisogno, T., Laezza, C., Bifulco, M., & Di Marzo, V. (1998). The endogenous cannabinoid anandamide inhibits human breast cancer cell proliferation. Proceedings of the National Academy of Sciences, 95(14), 8375-8380.

DeOme, K. B., Faulkin, L. J., Bern, H. A., & Blair, P. B. (1959). Development of mammary tumors from hyperplastic alveolar nodules transplanted into gland-free mammary fat pads of female C3H mice. Cancer research, 19(5), 515.

Devane, W. A., Dysarz, F. 3., Johnson, M. R., Melvin, L. S., & Howlett, A. C. (1988). Determination and characterization of a cannabinoid receptor in rat brain. Molecular pharmacology, 34(5), 605-613.

Devane, W. A., Hanus, L., Breuer, A., Pertwee, R. G., Stevenson, L. A., Griffin, G., ... & Mechoulam, R. (1992). Isolation and structure of a brain constituent that binds to the cannabinoid receptor. Science, 258(5090), 1946-1949.

Di Marzo, V., & Maccarrone, M. (2008). FAAH and anandamide: is 2-AG really the odd one out?. Trends in pharmacological sciences, 29(5), 229-233.

Di Marzo, V., Melck, D., Orlando, P., Bisogno, T., Zagoory, O., Bifulco, M., ... & de Petrocellis, L. (2001). Palmitoylethanolamide inhibits the expression of fatty acid amide hydrolase and enhances the anti-proliferative effect of anandamide in human breast cancer cells. Biochemical Journal, 358(1), 249-255.

Elbaz, M., Ahirwar, D., Xiaoli, Z., Zhou, X., Lustberg, M., Nasser, M. W., ... & Ganju, R. K. (2018). TRPV2 is a novel biomarker and therapeutic target in triple negative breast cancer. Oncotarget, 9(71), 33459.

Elbaz, M., Ahirwar, D., Ravi, J., Nasser, M. W., & Ganju, R. K. (2017). Novel role of cannabinoid receptor 2 in inhibiting EGF/EGFR and IGF-I/IGF-IR pathways in breast cancer. Oncotarget, 8(18), 29668.

Elston, C. W., & Ellis, I. O. (1991). Pathological prognostic factors in breast cancer. I. The value of histological grade in breast cancer: experience from a large study with long-term follow-up. Histopathology, 19(5), 403-410.

Endsley, M. P., Thill, R., Choudhry, I., Williams, C. L., Kajdacsy-Balla, A., Campbell, W. B., & Nithipatikom, K. (2008). Expression and function of fatty acid amide hydrolase in prostate cancer. International journal of cancer, 123(6), 1318-1326.

Ewing, J. (1928). Neoplastic Disease. A Treatment on Tumors.

Feng, Y., Broder, C. C., Kennedy, P. E., & Berger, E. A. (1996). HIV-1 entry cofactor: functional cDNA cloning of a seven-transmembrane, G protein-coupled receptor. Science, 272(5263), 872-877.

FlowJo™ Software for Windows Version 10.6.2. Ashland, OR: Becton, Dickinson and Company; 2019.

Fraguas-Sánchez, A. I., Martín-Sabroso, C., & Torres-Suárez, A. I. (2018). Insights into the effects of the endocannabinoid system in cancer: a review. British journal of pharmacology, 175(13), 2566-2580.

Fuentes, P., Sesé, M., Guijarro, P. J., Emperador, M., Sánchez-Redondo, S., Peinado, H., ... & y Cajal, S. R. (2020). ITGB3-mediated uptake of small extracellular vesicles facilitates intercellular communication in breast cancer cells. Nature communications, 11(1), 1-15.

Furuta, S., Jiang, X., Gu, B., Cheng, E., Chen, P. L., & Lee, W. H. (2005). Depletion of BRCA1 impairs differentiation but enhances proliferation of mammary epithelial cells. Proceedings of the National Academy of Sciences, 102(26), 9176-9181.

Galve-Roperh, I., Chiurchiù, V., Díaz-Alonso, J., Bari, M., Guzmán, M., & Maccarrone, M. (2013). Cannabinoid receptor signaling in progenitor/stem cell proliferation and differentiation. Progress in lipid research, 52(4), 633-650.

Galve-Roperh, I., Sánchez, C., Cortés, M. L., del Pulgar, T. G., Izquierdo, M., & Guzmán, M. (2000). Anti-tumoral action of cannabinoids: involvement of sustained ceramide accumulation and extracellular signal-regulated kinase activation. Nature medicine, 6(3), 313-319.

Gardner, B., Zhu, L. X., Sharma, S., Tashkin, D. P., & Dubinett, S. M. (2003). Methanandamide increases COX-2 expression and tumor growth in murine lung cancer. The FASEB journal, 17(14), 1-18.

Gaoni, Y., & Mechoulam, R. (1964). Isolation, structure, and partial synthesis of an active constituent of hashish. Journal of the American chemical society, 86(8), 1646-1647.

Gjerstorff, M. F., Benoit, V. M., Laenkholm, A. V., Nielsen, O., Johansen, L. E., & Ditzel, H. J. (2006). Identification of genes with altered expression in medullary breast cancer vs. ductal breast cancer and normal breast epithelia. International journal of oncology, 28(6), 1327-1335.

Giraddi, R. R., Chung, C. Y., Heinz, R. E., Balcioglu, O., Novotny, M., Trejo, C. L., ... & Hwang, J. Y. (2018). Single-cell transcriptomes distinguish stem cell state changes and lineage specification programs in early mammary gland development. Cell reports, 24(6), 1653-1666.

Glass, M., & Felder, C. C. (1997). Concurrent stimulation of cannabinoid CB1 and dopamine D2 receptors augments cAMP accumulation in striatal neurons: evidence for a Gs linkage to the CB1 receptor. Journal of Neuroscience, 17(14), 5327-5333.

Gorzalka, B. B., & Dang, S. S. (2012). Minireview: Endocannabinoids and gonadal hormones: bidirectional interactions in physiology and behavior. Endocrinology, 153(3), 1016-1024.

Grimaldi, C., Pisanti, S., Laezza, C., Malfitano, A. M., Santoro, A., Vitale, M., ... & Di Marzo, V. (2006). Anandamide inhibits adhesion and migration of breast cancer cells. Experimental cell research, 312(4), 363-373.

Grimaldi, P., Pucci, M., Di Siena, S., Di Giacomo, D., Pirazzi, V., Geremia, R., & Maccarrone, M. (2012). The faah gene is the first direct target of estrogen in the testis: role of histone demethylase LSD1. Cellular and molecular life sciences, 69(24), 4177-4190.

Guo, F., Wang, Y., Liu, J., Mok, S. C., Xue, F., & Zhang, W. (2016). CXCL12/CXCR4: a symbiotic bridge linking cancer cells and their stromal neighbors in oncogenic communication networks. Oncogene, 35(7), 816-826.

Guy, C. T., Webster, M. A., Schaller, M., Parsons, T. J., Cardiff, R. D., & Muller, W. J. (1992). Expression of the neu protooncogene in the mammary epithelium of transgenic mice induces metastatic disease. Proceedings of the National Academy of Sciences, 89(22), 10578-10582.

Guzmán, M., Galve-Roperh, I., & Sánchez, C. (2001). Ceramide: a new second messenger of cannabinoid action. Trends in pharmacological sciences, 22(1), 19-22.

Györffy, B. (2021). Survival analysis across the entire transcriptome identifies biomarkers with the highest prognostic power in breast cancer. Computational and Structural Biotechnology Journal, 19, 4101-4109.

Hanahan, D., & Weinberg, R. A. (2011). Hallmarks of cancer: the next generation. cell, 144(5), 646-674.

Hanlon, K. E., Lozano-Ondoua, A. N., Umaretiya, P. J., Symons-Liguori, A. M., Chandramouli, A., Moy, J. K., ... & Vanderah, T. W. (2016). Modulation of breast cancer cell viability by a cannabinoid receptor 2 agonist, JWH-015, is calcium dependent. Breast Cancer: Targets and Therapy, 8, 59.

Harbeck, N., Penault-Llorca, F., Cortes, J., Gnant, M., Houssami, N., Poortmans, P., Ruddy, K., Tsang, J., Cardoso, F (2019). Breast cancer. Nature Reviews Disease Primers, 5(1), 66.

Hart, S., Fischer, O. M., & Ullrich, A. (2004). Cannabinoids induce cancer cell proliferation via tumor necrosis factor α-converting enzyme (TACE/ADAM17)-mediated transactivation of the epidermal growth factor receptor. Cancer research, 64(6), 1943-1950.

Hennighausen, L., Robinson, G. W., Wagner, K. U., & Liu, X. (1997). Prolactin signaling in mammary gland development. Journal of Biological Chemistry, 272(12), 7567-7569.

Henry, M. D., Triplett, A. A., Oh, K. B., Smith, G. H., & Wagner, K. U. (2004). Parity-induced mammary epithelial cells facilitate tumorigenesis in MMTV-neu transgenic mice. Oncogene, 23(41), 6980-6985.

Hermanson, D. J., Hartley, N. D., Gamble-George, J., Brown, N., Shonesy, B. C., Kingsley, P. J., ... & Patel, S. (2013). Substrate-selective COX-2 inhibition decreases anxiety via endocannabinoid activation. Nature neuroscience, 16(9), 1291.

Herschkowitz, J. I., Simin, K., Weigman, V. J., Mikaelian, I., Usary, J., Hu, Z., ... & Backlund, M. G. (2007). Identification of conserved gene expression features between murine mammary carcinoma models and human breast tumors. Genome biology, 8(5), R76.

Higgins, M. J., & Baselga, J. (2011). Targeted therapies for breast cancer. The Journal of clinical investigation, 121(10), 3797-3803.

Hollern, D. P., & Andrechek, E. R. (2014). A genomic analysis of mouse models of breast cancer reveals molecular features ofmouse models and relationships to human breast cancer. Breast Cancer Research, 16(3), 1-16.

Ianotti, F.A., Piscitelli, F (2018). Endocannabinoidome. In: eLS. John Wiley & Sons, Ltd.

Ibsen, M. S., Connor, M., & Glass, M. (2017). Cannabinoid CB1 and CB2 receptor signaling and bias. Cannabis and cannabinoid research, 2(1), 48-60.

Inman, J. L., Robertson, C., Mott, J. D., & Bissell, M. J. (2015). Mammary gland development: cell fate specification, stem cells and the microenvironment. Development, 142(6), 1028-1042.

Jaiswal, S., & Ayyannan, S. R. (2021). Anticancer Potential of Small-Molecule Inhibitors of Fatty Acid Amide Hydrolase and Monoacylglycerol Lipase. ChemMedChem.

Jézéquel, P., Campone, M., Gouraud, W., Guérin-Charbonnel, C., Leux, C., Ricolleau, G., & Campion, L. (2012). bc-GenExMiner: an easy-to-use online platform for gene prognostic analyses in breast cancer. Breast cancer research and treatment, 131(3), 765-775.

Jézéquel, P., Gouraud, W., Ben Azzouz, F., Guérin-Charbonnel, C., Juin, P. P., Lasla, H., & Campone, M. (2021). bc-GenExMiner 4.5: new mining module computes breast cancer differential gene expression analyses. Database, 2021.

Jin, F., Brockmeier, U., Otterbach, F., & Metzen, E. (2012). New insight into the SDF-1/CXCR4 axis in a breast carcinoma model: hypoxia-induced endothelial SDF-1 and tumor cell CXCR4 are required for tumor cell intravasation. Molecular Cancer Research, 10(8), 1021-1031.

JingSong, H., Hong, G., Yang, J., Duo, Z., Li, F., WeiCai, C., ... & Zou, C. (2017). siRNA-mediated suppression of collagen type iv alpha 2 (COL4A2) mRNA inhibits triple-negative breast cancer cell proliferation and migration. Oncotarget, 8(2), 2585.

Kang, Y., Siegel, P. M., Shu, W., Drobnjak, M., Kakonen, S. M., Cordón-Cardo, C., ... & Massagué, J. (2003). A multigenic program mediating breast cancer metastasis to bone. Cancer cell, 3(6), 537-549.

Kanehisa, M., & Goto, S. (2000). KEGG: kyoto encyclopedia of genes and genomes. Nucleic acids research, 28(1), 27-30.

Kang, Y., Siegel, P. M., Shu, W., Drobnjak, M., Kakonen, S. M., Cordón-Cardo, C., ... & Massagué, J. (2003). A multigenic program mediating breast cancer metastasis to bone. Cancer cell, 3(6), 537-549.

Kannan, N., Huda, N., Tu, L., Droumeva, R., Aubert, G., Chavez, E., ... & Gilley, D. (2013). The luminal progenitor compartment of the normal human mammary gland constitutes a unique site of telomere dysfunction. Stem Cell Reports, 1(1), 28-37.

Kent, J. C., Prime, D. K., & Garbin, C. P. (2012). Principles for maintaining or increasing breast milk production. Journal of Obstetric, Gynecologic & Neonatal Nursing, 41(1), 114-121.

Kerbrat, A., Ferré, J. C., Fillatre, P., Ronzière, T., Vannier, S., Carsin-Nicol, B., ... & Edan, G. (2016). Acute neurologic disorder from an inhibitor of fatty acid amide hydrolase. New England Journal of Medicine, 375(18), 1717-1725.

Khan, B. R., Faure, L., Chapman, K. D., & Blancaflor, E. B. (2017). A chemical genetic screen uncovers a small molecule enhancer of the N-acylethanolamine degrading enzyme, fatty acid amide hydrolase, in Arabidopsis. Scientific reports, 7(1), 1-12.

Kim, S., Roopra, A., & Alexander, C. M. (2012). A phenotypic mouse model of basaloid breast tumors. PloS one, 7(2), e30979.

Kitamura, T., Kato, Y., Brownlie, D., Soong, D. Y., Sugano, G., Kippen, N., ... & Pollard, J. W. (2019). Mammary tumor cells with high metastatic potential are hypersensitive to macrophage-derived HGF. Cancer immunology research, 7(12), 2052-2064.

Koboldt, D. C. F. R., Fulton, R., McLellan, M., Schmidt, H., Kalicki-Veizer, J., McMichael, J., ... & Iglesia, M. (2012). Comprehensive molecular portraits of human breast tumours. Nature, 490(7418), 61-70.

Kufe, D. W., Holland, J. F., & Frei, E. (2003). Cancer medicine 6 (Vol. 2). BC Decker.

Kumar, S., Clarke, A. R., Hooper, M. L., Horne, D. S., Law, A. J., Leaver, J., ... & Simons, J. P. (1994). Milk composition and lactation of beta-casein-deficient mice. Proceedings of the National Academy of Sciences, 91(13), 6138-6142.

Kunos, G., Osei-Hyiaman, D., Bátkai, S., Sharkey, K. A., & Makriyannis, A. (2009). Should peripheral CB1 cannabinoid receptors be selectively targeted for therapeutic gain?. Trends in pharmacological sciences, 30(1), 1-7.

Ladin, D. A., Soliman, E., Escobedo, R., Fitzgerald, T. L., Yang, L. V., Burns, C., & Van Dross, R. (2017). Synthesis and Evaluation of the Novel Prostamide, 15-Deoxy, Δ12, 14-Prostamide J2, as a Selective Antitumor Therapeutic. Molecular cancer therapeutics, 16(5), 838-849.

Laezza, C., D'Alessandro, A., Paladino, S., Malfitano, A. M., Proto, M. C., Gazzerro, P., ... & Endocannabinoid Research Group. (2012). Anandamide inhibits the Wnt/β-catenin signalling pathway in human breast cancer MDA MB 231 cells. European Journal of Cancer, 48(16), 3112-3122.

Laezza, C., Pisanti, S., Crescenzi, E., & Bifulco, M. (2006). Anandamide inhibits Cdk2 and activates Chk1 leading to cell cycle arrest in human breast cancer cells. FEBS letters, 580(26), 6076-6082.

Li, R. J., Ying, X., Zhang, Y., Ju, R. J., Wang, X. X., Yao, H. J., ... & Lu, W. L. (2011). All-trans retinoic acid stealth liposomes prevent the relapse of breast cancer arising from the cancer stem cells. Journal of controlled release, 149(3), 281-291.

Lim, E., Vaillant, F., Wu, D., Forrest, N. C., Pal, B., Hart, A. H., ... & Feleppa, F. (2009). Aberrant luminal progenitors as the candidate target population for basal tumor development in BRCA1 mutation carriers. Nature medicine, 15(8), 907.

Lim, E., Wu, D., Pal, B., Bouras, T., Asselin-Labat, M. L., Vaillant, F., ... & Visvader, J. E. (2010). Transcriptome analyses of mouse and human mammary cell subpopulations reveal multiple conserved genes and pathways. Breast Cancer Research, 12(2), 1-14.

Liu, Y., Cai, Y., Liu, L., Wu, Y., & Xiong, X. (2018). Crucial biological functions of CCL7 in cancer. PeerJ, 6, e4928.

Lonsdale, J., Thomas, J., Salvatore, M., Phillips, R., Lo, E., Shad, S., ... & Moore, H. F. (2013). The genotype-tissue expression (GTEx) project. Nature genetics, 45(6), 580-585.

Lu, H. C., & Mackie, K. (2016). An introduction to the endogenous cannabinoid system. Biological psychiatry, 79(7), 516-525.

Maccarrone, M., Bab, I., Bíró, T., Cabral, G. A., Dey, S. K., Di Marzo, V., ... & Sharkey, K. A. (2015). Endocannabinoid signaling at the periphery: 50 years after THC. Trends in pharmacological sciences, 36(5), 277-296.

Maccarrone, M., Bari, M., Di Rienzo, M., Finazzi-Agrò, A., & Rossi, A. (2003). Progesterone activates fatty acid amide hydrolase (FAAH) promoter in human T lymphocytes through the transcription factor Ikaros: evidence for a synergistic effect of leptin. Journal of Biological Chemistry, 278(35), 32726-32732.

Maccarrone, M., Dainese, E., & Oddi, S. (2010). Intracellular trafficking of anandamide: new concepts for signaling. Trends in biochemical sciences, 35(11), 601-608.

Maccarrone, M., De Felici, M., Bari, M., Klinger, F., Siracusa, G., & Finazzi-Agrò, A. (2000). Down-regulation of anandamide hydrolase in mouse uterus by sex hormones. European journal of Biochemistry, 267(10), 2991-2997.

Iglesias, J.M., Beloqui, I., Garcia-Garcia, F., Leis, O., Vazquez-Martin, A., Eguiara, A., ... & Martin, A. G. (2013). Mammosphere formation in breast carcinoma cell lines depends upon expression of E-cadherin. PloS one, 8(10), e77281.

Matsuda, L. A., Lolait, S. J., Brownstein, M. J., Young, A. C., & Bonner, T. I. (1990). Structure of a cannabinoid receptor and functional expression of the cloned cDNA. Nature, 346(6284), 561-564.

McFarlane, S., Coulter, J. A., Tibbits, P., O'Grady, A., McFarlane, C., Montgomery, N., ... & Waugh, D. J. (2015). CD44 increases the efficiency of distant metastasis of breast cancer. Oncotarget, 6(13), 11465.

McKallip, R. J., Nagarkatti, M., & Nagarkatti, P. S. (2005). Δ-9-tetrahydrocannabinol enhances breast cancer growth and metastasis by suppression of the antitumor immune response. The Journal of Immunology, 174(6), 3281-3289.

McKinney, M. K., & Cravatt, B. F. (2005). Structure and function of fatty acid amide hydrolase. Annu. Rev. Biochem., 74, 411-432.

Mechoulam, R., Ben-Shabat, S., Hanus, L., Ligumsky, M., Kaminski, N. E., Schatz, A. R., ... Vogel, Z. (1995). Identification of an endogenous 2-monoglyceride, present in canine gut, that binds to cannabinoid receptors. Biochemical Pharmacology, 50(1), 83-90.

Melck, D., Rueda, D., Galve-Roperh, I., De Petrocellis, L., Guzmán, M., & Di Marzo, V. (1999). Involvement of the cAMP/protein kinase A pathway and of mitogen-activated protein kinase in the anti-proliferative effects of anandamide in human breast cancer cells. FEBS letters, 463(3), 235-240.

Mi, H., Muruganujan, A., Ebert, D., Huang, X., & Thomas, P. D. (2019). PANTHER version 14: more genomes, a new PANTHER GO-slim and improvements in enrichment analysis tools. Nucleic acids research, 47(D1), D419-D426.

Michalski, C. W., Oti, F. E., Erkan, M., Sauliunaite, D., Bergmann, F., Pacher, P., ... & Kleeff, J. (2008). Cannabinoids in pancreatic cancer: correlation with survival and pain. International journal of cancer, 122(4), 742-750.

Middelbeek, J., Kuipers, A. J., Henneman, L., Visser, D., Eidhof, I., van Horssen, R., ... & Jalink, K. (2012). TRPM7 is required for breast tumor cell metastasis. Cancer research, 72(16), 4250-4261.

Minn, A. J., Gupta, G. P., Siegel, P. M., Bos, P. D., Shu, W., Giri, D. D., ... & Massagué, J. (2005). Genes that mediate breast cancer metastasis to lung. Nature, 436(7050), 518-524.

Minn, A. J., Gupta, G. P., Padua, D., Bos, P., Nguyen, D. X., Nuyten, D., ... & Massague, J. (2007). Lung metastasis genes couple breast tumor size and metastatic spread. Proceedings of the National Academy of Sciences, 104(16), 6740-6745.

Miyato, H., Kitayama, J., Yamashita, H., Souma, D., Asakage, M., Yamada, J., & Nagawa, H. (2009). Pharmacological synergism between cannabinoids and paclitaxel in gastric cancer cell lines. Journal of Surgical Research, 155(1), 40-47.

Moreno, E., Andradas, C., Medrano, M., Caffarel, M. M., Pérez-Gómez, E., Blasco-Benito, S., ... & Canela, E. I. (2014). Targeting CB2-GPR55 receptor heteromers modulates cancer cell signaling. Journal of Biological Chemistry, 289(32), 21960-21972.

Müller, A., Homey, B., Soto, H., Ge, N., Catron, D., Buchanan, M. E., ... & Barrera, J. L. (2001). Involvement of chemokine receptors in breast cancer metastasis. nature, 410(6824), 50-56.

Munro, S., Thomas, K. L., & Abu-Shaar, M. (1993). Molecular characterization of a peripheral receptor for cannabinoids. Nature, 365(6441), 61.

Munson, A. E., Harris, L. S., Friedman, M. A., Dewey, W. L., & Carchman, R. A. (1975). Antineoplastic activity of cannabinoids. Journal of the National Cancer Institute, 55(3), 597-602.

Narayanaswamy, P. B., Baral, T. K., Haller, H., Dumler, I., Acharya, K., & Kiyan, Y. (2017). Transcriptomic pathway analysis of urokinase receptor silenced breast cancer cells: a microarray study. Oncotarget, 8(60), 101572.

Nasser, M. W., Qamri, Z., Deol, Y. S., Smith, D., Shilo, K., Zou, X., & Ganju, R. K. (2011). Crosstalk between chemokine receptor CXCR4 and cannabinoid receptor CB2 in modulating breast cancer growth and invasion. PloS one, 6(9).

Neve, R. M., Chin, K., Fridlyand, J., Yeh, J., Baehner, F. L., Fevr, T., ... & Gray, J. W. (2006). A collection of breast cancer cell lines for the study of functionally distinct cancer subtypes. Cancer cell, 10(6), 515-527.

Nguyen, Q. H., Pervolarakis, N., Blake, K., Ma, D., Davis, R. T., James, N., ... & Driver, I. (2018). Profiling human breast epithelial cells using single cell RNA sequencing identifies cell diversity. Nature communications, 9(1), 1-12.

Nilsson, S., Koehler, K. F., & Gustafsson, J. Å. (2011). Development of subtype-selective oestrogen receptor-based therapeutics. Nature reviews Drug discovery, 10(10), 778-792.

Nomura, D. K., Long, J. Z., Niessen, S., Hoover, H. S., Ng, S. W., & Cravatt, B. F. (2010). Monoacylglycerol lipase regulates a fatty acid network that promotes cancer pathogenesis. Cell, 140(1), 49-61.

Olsen, C. G., & Gordon Jr, R. E. (1990). Breast disorders in nursing mothers. American family physician, 41(5), 1509-1516.

Orimo, A., Gupta, P. B., Sgroi, D. C., Arenzana-Seisdedos, F., Delaunay, T., Naeem, R., ... & Weinberg, R. A. (2005). Stromal fibroblasts present in invasive human breast carcinomas promote tumor growth and angiogenesis through elevated SDF-1/CXCL12 secretion. Cell, 121(3), 335-348.

Ormandy, C. J., Binart, N., & Kelly, P. A. (1997). Mammary gland development in prolactin receptor knockout mice. Journal of mammary gland biology and neoplasia, 2(4), 355-364.

Paradisi, A., Pasquariello, N., Barcaroli, D., & Maccarrone, M. (2008). Anandamide regulates keratinocyte differentiation by inducing DNA methylation in a CB1 receptor-dependent manner. Journal of Biological Chemistry, 283(10), 6005-6012.

Pacher, P., Bátkai, S., & Kunos, G. (2006). The endocannabinoid system as an emerging target of pharmacotherapy. Pharmacological reviews, 58(3), 389-462.

Pacher, P., & Mechoulam, R. (2011). Is lipid signaling through cannabinoid 2 receptors part of a protective system?. Progress in lipid research, 50(2), 193-211.

Paget, S. (1889). The distribution of secondary growths in cancer of the breast. Lancet, 571-573.

Pérez-Gómez, E., Andradas, C., Blasco-Benito, S., Caffarel, M. M., García-Taboada, E., Villa-Morales, M., ... & Wenners, A. (2015). Role of cannabinoid receptor CB2 in HER2 pro-oncogenic signaling in breast cancer. Journal of the National Cancer Institute, 107(6), djv077.

Perou, C. M., Sørlie, T., Eisen, M. B., Van De Rijn, M., Jeffrey, S. S., Rees, C. A., ... & Fluge, Ø. (2000). Molecular portraits of human breast tumours. nature, 406(6797), 747-752.

Petrelli, A., Carollo, R., Cargnelutti, M., Iovino, F., Callari, M., Cimino, D., ... & Giordano, S. (2015). By promoting cell differentiation, miR-100 sensitizes basal-like breast cancer stem cells to hormonal therapy. Oncotarget, 6(4), 2315.

Pfefferle, A. D., Herschkowitz, J. I., Usary, J., Harrell, J. C., Spike, B. T., Adams, J. R., ... & Perou, C. M. (2013). Transcriptomic classification of genetically engineered mouse models of breast cancer identifies human subtype counterparts. Genome biology, 14(11), 1-16.

Picardi, P., Ciaglia, E., Proto, M. C., & Pisanti, S. (2014). Anandamide inhibits breast tumor-induced angiogenesis. Translational Medicine@ UniSa, 10, 8.

Pisanti, S., Picardi, P., D'Alessandro, A., Laezza, C., & Bifulco, M. (2013). The endocannabinoid signaling system in cancer. Trends in pharmacological sciences, 34(5), 273-282.

Plaks, V., Brenot, A., Lawson, D. A., Linnemann, J. R., Van Kappel, E. C., Wong, K. C., ... & Werb, Z. (2013). Lgr5-expressing cells are sufficient and necessary for postnatal mammary gland organogenesis. Cell reports, 3(1), 70-78.

Polyak, K. (2007). Breast cancer: origins and evolution. The Journal of clinical investigation, 117(11), 3155-3163.

Prat, A., Parker, J. S., Karginova, O., Fan, C., Livasy, C., Herschkowitz, J. I., ... & Perou, C. M. (2010). Phenotypic and molecular characterization of the claudin-low intrinsic subtype of breast cancer. Breast cancer research, 12(5), R68.

Qamri, Z., Preet, A., Nasser, M. W., Bass, C. E., Leone, G., Barsky, S. H., & Ganju, R. K. (2009). Synthetic cannabinoid receptor agonists inhibit tumor growth and metastasis of breast cancer. Molecular cancer therapeutics, 8(11), 3117-3129.

Ramer, R., Schwarz, R., & Hinz, B. (2019). Modulation of the endocannabinoid system as a potential anticancer strategy. Frontiers in pharmacology, 10, 430.

Raouf, A., Zhao, Y., To, K., Stingl, J., Delaney, A., Barbara, M., ... & Eaves, C. (2008). Transcriptome analysis of the normal human mammary cell commitment and differentiation process. Cell stem cell, 3(1), 109-118.

Reader, J., Holt, D., & Fulton, A. (2011). Prostaglandin E 2 EP receptors as therapeutic targets in breast cancer. Cancer and Metastasis Reviews, 30(3), 449-463.

Richert, M. M., Schwertfeger, K. L., Ryder, J. W., & Anderson, S. M. (2000). An atlas of mouse mammary gland development. Journal of mammary gland biology and neoplasia, 5(2), 227-241.

Rios, A. C., Fu, N. Y., Lindeman, G. J., & Visvader, J. E. (2014). In situ identification of bipotent stem cells in the mammary gland. Nature, 506(7488), 322-327.

Rueda, D., Navarro, B., Martínez-Serrano, A., Guzmán, M., & Galve-Roperh, I. (2002). The endocannabinoid anandamide inhibits neuronal progenitor cell differentiation through attenuation of the Rap1/B-Raf/ERK pathway. Journal of Biological Chemistry, 277(48), 46645-46650.

Sen, N., Gui, B., & Kumar, R. (2014). Role of MTA1 in cancer progression and metastasis. Cancer and Metastasis Reviews, 33(4), 879-889.

Sailler, S., Schmitz, K., Jäger, E., Ferreiros, N., Wicker, S., Zschiebsch, K., ... & Lötsch, J. (2014). Regulation of circulating endocannabinoids associated with cancer and metastases in mice and humans. Oncoscience, 1(4), 272.

Saez, E., Rosenfeld, J., Livolsi, A., Olson, P., Lombardo, E., Nelson, M., ... & Evans, R. M. (2004). PPARγ signaling exacerbates mammary gland tumor development. Genes & development, 18(5), 528-540.

Sánchez, C., Galve-Roperh, I., Canova, C., Brachet, P., & Guzmán, M. (1998). $\triangle$9-Tetrahydrocannabinol induces apoptosis in C6 glioma cells. FEBS letters, 436(1), 6-10.

Sánchez, M. G., Sánchez, A. M., Ruiz-Llorente, L., & Díaz-Laviada, I. (2003). Enhancement of androgen receptor expression induced by (R)-methanandamide in prostate LNCaP cells. FEBS letters, 555(3), 561-566.

Sarnataro, D., Pisanti, S., Santoro, A., Gazzerro, P., Malfitano, A. M., Laezza, C., & Bifulco, M. (2006). The cannabinoid CB1 receptor antagonist rimonabant (SR141716) inhibits human breast cancer cell proliferation through a lipid raft-mediated mechanism. Molecular pharmacology, 70(4), 1298-1306.

Sarrió, D., Rodriguez-Pinilla, S. M., Hardisson, D., Cano, A., Moreno-Bueno, G., & Palacios, J. (2008). Epithelial-mesenchymal transition in breast cancer relates to the basal-like phenotype. Cancer research, 68(4), 989-997.

Schaefer, C. F., Anthony, K., Krupa, S., Buchoff, J., Day, M., Hannay, T., & Buetow, K. H. (2009). PID: the pathway interaction database. Nucleic acids research, 37(suppl_1), D674-D679.

Schneider, C. A., Rasband, W. S., & Eliceiri, K. W. (2012). NIH Image to ImageJ: 25 years of image analysis. Nature methods, 9(7), 671-675

Schmid, P. C., Wold, L. E., Krebsbach, R. J., Berdyshev, E. V., & Schmid, H. H. (2002). Anandamide and other N-acylethanolamines in human tumors. *Lipids*, *37*(9), 907-912.

Schwertfeger, K. L., Richert, M. M., & Anderson, S. M. (2001). Mammary gland involution is delayed by activated Akt in transgenic mice. Molecular endocrinology, 15(6), 867-881.

Scorticati, C., Mohn, C., De Laurentiis, A., Vissio, P., Solari, J. F., Seilicovich, A., ... & Rettori, V. (2003). The effect of anandamide on prolactin secretion is modulated by estrogen. Proceedings of the National Academy of Sciences, 100(4), 2134-2139.

Shackleton, M., Vaillant, F., Simpson, K. J., Stingl, J., Smyth, G. K., Asselin-Labat, M. L., ... & Visvader, J. E. (2006). Generation of a functional mammary gland from a single stem cell. Nature, 439(7072), 84-88.

Shah, S. P., Roth, A., Goya, R., Oloumi, A., Ha, G., Zhao, Y., ... & Aparicio, S. (2012). The clonal and mutational evolution spectrum of primary triple-negative breast cancers. Nature, 486(7403), 395-399.

Simões, B. M., Piva, M., Iriondo, O., Comaills, V., López-Ruiz, J. A., Zabalza, I., ... & dM Vivanco, M. (2011). Effects of estrogen on the proportion of stem cells in the breast. Breast cancer research and treatment, 129(1), 23-35.

Skibinski, A., & Kuperwasser, C. (2015). The origin of breast tumor heterogeneity. Oncogene, 34(42), 5309-5316.

Slepicka, P. F., Somasundara, A. V. H., & Dos Santos, C. O. (2021, June). The molecular basis of mammary gland development and epithelial differentiation. In Seminars in Cell & Developmental Biology (Vol. 114, pp. 93-112). Academic Press.

Smith, M. C., Luker, K. E., Garbow, J. R., Prior, J. L., Jackson, E., Piwnica-Worms, D., & Luker, G. D. (2004). CXCR4 regulates growth of both primary and metastatic breast cancer. Cancer research, 64(23), 8604-8612.

Smith, P. B., Compton, D. R., Welch, S. P., Razdan, R. K., Mechoulam, R., & Martin, B. R. (1994). The pharmacological activity of anandamide, a putative endogenous cannabinoid, in mice. Journal of pharmacology and Experimental Therapeutics, 270(1), 219-227.

Song, Z. H., & Zhong, M. (2000). CB1 cannabinoid receptor-mediated cell migration. Journal of Pharmacology and Experimental Therapeutics, 294(1), 204-209.

Sørlie, T., Perou, C. M., Tibshirani, R., Aas, T., Geisler, S., Johnsen, H., ... & Thorsen, T. (2001). Gene expression patterns of breast carcinomas distinguish tumor subclasses with clinical implications. Proceedings of the National Academy of Sciences, 98(19), 10869-10874.

Spike, B. T., Engle, D. D., Lin, J. C., Cheung, S. K., La, J., & Wahl, G. M. (2012). A mammary stem cell population identified and characterized in late embryogenesis reveals similarities to human breast cancer. Cell stem cell, 10(2), 183-197.

Stingl, J., Eirew, P., Ricketson, I., Shackleton, M., Vaillant, F., Choi, D., ... & Eaves, C. J. (2006). Purification and unique properties of mammary epithelial stem cells. Nature, 439(7079), 993-997.

Subramanian, A., Tamayo, P., Mootha, V. K., Mukherjee, S., Ebert, B. L., Gillette, M. A., ... & Mesirov, J. P. (2005). Gene set enrichment analysis: a knowledge-based approach for interpreting genome-wide expression profiles. Proceedings of the National Academy of Sciences, 102(43), 15545-15550.

Sugiura, T., Kondo, S., Sukagawa, A., Nakane, S., Shinoda, A., Itoh, K., ... & Waku, K. (1995). 2-Arachidonoylgylcerol: a possible endogenous cannabinoid receptor ligand in brain. Biochemical and biophysical research communications, 215(1), 89-97.

Suk, K. T., Mederacke, I., Gwak, G. Y., Cho, S. W., Adeyemi, A., Friedman, R., & Schwabe, R. F. (2016). Opposite roles of cannabinoid receptors 1 and 2 in hepatocarcinogenesis. Gut, 65(10), 1721-1732.

Sun, H., Jiang, L., Luo, X., Jin, W., He, Q., An, J., ... & Lucchesi, C. (2013). Potential tumor-suppressive role of monoglyceride lipase in human colorectal cancer. Oncogene, 32(2), 234-241.

Sun, H., Miao, Z., Zhang, X., Chan, U. I., Su, S. M., Guo, S., ... & Deng, C. X. (2018). Single-cell RNA-Seq reveals cell heterogeneity and hierarchy within mouse mammary epithelia. Journal of Biological Chemistry, 293(22), 8315-8329.

Sun, X., Zhang, G., Nian, J., Yu, M., Chen, S., Zhang, Y., ... & Li, J. P. (2017). Elevated heparanase expression is associated with poor prognosis in breast cancer: a study based on systematic review and TCGA data. Oncotarget, 8(26), 43521.

Tabor, S., Szostakowska-Rodzos, M., Fabisiewicz, A., & Grzybowska, E. A. (2020). How to predict metastasis in luminal breast cancer? current solutions and future prospects. International Journal of Molecular Sciences, 21(21), 8415.

Thors, L., Bergh, A., Persson, E., Hammarsten, P., Stattin, P., Egevad, L., ... & Fowler, C. J. (2010). Fatty acid amide hydrolase in prostate cancer: association with disease severity and outcome, CB1 receptor expression and regulation by IL-4. PloS one, 5(8), e12275.

Tiede, B., & Kang, Y. (2011). From milk to malignancy: the role of mammary stem cells in development, pregnancy and breast cancer. Cell research, 21(2), 245-257.

Twelves, C., Sabel, M., Checketts, D., Miller, S., Tayo, B., Jove, M., ... & Short, S. C. (2021). A phase 1b randomised, placebo-controlled trial of nabiximols cannabinoid oromucosal spray with temozolomide in patients with recurrent glioblastoma. British journal of cancer, 124(8), 1379-1387.

Van De Vijver, M. J., He, Y. D., Van't Veer, L. J., Dai, H., Hart, A. A., Voskuil, D. W., ... & Bernards, R. (2002). A gene-expression signature as a predictor of survival in breast cancer. New England Journal of Medicine, 347(25), 1999-2009.

Van Egmond, N., Straub, V. M., & van der Stelt, M. (2021). Targeting endocannabinoid signaling: FAAH and MAG lipase inhibitors. Annual Review of Pharmacology and Toxicology, 61, 441-463.

Van Esbroeck, A. C., Janssen, A. P., Cognetta, A. B., Ogasawara, D., Shpak, G., Van Der Kroeg, M., ... & Van Der Stelt, M. (2017). Activity-based protein profiling reveals off-target proteins of the FAAH inhibitor BIA 10-2474. Science, 356(6342), 1084-1087.

Van Keymeulen, A., Rocha, A. S., Ousset, M., Beck, B., Bouvencourt, G., Rock, J., ... & Blanpain, C. (2011). Distinct stem cells contribute to mammary gland development and maintenance. Nature, 479(7372), 189-193.

Van't Veer, L. J., Dai, H., Van De Vijver, M. J., He, Y. D., Hart, A. A., Mao, M., ... & Friend, S. H. (2002). Gene expression profiling predicts clinical outcome of breast cancer. nature, 415(6871), 530-536.

Velasco, G., Hernández-Tiedra, S., Dávila, D., & Lorente, M. (2016). The use of cannabinoids as anticancer agents. Progress in neuro-psychopharmacology and biological psychiatry, 64, 259-266.

Velasco, G., Sánchez, C., & Guzmán, M. (2012). Towards the use of cannabinoids as antitumour agents. Nature Reviews Cancer, 12(6), 436-444.

Vercelli, C., Barbero, R., Cuniberti, B., Racca, S., Abbadessa, G., Piccione, F., & Re, G. (2014). Transient receptor potential vanilloid 1 expression and functionality in mcf-7 cells: a preliminary investigation. Journal of breast cancer, 17(4), 332-338.

Visvader, J. E., & Stingl, J. (2014). Mammary stem cells and the differentiation hierarchy: current status and perspectives. *Genes & development*, *28*(11), 1143-1158.

Wagner, K. U., Wall, R. J., St-Onge, L., Gruss, P., Wynshaw-Boris, A., Garrett, L., ... & Hennighausen, L. (1997). Cre-mediated gene deletion in the mammary gland. Nucleic acids research, 25(21), 4323-4330.

Waleh, N. S., Cravatt, B. F., Apte-Deshpande, A., Terao, A., & Kilduff, T. S. (2002). Transcriptional regulation of the mouse fatty acid amide hydrolase gene. Gene, 291(1-2), 203-210.

Wang, D., Cai, C., Dong, X., Yu, Q. C., Zhang, X. O., Yang, L., & Zeng, Y. A. (2015). Identification of multipotent mammary stem cells by protein C receptor expression. Nature, 517(7532), 81-84.

Wang, Y., Klijn, J. G., Zhang, Y., Sieuwerts, A. M., Look, M. P., Yang, F., ... & Foekens, J. A. (2005). Gene-expression profiles to predict distant metastasis of lymph-node-negative primary breast cancer. The Lancet, 365(9460), 671-679.

Wei, B. Q., Mikkelsen, T. S., McKinney, M. K., Lander, E. S., & Cravatt, B. F. (2006). A second fatty acid amide hydrolase with variable distribution among placental mammals. Journal of Biological Chemistry, 281(48), 36569-36578.

Weigelt, B., Glas, A. M., Wessels, L. F., Witteveen, A. T., Peterse, J. L., & van't Veer, L. J. (2003). Gene expression profiles of primary breast tumors maintained in distant metastases. Proceedings of the National Academy of Sciences, 100(26), 15901-15905.

Wiercinska, E., Naber, H. P., Pardali, E., van der Pluijm, G., van Dam, H., & Ten Dijke, P. (2011). The TGF-β/Smad pathway induces breast cancer cell invasion through the up-regulation of matrix metalloproteinase 2 and 9 in a spheroid invasion model system. Breast cancer research and treatment, 128(3), 657-666.

Witt, A. E., Lee, C. W., Lee, T. I., Azzam, D. J., Wang, B., Caslini, C., ... & Ince, T. A. (2017). Identification of a cancer stem cell-specific function for the histone deacetylases, HDAC1 and HDAC7, in breast and ovarian cancer. Oncogene, 36(12), 1707-1720.

Wollank, Y., Ramer, R., Ivanov, I., Salamon, A., Peters, K., & Hinz, B. (2015). Inhibition of FAAH confers increased stem cell migration via PPARα. Journal of lipid research, 56(10), 1947-1960.

World Health Organisation (2019). WHO Classification of Tumours of the Breast, 5th Edition.

Wu, X., Han, L., Zhang, X., Li, L., Jiang, C., Qiu, Y., ... & Fu, J. (2012). Alteration of endocannabinoid system in human gliomas. Journal of neurochemistry, 120(5), 842-849.

Yuan, Z. Y., Dai, T., Wang, S. S., Peng, R. J., Li, X. H., Qin, T., ... & Wang, X. (2014). Overexpression of ETV4 protein in triple-negative breast cancer is associated with a higher risk of distant metastasis. OncoTargets and therapy, 7, 1733.

Zeng, Y. A., & Nusse, R. (2010). Wnt proteins are self-renewal factors for mammary stem cells and promote their long-term expansion in culture. Cell stem cell, 6(6), 568-577.

Zhang, H., Berezov, A., Wang, Q., Zhang, G., Drebin, J., Murali, R., & Greene, M. I. (2007). ErbB receptors: from oncogenes to targeted cancer therapies. The Journal of clinical investigation, 117(8), 2051-2058.

Zhu, L. X., Sharma, S., Stolina, M., Gardner, B., Roth, M. D., Tashkin, D. P., & Dubinett, S. M. (2000). Δ-9-Tetrahydrocannabinol inhibits antitumor immunity by a CB2 receptor-mediated, cytokine-dependent pathway. The Journal of Immunology, 165(1), 373-380.

Zlotnik, A., & Yoshie, O. (2000). Chemokines: a new classification system and their role in immunity. Immunity, 12(2), 121-127.

ADDENDUM

SUPPLEMENTARY FIGURES

Supplementary Table 1: Gene Ontology (GO) Cellular Component (CC)

Pathway	Fold Enrichment	p	Upregulated	Downregulated
adherens junction	14,992	1,34E-05	*ALCAM, CD44, HMGA1, ITGA6, LAP3, NDRG1, RSU1, SHROOM3, TNC*	*ANXA6, CAPN1, CSPG4, FGFR3, FLNC, HNRNPK, KIF23, PKP2, PPIA, RPL4, RPS17, RPS2, RPS3, TSPAN4*
anchoring junction	14,702	1,57E-05	*ALCAM, CD44, HMGA1, ITGA6, LAP3, NDRG1, RSU1, SHROOM3, TNC*	*ANXA6, CAPN1, CSPG4, FGFR3, FLNC, HNRNPK, KIF23, PKP2, PPIA, RPL4, RPS17, RPS2, RPS3, TSPAN4*
cell substrate junction	9,830	8,23E-05	*ALCAM, CD44, HMGA1, ITGA6, LAP3, RSU1, TNC*	*ANXA6, CAPN1, CSPG4, FGFR3, FLNC, HNRNPK, ITGB4, KIF23, PPIA, RPL4, RPS17, RPS2, RPS3, TSPAN4*
ribonucleoprotein complex	11,768	1,67E-04	*RPL24, SNRPN*	*BTBD1, HNRNPH1, HNRNPK, PSMA4, RPL4, RPS17, RPS2, RPS3, WTIP*
focal adhesion	14,112	1,69E-04	*ALCAM, CD44, HMGA1, ITGA6, LAP3, RSU1, TNC*	*ANXA6, CAPN1, CSPG4, FGFR3, FLNC, HNRNPK, KIF23, PPIA, RPL4, RPS17, RPS2, RPS3, TSPAN4*
cell substrate adherens junction	14,069	1,72E-04	*ALCAM, CD44, HMGA1, ITGA6, LAP3, RSU1, TNC*	*ANXA6, CAPN1, CSPG4, FGFR3, FLNC, HNRNPK, KIF23, PPIA, RPL4, RPS17, RPS2, RPS3, TSPAN4*
cytosolic ribosome	32,890	1,78E-04	*RPL24*	*RPL4, RPS17, RPS2, RPS3*
cell junction	10,118	3,99E-04	*ALCAM, CD44, HMGA1, ITGA6, LAP3, NDRG1, NEU1, RSU1, SHROOM3, TIAM1, TNC*	*ANXA6, CAPN1, CSPG4, FGFR3, FLNC, GTF2A2, HNRNPK, ITGB4, KIF23, MICALL2, PKP2, PPIA, RPL4, RPS17, RPS2, RPS3, TGFBR1, TSPAN4*
nuclear replication fork	147,838	4,81E-04		*POLA1, RPA3*
ribosomal subunit	26,855	5,79E-04	*RPL24*	*RPL4, RPS17, RPS2, RPS3*
cytosolic part	16,557	7,06E-04	*RPL24*	*CCT6A, RPL4, RPS17, RPS2, RPS3*
replisome & nuclear replisome	122,992	8,03E-04		*POLA1, RPA3*
chromosomal part	15,283	8,70E-04	*ESR1, HIST1H1C, HIST1H3H, HIST1H4H, HMGA1, STAT1*	*FAM111A, HELLS, HNRNPK, ICE2, KNSTRN, MORF4L1, PIF1, POLA1, RPA3, SKA2, TP53BP1, ZWILCH*
cyclin dependent protein kinase holoenzyme complex	105,043	1,14E-03	*CCND3, CDKN1A*	
chromosome	14,102	1,39E-03	*ESR1, HIST1H1C, HIST1H3H, HIST1H4H, HMGA1, STAT1*	*FAM111A, FIGNL1, HELLS, HNRNPK, ICE2, KNSTRN, MORF4L1, PIF1, POLA1, RPA3, SKA2, TP53BP1, ZWILCH*
ribosome	22,345	1,43E-03	*RPL24*	*RPL4, RPS17, RPS2, RPS3*
microtubule	35,098	1,55E-03	*NDRG1, TUBA4A*	*CCT6A, KNSTRN, PRC1, SKA2*
chromatin	10,474	1,62E-03	*ESR1, HIST1H1C, HIST1H3H, HIST1H4H, HMGA1, STAT1*	*FAM111A, HELLS, HNRNPK, ICE2, MORF4L1, POLA1*
replication fork	97,357	1,68E-03		*POLA1, RPA3*
spindle	32,524	1,91E-03		*CLTCL1, KIF23, KNSTRN, PRC1, SKA2*
endoplasmic reticulum membrane	19,339	7,57E-03	*AGPAT1, ASPH, CYP2B6, DERL3, ELOVL5, EMC3, HLA-DRB1, NOS1AP, PLA2G4C, SEC11C, SPINK5, STS, TBC1D20*	*PCYT2, PIGB, SEC11A, SPPL2A, STX17, TYRO3*
nuclear outer membrane endoplasmic reticulum membrane network	18,793	8,51E-03	*AGPAT1, ASPH, CYP2B6, DERL3, ELOVL5, EMC3, HLA-DRB1, NOS1AP, PLA2G4C, SEC11C, SPINK5, STS, TBC1D20*	*PCYT2, PIGB, SEC11A, SPPL2A, STX17, TYRO3*
cytosolic small ribosomal subunit	55,023	9,77E-03		*RPS17, RPS2, RPS3*
kinetochore	50,123	1,05E-02		*KNSTRN, SKA2, ZWILCH*
protein DNA complex	28,586	1,16E-02	*HIST1H3H, HIST1H4H, PAX2*	*POLA1, RPA3*
nuclear chromosome	10,240	1,35E-02	*HIST1H1C, HIST1H3H, HIST1H4H, STAT1*	*FIGNL1, HNRNPK, MORF4L1, PIF1, POLA1, RPA3*
catalytic step 2 spliceosome	46,910	1,57E-02		*HNRNPH1, HNRNPK*
small ribosomal subunit	43,560	2,25E-02		*RPS17, RPS2, RPS3*
chromosome centromeric region	37,337	2,52E-02		*HELLS, KNSTRN, SKA2, ZWILCH*
endoplasmic reticulum part	14,784	2,91E-02	*AGPAT1, ASPH, COL4A5, COL4A6, CYP2B6, DERL3, ELOVL5, EMC3, HLA-DRB1, NOS1AP, P3H1, PLA2G4C, SEC11C, SPINK5, STS, TBC1D20, THBS1*	*COL12A1, COL9A3, NTF4, PCYT2, PIGB, SEC11A, SERPINH1, SPPL2A, STX17, TYRO3*
clathrin coated vesicle	40,209	3,34E-02	*HLA-DRB1, SNX9*	*CLTCL1, ROR2*
protein kinase complex	35,014	3,88E-02	*CCND3, CDKN1A*	
spliceosomal complex	33,569	4,29E-02	*SNRPN*	*HNRNPH1, HNRNPK*
nucleolus	5,670	4,96E-02	*ABHD14B, BHLHE40, HOMEZ, ISG20, MPHOSPH6, MXI1, MYO10, OASL, SP110, STAT1, TXNRD1*	*CHD2, IMP3, NFIB, NUSAP1, POLA1, RCN2, RPL4, ZBED6*

Supplementary Table 1. Complete list of differentially expressed genes (DEGs) included in the Gene Ontology (GO) Cellular Component (CC) analysis of RNA-seq data. Fold enrichment and Student's t-test p-values are shown.

Supplementary Table 2: Gene Ontology (GO) Molecular Function (MF)

Pathway	Fold Enrichment	p	Upregulated	Downregulated
activating transcription factor binding	93,821	6,51E-05	*BHLHE40, GATA4, IFI27, MEF2D*	*TP53BP1*
nucleic acid binding transcription factor activity & sequence specific DNA binding transcription factor activity	10,948	2,42E-04	*BCL11A, BHLHE40, ESR1, GATA4, MEF2D, STAT1*	*GLIS2, HNRNPK, LMO4, NFIB, RORC*
transcription factor binding	16,508	3,32E-04	*BHLHE40, ESR1, GATA4, HMGA1, IFI27, MEF2D, OASL, PAX2, ZMYND8*	*GTF2A2, LMO4, RPS3, TP53BP1*
sequence specific DNA binding	11,570	4,33E-04	*BCL11A, ESR1, GATA4, HMGA1, MBD4, MEF2D, PAX2, STAT1*	*CHD2, HNRNPK, MEIS3, NFIB, PIF1, RORC*
protein kinase activity	11,392	8,64E-04	*CDKN1A, DYRK3*	*CLK3, CSK, FGFR3, IGF1R, NEK9, TGFBR1, TYRO3, ULK3*
phosphotransferase activity alcohol group as acceptor	10,101	2,00E-03	*CDKN1A, DYRK3*	*CLK3, CSK, FGFR3, IGF1R, NEK9, TGFBR1, TYRO3, ULK3*
sequence specific DNA binding RNA polymerase II transcription factor activity	21,989	2,00E-03	*BCL11A, BHLHE40, ESR1, MEF2D, STAT1*	*GLIS2, HNRNPK, NFIB*
kinase activity	9,338	3,42E-03	*CDKN1A, DYRK3*	*CLK3, CSK, FGFR3, IGF1R, NEK9, TGFBR1, TYRO3, ULK3*
RNA polymerase II transcription factor binding transcription factor activity involved in negative regulation of transcription	83,002	5,19E-03	*BHLHE40, ZMYND8*	*NFIB*
RNA polymerase II core promoter proximal region sequence specific DNA binding	31,058	6,33E-03	*BCL11A, ESR1, STAT1*	*HNRNPK, NFIB*
core promoter proximal region sequence specific DNA binding	29,434	7,69E-03	*BCL11A, ESR1, PAX2, STAT1*	*HNRNPK, NFIB*
core promoter proximal region DNA binding	29,243	7,88E-03	*BCL11A, ESR1, PAX2, STAT1*	*HNRNPK, NFIB*
RNA polymerase II core promoter proximal region sequence specific DNA binding transcription factor activity	29,243	8,25E-03	*BCL11A, BHLHE40, ESR1*	*GLIS2, HNRNPK, NFIB*
transferase activity transferring phosphorus containing groups	8,280	8,45E-03	*CDKN1A, DYRK3, OAS2*	*CLK3, CSK, FGFR3, IGF1R, NEK9, PCYT2, POLA1, POLG, TGFBR1, TYRO3, ULK3*
RNA polymerase II regulatory region sequence specific DNA binding & RNA polymerase II regulatory region DNA binding	14,204	8,64E-03	*BCL11A, ESR1, MEF2D, STAT1*	*HNRNPK, NFIB*
single stranded DNA binding	53,809	8,91E-03	*NABP1*	*HNRNPK, RPA3*
antigen binding	76,762	9,43E-03	*HLA-DRB1, IGHG1*	*TSPAN4*
transcription cofactor activity	15,214	1,05E-02	*BHLHE40, GATA4, HELZ2, HMGA1, LMCD1, MXI1, ZMYND8*	*EID1, GTF2A2, NCOA2, NFIB, TP53BP1*
transcription factor binding transcription factor activity	14,471	1,38E-02	*BHLHE40, GATA4, HELZ2, HMGA1, LMCD1, MXI1, ZMYND8*	*EID1, GTF2A2, NCOA2, NFIB, TP53BP1*
protein binding transcription factor activity	14,324	1,44E-02	*BHLHE40, GATA4, HELZ2, HMGA1, LMCD1, MXI1, ZMYND8*	*EID1, GTF2A2, NCOA2, NFIB, TP53BP1*
poly U RNA binding	243,933	1,64E-02	*ATXN1*	*HNRNPH1*
chaperone binding	51,901	1,98E-02	*CLU*	*DNAJA4, RNF207*
poly pyrimidine tract binding	221,758	2,01E-02	*ATXN1*	*HNRNPH1*
regulatory region nucleic acid binding regulatory region DNA binding & transcription regulatory region DNA binding	13,499	2,08E-02	*BCL11A, BHLHE40, ESR1, GATA4, MEF2D, PAX2, STAT1*	*CHD2, GLIS2, HNRNPK, NFIB*
transcription regulatory region sequence specific DNA binding	14,006	2,26E-02	*BCL11A, ESR1, MEF2D, PAX2, STAT1*	*CHD2, HNRNPK, NFIB*
ubiquitin protein ligase binding	21,273	2,29E-02	*ARRB2, CDKN1A, CLU, CXCR4, SNX9, TXNIP*	
ubiquitin like protein ligase binding	21,029	2,39E-02	*ARRB2, CDKN1A, CLU, CXCR4, SNX9, TXNIP*	
structural molecule activity	23,094	2,53E-02	*ARRB2, ASPH, MGP*	*LAMB1, PKP2, RPS2, RPS3, SORBS2*
protein complex binding	13,630	2,61E-02	*HLA-DRB1, MYO10, NDRG1, P3H1, PGAM5, PRNP, SNX9, THBS1*	*IGF1R, KIF23, MICALL2, PKP2, SKA2, SLC6A4, TNNC1, TSPAN4*
protein tyrosine kinase activity	43,387	3,29E-02		*CSK, FGFR3, IGF1R, TYRO3*
NAD ADP ribosyltransferase activity	204,699	3,41E-02	*PARP9*	
insulin receptor binding	177,406	3,82E-02		*IGF1R*
core promoter binding	37,528	4,99E-02	*ESR1, STAT1*	*CHD2*

Supplementary Table 2. Complete list of DEGs included in the Gene Ontology (GO) Molecular Function (MF) analysis of RNA-seq data. Fold enrichment and Student's t-test p-values are shown.

Supplementary Table 3: Gene Ontology (GO) Biological Process (BP) (1/2)

Pathway	Fold Enrichment	p	Upregulated	Downregulated
nuclear transcribed mRNA catabolic process	16,823	3,59E-05	*RPL24*	*RPL4, RPS17, RPS2, RPS3*
mRNA catabolic process	34,276	4,95E-05	*RPL24*	*RPL4, RPS17, RPS2, RPS3*
nucleobase containing compound catabolic process	22,940	5,23E-05	*CECR2, HMGA1, ISG20, MBD4, RPL24*	*RPA3, RPL4, RPS17, RPS2, RPS3*
cellular nitrogen compound catabolic process	21,029	9,69E-05	*CECR2, HMGA1, ISG20, MBD4, RPL24*	*RPA3, RPL4, RPS17, RPS2, RPS3*
heterocycle catabolic process	20,968	9,69E-05	*CECR2, HMGA1, ISG20, MBD4, RPL24*	*RPA3, RPL4, RPS17, RPS2, RPS3*
RNA catabolic process	31,052	9,78E-05	*ISG20, RPL24*	*RPL4, RPS17, RPS2, RPS3*
aromatic compound catabolic process	20,672	1,08E-04	*CECR2, HGD, HMGA1, ISG20, MBD4, RPL24*	*RPA3, RPL4, RPS17, RPS2, RPS3*
SRP dependent cotranslational protein targeting to membrane	28,146	1,49E-04	*RPL24, SEC11C*	*RPL4, RPS17, RPS2, RPS3, SEC11A*
organic cyclic compound catabolic process	19,832	1,49E-04	*CECR2, HGD, HMGA1, ISG20, MBD4, RPL24, STS*	*RPA3, RPL4, RPS17, RPS2, RPS3*
cotranslational protein targeting to membrane	28,146	1,56E-04	*RPL24, SEC11C*	*RPL4, RPS17, RPS2, RPS3, SEC11A*
protein targeting to ER	27,615	1,71E-04	*RPL24, SEC11C*	*RPL4, RPS17, RPS2, RPS3, SEC11A*
establishment of protein localization to endoplasmic reticulum	26,611	2,05E-04	*RPL24, SEC11C*	*RPL4, RPS17, RPS2, RPS3, SEC11A*
mRNA metabolic process	9,851	2,10E-04	*RPL24*	*HNRNPH1, HNRNPK, RPL4, RPS17, RPS2, RPS3*
nuclear transcribed mRNA catabolic process nonsense mediated decay	25,904	2,14E-04	*RPL24*	*RPL4, RPS17, RPS2, RPS3*
protein complex disassembly	17,600	2,19E-04	*BNIP3, HMGA1, RPL24*	*RPL4, RPS17, RPS2, RPS3, SUPT16H*
macromolecular complex disassembly	17,082	2,78E-04	*BNIP3, HMGA1, RPL24*	*RPL4, RPS17, RPS2, RPS3, SUPT16H*
protein localization to endoplasmic reticulum	24,192	3,37E-04	*RPL24, SEC11C*	*RPL4, RPS17, RPS2, RPS3, SEC11A*
viral life cycle	16,840	4,82E-04	*ISG15, ISG20, NEDD4L, OASL, RAB43, RPL24, TBC1D20*	*FAM111A, PPIA, RPL4, RPS17, RPS2, RPS3, SUPT16H*
establishment of protein localization to membrane	18,692	5,60E-04	*RPL24, SEC11C*	*CSK, PACS1, PKP2, RPL4, RPS17, RPS2, RPS3, SEC11A*
double strand break repair	37,761	8,69E-04	*NABP1, PARP9*	*FIGNL1, MORF4L1, POLA1, RAD54B, RPA3, TP53BP1*
DNA replication	34,650	8,94E-04		*DUT, FAM111A, HRAS, IGF1R, KIAA0101, PIF1, POLA1, POLG, PPIA, RPA3, TICRR*
protein targeting to membrane	19,778	1,17E-03	*RPL24, SEC11C*	*PACS1, RPL4, RPS17, RPS2, RPS3, SEC11A*
translational termination	17,634	1,58E-03	*RPL24*	*RPL4, RPS17, RPS2, RPS3*
translational elongation	14,759	1,82E-03	*RPL24*	*EEF1B2, RPL4, RPS17, RPS2, RPS3*
viral process	10,029	2,18E-03	*CXCR4, GTF2E1, HMGA1, ISG15, ISG20, NEDD4L, OASL, RAB43, RPL24, STAT1, TBC1D20*	*FAM111A, GTF2A2, PACS1, PPIA, PSMA4, RPL4, RPS17, RPS2, RPS3, SUPT16H*
telomere maintenance via semi conservative replication	173,549	2,19E-03		*POLA1, RPA3*
protein localization to membrane	14,965	2,23E-03	*RPL24, SEC11C*	*CSK, PACS1, PKP2, RPL4, RPS17, RPS2, RPS3, SEC11A*
viral transcription	22,462	2,26E-03	*RPL24*	*RPL4, RPS17, RPS2, RPS3, SUPT16H*
multi organism cellular process	9,737	2,60E-03	*CXCR4, GTF2E1, HMGA1, IFIH1, ISG15, ISG20, NEDD4L, OASL, RAB43, RPL24, STAT1, TBC1D20*	*FAM111A, GTF2A2, PACS1, PPIA, PSMA4, RPL4, RPS17, RPS2, RPS3, SUPT16H*
viral gene expression	21,286	2,93E-03	*RPL24*	*RPL4, RPS17, RPS2, RPS3, SUPT16H*
multi organism metabolic process	20,849	3,40E-03	*RPL24*	*RPL4, RPS17, RPS2, RPS3, SUPT16H*
interspecies interaction between organisms & symbiosis encompassing mutualism through parasitism	14,462	3,53E-03	*ATP6V1C1, CXCR4, GTF2E1, HMGA1, ISG15, ISG20, NEDD4L, OASL, RAB43, RPL24, STAT1, TBC1D20*	*FAM111A, GTF2A2, PACS1, PPIA, PSMA4, RPL4, RPS17, RPS2, RPS3, SUPT16H*
telomere maintenance via recombination	147,838	3,61E-03		*POLA1, RPA3*
nuclear DNA replication	128,762	5,53E-03		*POLA1, RPA3*
cellular protein complex disassembly	25,010	5,54E-03	*RPL24*	*RPL4, RPS17, RPS2, RPS3*
DNA strand elongation involved in DNA replication	124,739	6,10E-03		*POLA1, RPA3*
cellular senescence	42,889	7,28E-03	*CDKN1A, HMGA1*	*HRAS, ULK3*
mitotic recombination	120,959	7,35E-03		*POLA1, RAD54B, RPA3*
translational initiation	15,474	7,79E-03	*RPL24*	*RPL4, RPS17, RPS2, RPS3, TICRR*
response to organic cyclic compound	25,587	7,83E-03	*ASPH, ESR1, STAT1, THBS1*	*DRD4, RORC, TGFBR1*
DNA strand elongation	114,047	8,04E-03		*POLA1, RPA3*
telomere maintenance via telomere lengthening	114,047	8,77E-03		*POLA1, RPA3*
cell cycle DNA replication	105,043	1,12E-02		*POLA1, RPA3*

Supplementary Table 3. Complete list of DEGs included in the Gene Ontology (GO) Biological Process (BP) analysis of RNA-seq data. Fold enrichment and Student's t-test p-values are shown.

Supplementary Table 3: Gene Ontology (GO) Biological Process (2/2)

Pathway	Fold Enrichment	p	Upregulated	Downregulated
DNA metabolic process	7,744	1,40E-02	*CECR2, HIST1H3H, HIST1H4H, HMGA1, ISG20, MBD4, MTRR, NABP1, PARP9, TNFSF13*	*DUT, FAM111A, FANCI, FIGNL1, HELLS, HRAS, IGF1R, KIAA0101, MORF4L1, NEIL1, NUSAP1, PIF1, POLA1, POLG, PPIA, RAD54B, RPA3, RPS3, TICRR, TP53BP1*
positive regulation of receptor mediated endocytosis	97,573	1,47E-02	*ARRB2, NEDD4L, VEGFA*	*HNRNPK*
G2 M transition of mitotic cell cycle	35,961	1,49E-02	*CDKN1A, TUBA4A*	*TICRR, TUBGCP4*
cellular response to DNA damage stimulus	12,991	1,49E-02	*CD44, CDKN1A, CLU, HMGA1, MBD4, NABP1, NDRG1, PARP9*	*FANCI, FIGNL1, IER3, KIAA0101, MORF4L1, NEIL1, POLA1, POLG, PSMA4, RAD54B, RPA3, RPS3, TICRR, TP53BP1*
cell cycle G2 M phase transition	35,719	1,56E-02	*CDKN1A, TUBA4A*	*TICRR, TUBGCP4*
DNA repair	19,683	1,65E-02	*HMGA1, MBD4, NABP1, PARP9*	*FANCI, FIGNL1, KIAA0101, MORF4L1, NEIL1, POLA1, POLG, RAD54B, RPA3, RPS3, TICRR, TP53BP1*
inositol lipid mediated signaling & phosphatidylinositol mediated signaling	35,481	1,90E-02	*CDKN1A, FRS2*	*FGFR3, IGF1R, PLXNB1*
de novo posttranslational protein folding	86,604	1,94E-02	*TUBA4A*	*CCT6A*
positive regulation of nitric oxide biosynthetic process	92,438	1,94E-02	*CLU, ESR1, NOS1AP*	
regulation of response to DNA damage stimulus	35,183	1,95E-02	*CD44, CLU*	*FIGNL1, IER3, RPS3*
DNA biosynthetic process	92,829	2,54E-02		*KIAA0101, PIF1, POLA1, POLG*
positive regulation of reactive oxygen species metabolic process	76,229	2,54E-02	*CDKN1A, CLU, ESR1, NOS1AP, THBS1*	
positive regulation of reactive oxygen species biosynthetic process	83,634	2,62E-02	*CLU, ESR1, NOS1AP*	
de novo protein folding	76,762	2,80E-02	*TUBA4A*	*CCT6A*
positive regulation of transcription from RNA polymerase II promoter	12,260	2,87E-02	*ABHD14B, BCL11A, ESR1, GATA4, HELZ2, ITGA6, MEF2D, PAX2, STAT1, VEGFA*	*GLIS2, GTF2A2, HNRNPK, HRAS, NFIB, TP53BP1*
single organism membrane organization	12,275	3,14E-02	*BNIP3, CLU, CXCR4, RPL24, SEC11C, SNX9, STX18, TBC1D20*	*CNTNAP2, CSK, NEK9, PACS1, PKP2, RPL4, RPS17, RPS2, RPS3, SEC11A, SNX33, STX17*
negative regulation of response to DNA damage stimulus	78,407	3,21E-02	*CD44, CLU*	*RPS3*
peptidyl tyrosine phosphorylation & peptidyl tyrosine modification	17,507	3,43E-02	*CD44, VEGFA*	*CSPG4, FGFR3, IGF1R, ROR2, TYRO3*
cell aging	28,839	3,52E-02	*CDKN1A, HMGA1*	*HRAS, ULK3*
regulation of kidney development	80,713	3,58E-02	*PAX2, STAT1, VEGFA*	
protein folding	27,331	3,84E-02	*CLU, P3H1, TUBA4A*	*CCT6A, DNAJA4, PPIA*
blood coagulation	12,588	3,94E-02	*ADORA2A, ARRB2, CD36, CD44, CD47, CLU, GATA4, GNAT3, GRB14, HIST1H3H, ITGA6, KCNMA1, THBS1, TUBA4A, VEGFA*	*CAPZA1, CSK, DOCK8, HRAS, KIF23, PPIA, TYRO3*
coagulation	12,588	3,98E-02	*ADORA2A, ARRB2, CD36, CD44, CD47, CLU, GATA4, GNAT3, GRB14, HIST1H3H, ITGA6, KCNMA1, THBS1, TUBA4A, VEGFA*	*CAPZA1, CSK, DOCK8, HRAS, KIF23, PPIA, TYRO3*
hemostasis	12,502	4,12E-02	*ADORA2A, ARRB2, CD36, CD44, CD47, CLU, GATA4, GNAT3, GRB14, HIST1H3H, ITGA6, KCNMA1, THBS1, TUBA4A, VEGFA*	*CAPZA1, CSK, DOCK8, HRAS, KIF23, PPIA, TYRO3*
nephron morphogenesis nephron epithelium morphogenesis	78,267	4,22E-02	*PAX2, STAT1, VEGFA*	
regulation of nitric oxide biosynthetic process	70,253	4,40E-02	*CLU, ESR1, NOS1AP*	
G1 S transition of mitotic cell cycle	27,016	4,50E-02	*CDKN1A*	*POLA1, PSMA4, RPA3*
cellular component disassembly	11,971	4,99E-02	*BNIP3, CD44, CECR2, COL4A5, COL4A6, HMGA1, LAMA3, LMCD1, RPL24*	*CAPN1, COL12A1, COL9A3, LAMB1, NEK9, OBSCN, RPL4, RPS17, RPS2, RPS3, SUPT16H*

Supplementary Table 3. Complete list of DEGs included in the Gene Ontology (GO) Biological Process (BP) analysis of RNA-seq data. Fold enrichment and Student's t-test p-values are shown.

Supplementary Table 4: Kyoto Encyclopedia of Genes and Genomes (KEGG) pathway enrichment analysis

Pathway	Fold Enrichment	p	Upregulated	Downregulated
thyroid hormone signaling pathway	51,644	1,13E-05	*STAT1, ESR1, GATA4*	*HRAS, NCOA2, PLCD3*
proteoglycans in cancer	35,961	6,45E-05	*CD44, MRAS, ESR1, TIAM1, CDKN1A, VEGFA, TIMP3, THBS1, FRS2*	*HRAS, FLNC, IGF1R, GPC1*
endocytosis	30,103	1,69E-04	*NEDD4L, CXCR4, ARRB2*	*CLTCL1, TGFBR1, FGFR3, IGF1R, CAPZA1, HRAS, ARAP1*
DNA replication	114,047	7,14E-04		*POLA1, RPA3*
pathways in cancer	9,887	1,23E-03	*CXCR4, COL4A6, COL4A5, LAMA3, ITGA6, CDKN1A, STAT1, VEGFA, ESR1, CCND3, TXNRD1*	*LAMB1, IGF1R, FGFR3, HRAS, TGFBR1*
ribosome	23,418	1,36E-03	*RPL24*	*RPS2, RPS3, RPS17, RPL4*
hepatitis B	32,633	1,93E-03	*CDKN1A, STAT1, IFIH1*	*TGFBR1, HRAS*
endocrine and other factor-regulated calcium reabsorption	85,093	2,15E-03	*ESR1*	*CLTCL1*
epstein-barr virus infection	27,865	3,39E-03	*HLA-DRB1, STAT1, OAS2, ISG15, CDKN1A, CD44, CCND3*	
breast cancer	15,881	3,57E-03	*ESR1, CDKN1A*	*IGF1R, HRAS*
glioma	23,915	4,07E-03	*CDKN1A*	*IGF1R, HRAS*
melanoma	24,640	4,30E-03	*CDKN1A*	*IGF1R, HRAS*
prolactin signaling pathway	57,850	5,40E-03	*STAT1, ELF5, ESR1*	*HRAS*
pancreatic cancer	53,222	6,65E-03	*STAT1, VEGFA, CDKN1A*	*TGFBR1*
hepatocellular carcinoma	13,374	6,81E-03	*CDKN1A, TXNRD1*	*IGF1R, HRAS, TGFBR1*
bladder cancer	48,678	7,22E-03	*CDKN1A, THBS1, VEGFA*	*FGFR3, HRAS*
Fanconi anemia pathway	52,711	9,99E-03		*FANCI, RMI1, RPA3*
prostate cancer	17,676	1,40E-02	*CDKN1A*	*IGF1R, HRAS*
HIF-1 signaling pathway	43,387	1,58E-02	*VEGFA, CDKN1A*	*IGF1R*
thyroid cancer	33,880	1,85E-02	*CDKN1A*	*HRAS*
cellular senescence	19,258	1,87E-02	*CCND3, CDKN1A, MRAS, GATA4, VDAC1*	*TGFBR1, HRAS, TRPM7, CAPN1*
ECM-receptor interaction	22,176	1,88E-02	*COL4A6, COL4A5, LAMA3, THBS1, TNC, ITGA6, CD44, CD36, CD47*	*COL9A3, LAMB1, ITGB4*
PI3K-Akt signaling pathway	10,560	2,97E-02	*VEGFA, COL4A6, COL4A5, LAMA3, THBS1, TNC, ITGA6, CDKN1A, CCND3*	*NTF4, FGFR3, IGF1R, HRAS, COL9A3, LAMB1, ITGB4*
cell cycle	32,718	2,99E-02	*CCND3, CDKN1A*	
th17 cell differentiation	33,775	3,31E-02	*HLA-DRB1, STAT1*	*TGFBR1, RORC*
hepatitis C	33,827	3,52E-02	*OAS2, STAT1, CDKN1A*	*HRAS*
FoxO signaling pathway	31,430	3,60E-02	*CDKN1A, BNIP3*	*TGFBR1, IGF1R, HRAS*
p53 signaling pathway	32,285	3,93E-02	*CDKN1A, CCND3, THBS1*	
parathyroid hormone synthesis, secretion and action	34,848	4,07E-02	*ARRB2, MEF2D, CDKN1A*	
protein export	166,318	4,13E-02	*SEC11C*	*SEC11A*
mismatch repair	115,700	4,13E-02		*RPA3*
necroptosis	11,699	4,28E-02	*VDAC1, PLA2G4C, PGAM5, STAT1, HIST2H2AA4, HIST1H2AI*	*JMJD7-PLA2G4B, CAPN1, TRPM7, PPIA*
viral carcinogenesis	16,353	4,52E-02	*CDKN1A, HIST1H4H, GTF2E1, CCND3*	*HRAS, HNRNPK, GTF2A2*
focal adhesion	10,819	4,94E-02	*COL4A6, COL4A5, LAMA3, THBS1, TNC, ITGA6, VEGFA, CCND3*	*COL9A3, LAMB1, ITGB4, IGF1R, FLNC, HRAS*

Supplementary Table 4. Complete list of DEGs included in the Kyoto Encyclopedia of Genes and Genomes (KEGG) pathway enrichment analysis of RNA-seq data. Fold enrichment and Student's t-test p-values are shown.